ARTIFICIAL NEURAL NETWORK AND FUZZY LOGIC CONTROL FOR HVDC SYSTEMS

BY

ALIREZA DANESHPOOY

A Thesis
Submitted to the Faculty of Graduate Studies
in Partial Fulfillment of the Requirements
for the Degree of

DOCTOR OF PHILOSOPHY

Department of Electrical and Computer Engineering
University of Manitoba
Winnipeg, Manitoba

National Library
of Canada

Acquisitions and
Bibliographic Services

395 Wellington Street
Ottawa ON K1A 0N4
Canada

Bibliothèque nationale
du Canada

Acquisitions et
services bibliographiques

395, rue Wellington
Ottawa ON K1A 0N4
Canada

Your file Votre référence

Our file Notre référence

0-612-23593-9

Canada

THE UNIVERSITY OF MANITOBA

FACULTY OF GRADUATE STUDIES

*****

COPYRIGHT PERMISSION PAGE

ARTIFICIAL NEURAL NETWORK AND FUZZY LOGIC CONTROL FOR HVDC SYSTEMS

BY

ALIREZA DANESHPOOY

A Thesis/Practicum submitted to the Faculty of Graduate Studies of The University of Manitoba in partial fulfillment of the requirements of the degree

of

DOCTOR OF PHILOSOPHY

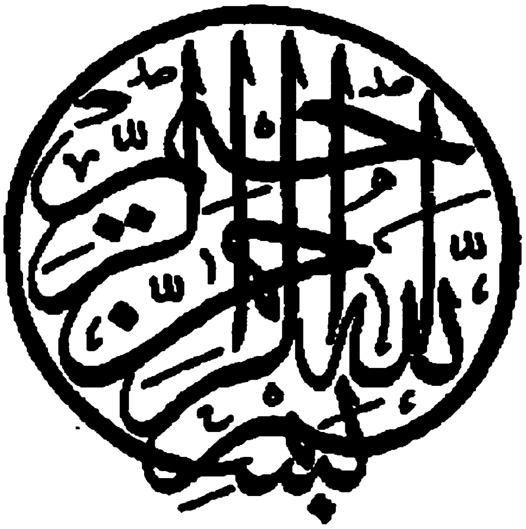

In the name of Allah, the Beneficent, the Merciful.

Acknowledgement

The author expresses his sincere gratitude to his advisor, Prof. A.M.Golé, for his continuous guidance and support through his study and research.

Especial thanks are due to Prof. D.G.Chapman and Mr. J.B.Davies of Manitoba Hydro for their technical advice and support. The financial support of Manitoba Hydro for this project is gratefully acknowledged.

The acknowledgement would be incomplete without thanking my wife, Rebecca, for her endurance, encouragement and priceless support.

Abstract

This thesis comprises the studies and results from the application of artificial neural networks (ANN) and fuzzy logic theory to the control of the high voltage direct current (HVdc) systems. The studies considered their implementation in both low and high level control systems in HVdc systems. The study is verified using the electromagnetic transients simulation software. The results demonstrated successful performance for single mode control (either constant extinction angle or constant current) using an ANN based on-line controller. The results for the fuzzy logic based controller showed many improvements compared to the conventional HVdc control scheme. The fuzzy logic based controller concept was further successfully extended to high level control problems such as the control of SSR and power swings. Finally in order to facilitate further application of new control techniques such as ANN or fuzzy logic, a MATLAB to transient simulation software interface was developed. Using this interface, all the MATALB commands and Toolboxes may be used within the transient simulation software.

Table of Contents

1. Introduction

High voltage direct current (HVdc) transmission plays an important role in today's electrical power transmission systems. The dc voltage in conjunction with fast acting power electronic devices in an HVdc system, makes it the most reliable method for power transmission over long distances, and power injection into load buses without much concern about system stability and dynamics.

HVdc systems have been in service for over half a century, and their performance is greatly affected by the control methods used. Application of advanced methods such as optimal control [4], adaptive control [51], multi-variable control [54,60] and different approaches such as microprocessor based controllers [38] and digital signal processing [39] have been investigated or under investigation. In this dissertation, the application of artificial neural networks and fuzzy logic techniques to various HVdc control levels have been evaluated.

Artificial neural networks (ANN) are gaining widespread application in several areas of engineering [66], especially where, due to non-linearity of the process, it is often too cumbersome to analyse the process or the plant under study. The ANN has the capability to learn and extract information in systems where the non-linearity and time dependency do not permit one to use methods such as frequency or modal analysis. Although it is always possible to linearize such a system around an operating point and conduct such studies, such derived models always remain valid only within the limited region.

ANN techniques have been applied extensively in the domain of power system. Among these works, the contributions of El-Sharkawi to various aspects of power system such as *security assessment* [1,2,17,18,64], *load forecasting* [19,47,48] and *drives control* [26,65] are notable. The ANN has also been applied widely to other fields such as *fault detection*.

ANN applications in HVdc system control have only recently become a topic of interest. The works of Sood in the application of ANN to HVdc control [39,43,56,57] are notable in this area. The application of the ANN has also been studied for fault detection in HVdc systems [36,58].

Adaptive control theory, in which the controller adapts its parameters and/or structure to changes in the operating point, is an attractive control technique for HVdc systems. This is because the dynamic response of the HVdc '*plant*' changes with variations in the operating point. However, adaptive controllers require for their design, a frequency domain model of the controlled plant. Due to the switched mode non-linear operation of the HVdc system, such a model is difficult to obtain. On the other hand, the ANN techniques can be applied even without the availability of frequency models and are thus potentially attractive.

The most widely used control block for control tracking is the proportional-integral (P-I) controller. It has been widely used in HVdc systems for the internal control loops. On the other hand, the ANN, through its adaptive [7] response offers the possibilities of good performance over a wide range.

In this thesis, after some preliminary introduction to the ANN theory, the application of the ANN based controller to HVdc systems, is studied. The results are presented and the advantages and disadvantages of the approach are discussed. It is deduced that the ANN controller performs in a manner comparable to, and even superior to the P-I controller when it is working under one control mode. However, during the course of the HVdc investigations, it was discovered that the ANN was not a suitable tool for multi-mode control of dc systems. This is because it is not possible to get an adequate description of the '*plant*'.

Following this, the application of the fuzzy logic method is investigated. The fuzzy logic technique is a simple method for encoding the verbal rules into a mathematical framework [34,49]. Thus the control rules of the HVdc plant are stated verbally and formulated into the fuzzy logic implementation.

The application of fuzzy logic technique to power systems and HVdc has also been widely studied. These application includes *gain scheduling* [11,12], *tuning of DC link controllers* [13] and *enhancement of the VDCL performance* [44].

In this dissertation a novel approach to apply fuzzy logic method to HVdc control is investigated. The method works in a supervisory technique, irrespective of the controller type (P-I, ANN, ...). It is shown that the fuzzy logic method improves the control system performance considerably, and the process to include more elaborate control rules is also demonstrated.

Later the application of the fuzzy logic to high level HVdc control schemes and the implementation of these methods to high level control such as power swing damping are also investigated.

In the course of the thesis investigations, a new technique for investigating advanced control methods in an EMTP[1]-type simulation framework was developed. This technique embodied the seamless integration of the PSCAD/EMTDC™ simulation program with the powerful MATLAB package. MATLAB has many built-in useful functions, and many practical Toolboxes such as neural network and fuzzy logic Toolboxes. Although not of direct relevance to the main thesis topic, this technique is an asset for investigation of new methods. It also saves a lot of time implementing the new technique during the preliminary studies. The technique has therefore been presented in Appendix.

[1] Electromagnetic transient program

2. Neural Network

2.1 Theory

An artificial neural network as defined by Hect-Nielsen [24], is a parallel, distributed information processing structure consisting of processing elements interconnected via unidirectional signal channels called connections or *weights*. Each processing element or *neuron* has a single output connection that branches (fans out) into as many collateral connections as desired; each carries the same signal -the processing output signal. The processing element output signal can be of any mathematical type desired. The information processing that goes on within each processing element can be defined arbitrarily with the restriction that it must be completely local; that is, it must depend only on the current values of the input signals arriving at the processing element via impinging connections and on values stored in the processing element's local memory. Neural systems encode sampled information in a parallel-distributed framework.

There are different types of ANN where each type is suitable for a specific application. The main interest here is applying the ANN for a non-linear mapping. Neural networks can also be used to estimate input-output functions. They are trainable dynamical systems. Unlike statistical estimators, they estimate a function without a mathematical model of how outputs depend on inputs. They are *model free* estimators. They learn from experience with numerical sample data.

Supervised feed forward models provide the most tractable, and most applicable neural models. Assume that we have a set of observations. This set consists of a group of input and output value pairs. Each of these pairs is of the form (x, y), where x is the input and y is the output. The set of these pairs inherits the mapping between the input and the output. The emphasis here is to extract the closest mapping from the input domain to the output range. The measure of this closeness can be chosen to conform to some appropriate form such as least squared error (though it is not the only function but it is quite simple). Therefore the objective is to estimate an unknown function $f(X \rightarrow Y)$ derived from observed set samples $(x_1, y_1), \ldots, (x_m, y_m)$ by minimizing an unknown expected error functional $E[w]$.

We define error as *desired* performance minus *actual* performance. Desired performance refers to the value (y_i), while the actual performance is the network output to the input (x_i). Supervision uses the desired performance and actual performance of the network to provide an ever-present error or teaching signal.

$E[w]$ defines an average error surface over the weight space. At each iteration, the current sample (x_i, y_i) and the previous initial conditions define an instantaneous error surface. We indirectly search $E[w]$ for the global minimum by using an optimization algorithm such as stochastic gradient descent [25]. Due to the nonlinear nature of the problem, we often converge to a local minimum (*w**). The local minimum *w** may differ significantly from the global minimum of $E[w]$. Some shallow local minima may be no better than expected error values determined by randomly picking network parameters. Since we do not know the shape of the $E[w]$, we do not know the depth of its local minima. In general, nonlinear multi-variable systems define complicated, and bumpy, average error surfaces. However, for small dimensional problems like the one reported in this thesis, no special technique is used to guarantee an absolute global minimum. This is in conformance with the current practice in the ANN field [55].

Consider a set of *Input* (x_i) and *Output* (y_i) which are derived from an actual measurement or simulation of a specific plant. It is desired to find a function which can resemble the whole plant based on this set of discrete vectors (x_i,y_i). In other words we want to find a function which approximates the plant to a specific degree of accuracy instead of analysing the nonlinear equation of the plants.

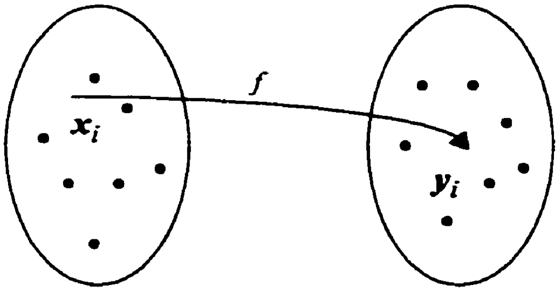

Figure 2-1-1 : Geometry of neural function estimation

A typical feed-forward ANN is shown in figure 2-1-2. It has one input node *x*, and one output node *o* along with *k* hidden nodes, V_1 to V_k. The objective is to produce the output o_i which is as close as possible to the desired target y_i, when x_i is the input of the network.

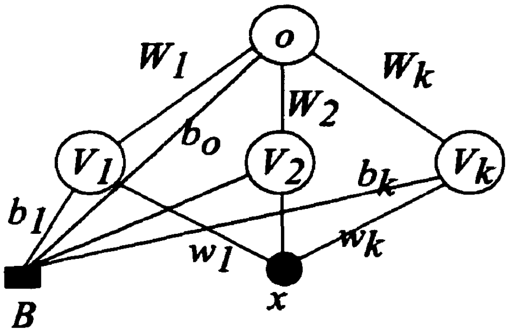

Figure 2-1-2 : A two layer feed-forward network

The output of any hidden or output neuron is calculated from a weighted sum of the inputs to that neuron. In addition to the inputs to each processing neuron, a bias level B (usually equal to one) may also be applied to each neuron. The bias is connected with an adjustable weight to each hidden and output neuron. Thus, for example, the excitation of node V_k is $h=w_k*x_i+b_k*B$. The output of the neuron V_k is generated by applying a sigmoid non-linearity as shown in figure 2-1-3 to the excitation [25]. The same nonlinear function is also used for the output neuron.

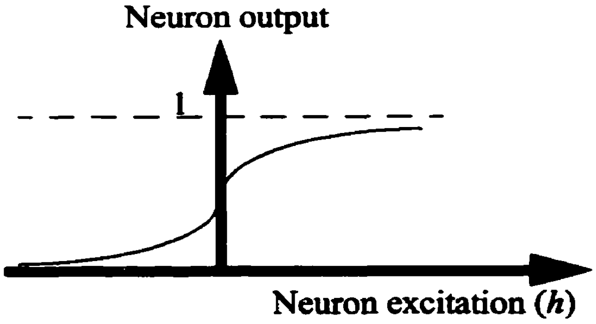

Figure 2-1-3 : Sigmoid nonlinear function

The sigmoid function used for this study has an input to output function given by eq. 2-1-1. The output range of the function presented in eq. 2-1-1 is the closed interval [0,1] (continuous interval between zero and one, including zero and one). Therefore, the output of each processing node (hidden and output) lies in the continuous interval between zero and one. The parameter β in eq. 2-1-1 decides the function's slope.

$$g[h] = \frac{1}{1+exp(-2\beta h)} \qquad (eq.\ 2\text{-}1\text{-}1)$$

Using an optimization technique, the weights are adjusted so as the error for the entire input-output set becomes as low as possible. Usually the mean square error, eq. 2-1-2, is chosen as the performance index or cost function:

$$E[w] = \frac{1}{2}\sum_{i}[y_i - o_i]^2 \qquad (eq.\ 2\text{-}1\text{-}2)$$

where *i* is the number of input pattern (*i* = *1,2,...,p*) and o_i is the i^{th} computed output. We seek the weight vector ***w*** which results in a global minimum for $E[w]$.

Learning or weight adjustment is carried out by determining the contribution of each connection to the output error and correcting that weight correspondingly. Applying the steepest descent algorithm [25], the adjustment in w_k yields as:

$$\Delta w_k = -\eta\frac{\partial E}{\partial w_k} \qquad (eq.\ 2\text{-}1\text{-}3)$$

where η is called the *learning rate* and is a very crucial parameter in the learning process. This procedure is also called *back propagation* [24], since the output error is back propagated through the network in order to determine the contribution of each single weight to it. It should be mentioned that $w_k$is chosen as an arbitrary weight, and the same derivation applies to all the weights either between two neurons or the weights between the bias and any neurons.

It is reported in the literature [25], that the cost function is usually full of valleys with steep sides but a shallow slope along the floor, and the aforementioned method usually gets stuck in these regions and the learning process becomes too slow. There are a number of ways of dealing with this problem, including the replacement of gradient descent by more sophisticated minimization algorithms. However a much simpler approach, the addition of a ***momentum*** [25], is often effective and is very commonly used.

The idea is to give each connection some inertia or momentum, so that it tends to change in the direction of the average downhill force that it feels, instead of oscillating wildly with every little kick. Then the effective learning rate can be made larger without divergent oscillations occurring. This scheme is implemented by giving a contribution from the previous time step to each weight change:

$$\Delta w_k(m+1) = -\eta\frac{\partial E}{\partial w_k(m)} + \alpha\Delta w_k(m) \qquad \textit{(eq. 2-1-4)}$$

Besides it can be shown [24] that "*Given any $\varepsilon > 0$ and any function $f; [0, 1]^n \subset R^n \rightarrow R^m$, there exists a three layer back-propagation neural network that can approximate f ($f \in L_2$) to within ε mean squared error accuracy*". Here L_2 is the mathematical space of functions that can be approximated by its Fourier series to any desired degree of accuracy in the mean squared error sense.

Although the above statement guarantees the ability of a multi-layer network with the *correct weights* to accurately implement an arbitrary function, it does not comment on whether or not these weights can be learned using any existing learning law. This is an open question [24].

In addition there is no guarantee that the function being approximated satisfies the above L_2 condition. Such a function would not be amenable to approximate by an ANN. However the above theorem suggests that assuming a reasonable function, a three layer ANN should normally suffice for most application with variable number of hidden units. There is no rule or theorem expressing the optimal number of hidden layer neurons, and is usually derived from empirical results or trial-error method.

The update rule, as defined by eq. 2-1-4, is written in the incremental form. In other words for each input-output pair (pattern i), the adjustment to individual weights are derived from this equation. The pattern i is presented to the ANN network, and then all the weights are updated before the next pattern is considered. This clearly decreases the cost function (for small enough η) at each time step, and lets successive steps adapt to the local gradient.

The developed neural network system can be trained and implemented in two different ways. In one approach, the network can be trained with a set of known input-output data pairs known as the training set and, after some standard verification, can be used for the actual application. For example a neural network can be trained with some known data for sonar target recognition and after achieving desired level of accuracy, it can be used for real sonar detection purpose. In this way the ANN network, after extracting the rules from examples or a training set, is known to perform some sort of generalization whenever it come across new inputs. This method is called *off-line* training because the weights adjustment is performed prior to implementing the network in the analysis. In the second method, the learning can be done while the network is being implemented in the process. In this way the network corrects itself as it comes across new inputs; learning while new sequences are being presented rather than after they are complete. It can thus deal with sequences of arbitrary length and there is no requirement to allocate memory proportional to the maximum sequence length. This method is called *on-line* training. In this method there is no generalization and all the input-output pairs are member of training set.

The neural network architecture used through out this dissertation, is as shown in figure 2-1-4. It is a two layer network with one input unit, two hidden units (adjustable) and one output unit. The weights are altered (learning process) in order to minimize the mean square error between the desired and actual outputs, using eq. 2-1-2. This is done by performing a gradient descent algorithm on eq. 2-1-4 which results in the normal back propagation algorithm (BP).

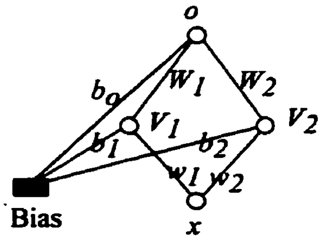

Figure 2-1-4 : Neural network architecture

This model is developed as a block and used in the digital simulation analysis program. Therefore at each time step an input x_i is represented to the neural network model and the error between o_i and y_i is then used to adjust the weights with back-propagation algorithm.

For on-line training (incremental), the weight update is done once each time step. Thus for this particular implementation eq. 2-1-2 takes the form:

$$E[w] = \left(o_i - y_i\right)^2 \qquad \textit{(eq. 2-1-5)}$$

2.2 ANN Based Control, Literature Survey

Various attempts have been carried out to use ANN for control purposes. Based on the learning method, the ANN based controllers can be divided in two categories. The first category are the controllers with off-line learning. Here, first the learning is performed, and then the trained ANN is implemented to the process which is under control. Nguyen and Widrow [45,46] have shown in a novel approach the use of this method for backing up a trailer in a two dimensional plane. Kong and Kosko [33] tried also the same approach, but used the truck kinematic equation instead of truck emulator as used by Nguyen. Beaufays et al. [6] have used this method for load frequency control in power systems. Generally, the off-line method is applicable to a process with explicit mathematical formulation.

The second category includes the controllers that use on-line learning. Chen [7] has investigated on-line learning for adaptive control, although his method is only applicable to single input, single output linearizable systems. It is shown that the learning process makes this controller an adaptive one. On-line learning has been successfully used for underwater vehicle control as reported [61]. The proposed learning algorithm and the network architecture provides stable and accurate tracking performance. For the on-line learning method, the mathematical formulation of the process under the control is needed.

Schiffmann et al. [55] have reported a comparative study for an ANN on-line controller and a P-I controller. The results show that the ANN controller is very effective. In their study the plant is treated as an additional and non-modifiable layer of the network and only simple qualitative knowledge of the plant is necessary.

The on-line training makes an ANN controller an adaptive controller. The learning process based on the back propagation, adjusts the ANN parameters (weights) such that the output follows its reference value.

2.3 On-line Training

Assume that a single input single output plant is cascaded to a neural network (feed forward connection). The single input single output plant is connected as a last level to the ANN, and can be taken as the last processing unit of this network, i.e. we can imagine that the whole system starting from input to the output of the plant is an additional processing unit (neuron) to the network. The last processing unit of this augmented network does not have a characteristic like the other ANN neurons, in fact the characteristics is non-linear and time-dependent and not explicitly known. As already explained in §2.1, the learning algorithm tries to set the system weights in order to make the output of the network be equal to some desired quantity. Thus by connecting an ANN as a controller connected to the input of the plant and implementing the learning process to adjust the weights, it is theoretically possible to make the plant output follow the reference order, provided that the network parameters and weights get adjusted by the output error.

Using a feed forward system for control purposes, a self-supervised learning system must be used. One such a system has been reported in [50]. Of the three proposed methods, specialized learning seems to be the best and is chosen for this study. This method requires knowledge of the *Jacobian* matrix of the plant. For a single input single output plant, the Jacobian reduces to derivative of the input-output function of the plant.

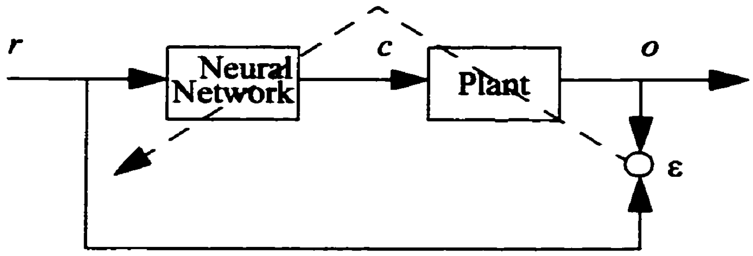

Figure 2-3-1 : Specialized Learning

The only difference of such a composite feed forward system is that the plant is the last layer of the network, (in this thesis this last layer is a single input single output system) and has the following differences with an ANN:

- The output unit (plant) does not have any adjustable parameters.
- The derivative of the output unit to the input is not explicitly known.

The first point implies that the plant does not take part in the learning process, while the second one tacitly reveals that the error can not be adjusted in order to get the modified error (c) at the neural network output. The back-propagation algorithm used for setting the ANN weights, requires the error at the output of the ANN, i.e. the error between the actual output c and the desired output (the desired output is the one that makes the plant error ε to be zero). However, the error of interest in the application is the error at the plant output. The value of c must be back-calculated from this error; and this is only possible if the plant derivative *do/dc* is known, either explicitly or approximately.

As already explained, the error that should be back propagated through the neural network is the error of *c* and not ε (figure 2-3-1), and the error of *c* can be derived if the derivative of the plant is known at any operating point. The plant is mostly viewed as a single input single output (SISO) plant and the sensitivity of the plant's input versus output for the cases under study never changes in sign. This is typically true, for example in an HVDC rectifier, where increasing the firing angle α results in a reduction in output voltage [32]. Therefore in this analysis, ε is treated as if it is the actual ANN output error. The controller implementation is shown in figure 2-3-2.

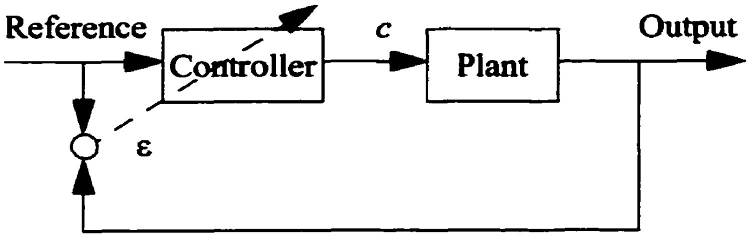

Figure 2-3-2 : On-line training

Here, the well known back-propagation rule [24] is used to perform gradient descent optimization on eq. 2-1-5 based on error ε. Here, the controller acts like a conventional type P-I controller and based on the error ε, the controller tries to change its output in order to minimize the error ε.

Similar works have been done by Sood et al. [56,57]. In contrast to this approach, they treated the error ε independently for each layer of ANN (using the delta [25] rule for each layer). Also they did not incorporate the activation functions slope (β) in their study and treated α and η as the only ANN parameters. In a recent publication [43] they considered the effect of the activation function slope on the system behaviour. The parameters α, β and η are described in §2.1.

2.4 Off-Line Training

Off-line training is not an adaptive process, but it is fastest to implement, because the weights are not changed in the field. One promising method for on-line training is using the recurrent ANN, and the method is briefly presented in this section. This model is trained in the manner shown in figure 2-4-1. This method is applied by Nguyen [45,46] and recently is used for load-frequency control [6]. The process is outlined as follows.

In this approach, before training the neural network controller, a separate neural network, which is called an *emulator*, is trained to behave like the plant. Training the emulator is similar to plant identification in control theory, except that the plant identification here is carried out by using the method of back-propagation.

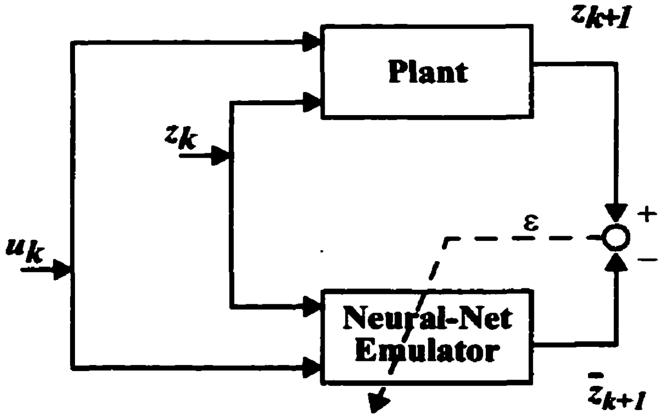

Figure 2-4-1 : Training the Neural Network Plant Emulator

The training process begins with the plant in an initial state. At time *k*, the input of the neural net is set equal to the current state of the plant z_k and the plant input u_k. The neural net is trained by back propagation to predict the next state of the plant, with the value of the next state of the plant z_{k+1} used as the desired respcnse during training.

Given that the emulator now closely matches the plant dynamics, we use it for the purpose of training the controller. The controller learns to derive the plant emulator from an initial state z_0 to the desired state z_d in "k" (determined by the designer) time steps. The objective of the learning process is to find a set of controller weights that minimizes the error function J, where J is averaged over the set of initial sets z_0.

$$J = E\left(\|z_d - z_k\|^2\right) \qquad \textit{(eq. 2-4-1)}$$

The training process for the controller is illustrated in the following figure.

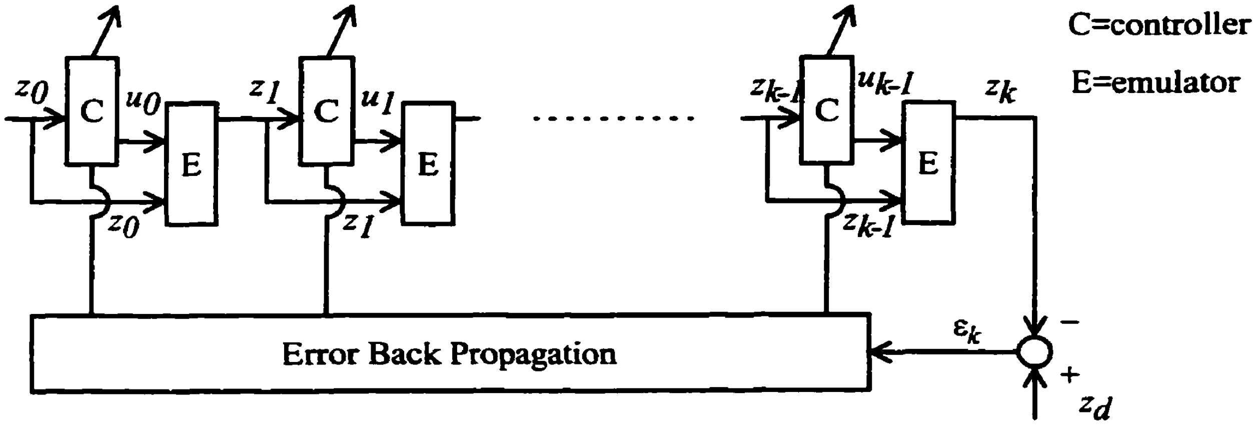

Figure 2-4-2 : Training the Controller with Back Propagation

Once the plant model is obtained, a candidate ANN controller is now designed to match the desired control characteristic of a conventional controller. After training, the ANN controller will mimic the conventional controller from which the training was derived. However, the performance of the off-line ANN controller can only be as good as that of the conventional one.

3. The Artificial Neural Network Controller

3.1 ANN Current Control

To gain familiarity with ANN control of power electronic circuits, the author first developed this concept on a simple three phase rectifier connected to an active load. The circuit layout is shown in figure 3-1-1.

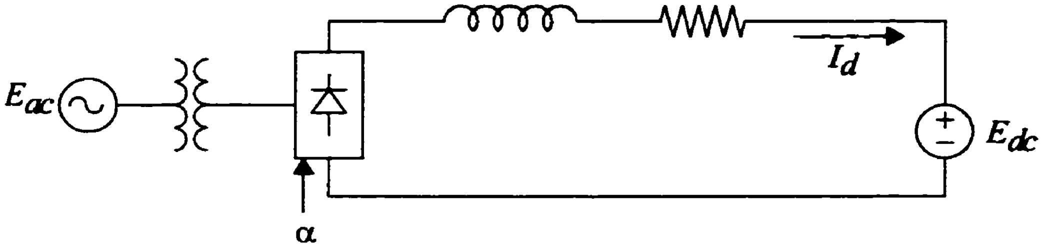

Figure 3-1-1 : Current Control Circuit Diagram

In the above circuit, the current I_d in the lagging load is controlled through the adjustment of the firing *delay angle* of the rectifier or α. The conventional method to control the converter is to apply a proportional integral type (P-I) controller as in the figure 3-1-2.

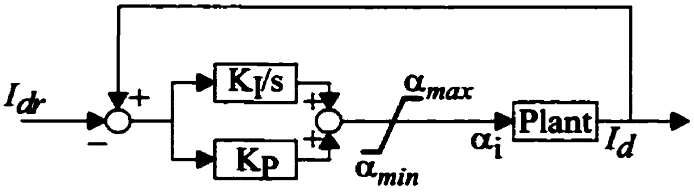

Figure 3-1-2 : Current Control Scheme

The proportional part reacts instantaneously to any difference in the measured and ordered current, whereas the integral part keeps varying α till there is no steady state error. The current error is fed into a P-I controller which adjusts α in turn in order to minimize the error. The P-I controller has two parameters K_I and K_P (integral and proportional gain), which should be tuned in order to get the best performance. This type of controller is not adaptive and thus following any system changes one has to tune the controller parameters accordingly.

For this analysis the P-I controllers is substituted with the ANN based on-line controller. The source code for back-propagation is incorporated in a model used in the PSCAD/EMTDC™ electromagnetic transients program. The model and the control diagram is depicted as figure 3-1-3. Since the output of ANN is between *zero* and *one* (see figure 2-1-3), a re-scaling of the output of ANN in the range of α_{min} and α_{max} is required and is carried out inside the block.

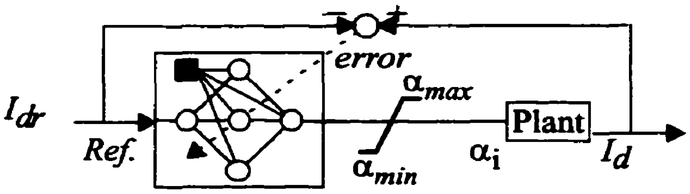

Figure 3-1-3 : Current control with ANN

As is shown in figure 3-1-3, the ANN model responds to two signals. These signals are as follows:

- *Ref.*: This is the ordered value of the controlled parameter. As has already been explained, the network is feed-forward in topology, and the only input to the ANN network is this signal.

- *Error*: This is the most important signal, and is the only measure of performance achievement and is used in the setting the ANN weights. The *gradient descent* moves the weights (*w*) so that *E*[*w*] approaches its (local) minimum value. The weights and their impacts on an ANN are explained in §2.1.

In addition to the two mentioned inputs described above, there exist other parameters associated with any ANN. The other parameters of this block are:

- the *momentum term* (α) which is usually between 0.5 and 0.9.
- the *learning rate* (η) which is normally between 0.5 and 0.9.
- the *slope term* (β). This term defines the slope of the sigmoid function and is usually between 0.01 and 0.1.

These last three terms are standard terms in ANN literatures [23,25] and were discussed briefly in §2.3.

The necessary ANN block was developed and added to the DRAFT user components. The electrical circuit developed within DRAFT is shown in figure 3-1-4 and the ANN block is shown along with the rest of the control scheme are shown in figure 3-1-5.

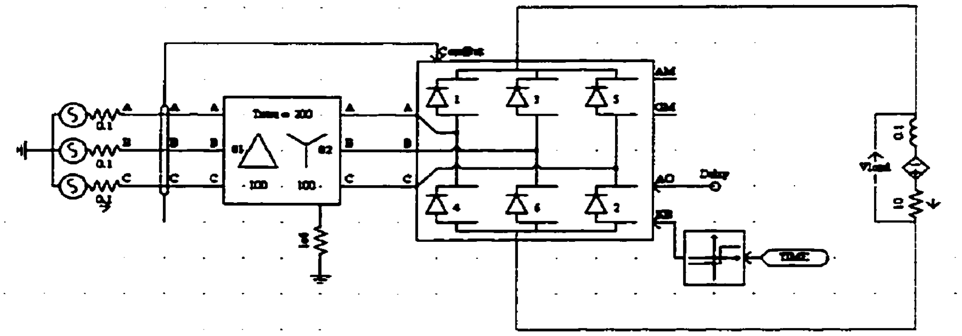

Figure 3-1-4 : Electric circuit

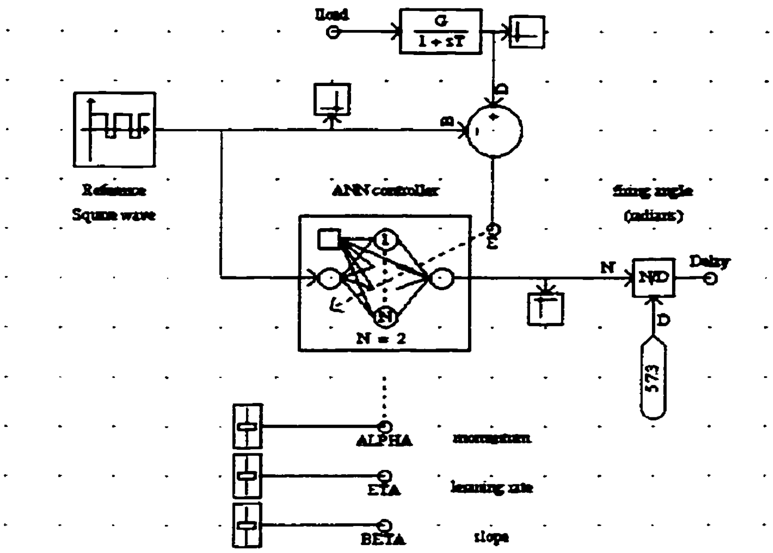

Figure 3-1-5 : ANN control scheme

With some experimentation, the parameter values selected were α=0.1, β=0.015 and η=0.6. These values appeared to provide the best learning performance. A simulation time-step of *5* μsec is used and the weights are continuously updated during each time step. The ANN topology is a two layer network with one input neuron, two hidden neurons and one output neuron. The voltage source in series with the load is set to zero, unless it is noted.

As the first performance and the evaluation test, the current reference change is investigated. The steady response with ANN control for this test is shown in figure 3-1-6.

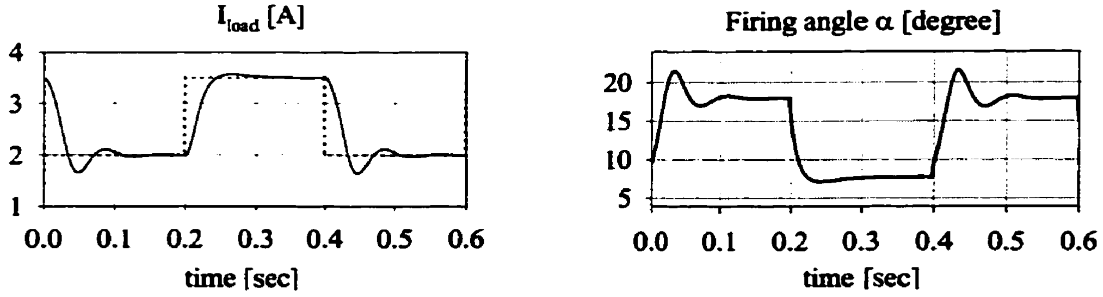

Figure 3-1-6 : Simple ANN current reference change response

The ANN based on-line controller as shown in figure 3-1-3, has the capability to adjust the firing angle (α) in order to minimize the dc current error and make the plant to follow the reference value. The methods and modifications to improve the response speed are discussed later.

3.2 Behaviour Analysis of the ANN

As shown in the previous section, an ANN based on-line controller has the capability to adjust the firing angle such that the dc current follows the reference change. The current reference change response shows that the ANN is capable of controlling the simple rectifier for simple current order change. Artificial neural networks have many variable parameter and characteristics such as learning rate and number of hidden units, where each has substantial effect on the ANN performance. The ANN parameters such as learning rate (η), momentum (α), activation function slope (β), the number of hidden units and the type of the input to the ANN are the parameters that should be further investigated and studied. Thus it is straightforward to follow the analysis by studying the effect of these parameters on the ANN and the system performance. In order to investigate the behaviour of this controller, following tests and simulations have been carried on.

- ***Operating point change***

As shown in figure 3-1-4 the load is in series with a dc voltage source. Any variation in this series voltage source, directly changes the firing angle and the operating condition of the rectifier. In order to study the behaviour of ANN due to the operating point changes on the performance of the system, the voltage is changed at $t=0.2$sec., and the response to a step change in current order is shown in figure 3-2-1. Figure 3-2-1 shows the response with two different values for the dc voltage: $E_{dc}=20$ and $E_{dc}=0$.

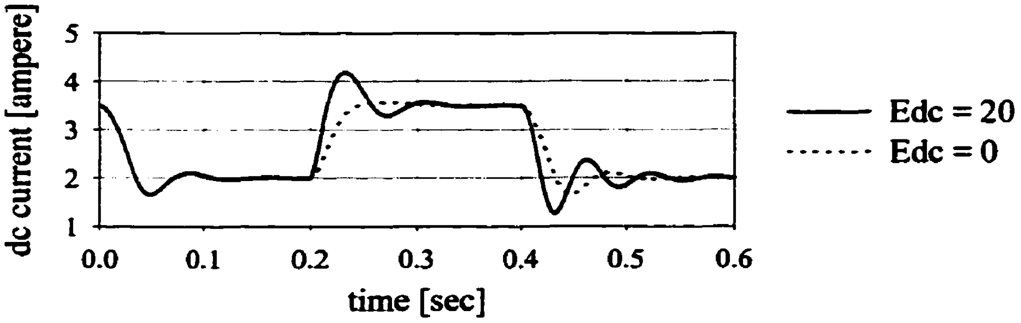

Figure 3-2-1 : Response of ANN with changes in E_{dc}

System changes as shown in figure 3-2-1 show that the behaviour of the system changes with change of the operating point. As shown, increasing the load voltage, brings about a faster and more oscillatory response.

With a constant ac bus voltage, the dc voltage ignoring the commutation reactance, is $V_d = kV_{ac}\cos\alpha$ (where V_{ac} is the rms value of the line voltage, α is the converter firing angle and $k = 3\sqrt{2}/\pi$) [32], which gives the sensitivity of converter dc voltage to α changes as $-kV_{ac}\sin\alpha$. Clearly, the controller is more sensitive for large α, i.e. smaller values of V_d, explaining the larger overshoot at the smaller voltages in figure 3-2-1.

- ***ANN parameters change***

In addition to the system change, ANN parameter changes should be considered as well. The ANN parameters such as activation function slope (β), the learning rate (η) and the momentum (α) have direct effect on the ANN performance. (The following tests were conducted for $E_{dc}=0$, unless otherwise noted). The following test (figure 3-2-2) shows the result of the activation function slope (β) change on the system response.

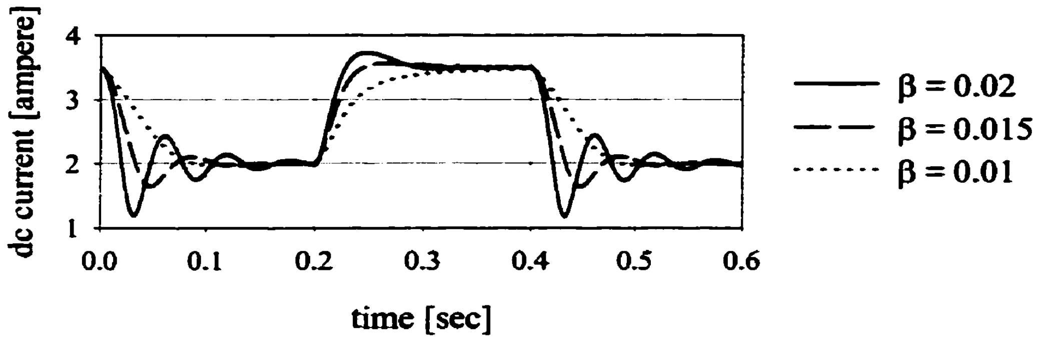

Figure 3-2-2 : Response of ANN with β change

Similarly the effects of learning rate (η) and momentum (α) on the system response are shown in figure 3-2-3 and figure 3-2-4 respectively.

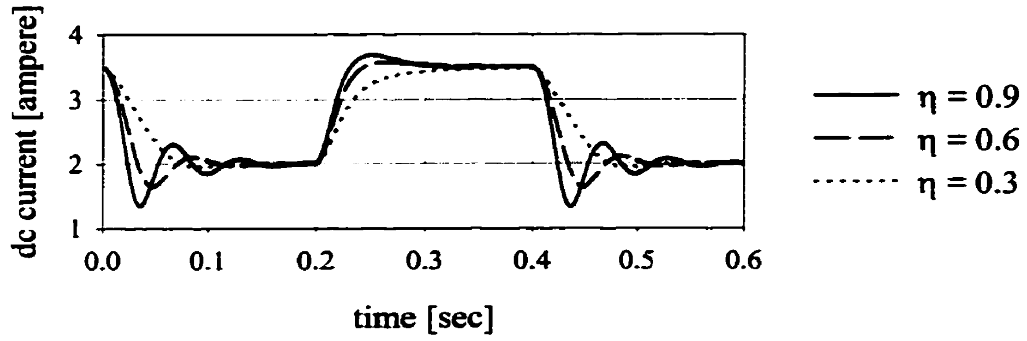

Figure 3-2-3 : Response of ANN with η change

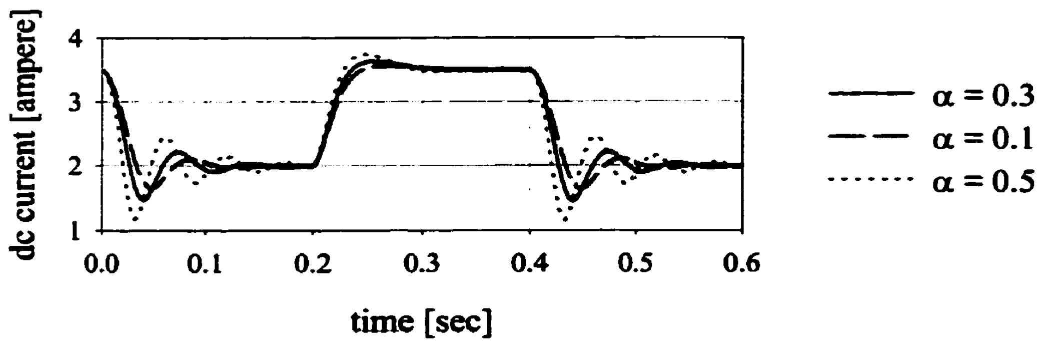

Figure 3-2-4 : Response of ANN with α change

Considering the results of the conducted tests, the following points are deduced:

1. The response is very sensitive to the slope (β) of the activation function. As shown in figure 3-2-2, higher β implies faster ANN performance. Therefore it seems very plausible to apply the slope change for increasing the ANN system response. Sood et al. have also pointed to this fact in their recent publication [43]. The method has some superficial similarity to the *simulated annealing* [35].
2. The learning rate η also determines the ANN performance. The learning rate as defined by its very first definition [25] adjusts the weights' updates in each epoch[1]. Hence the higher η implies larger adjustment and therefore faster response.
3. The momentum α incorporates the previous weight update in the recent weight update. As shown in figure 3-2-4 the value chosen for the momentum does not contribute significantly to the speed, except for a small increase in the oscillations observed for large α.

Of the two parameter slope and learning rate, it turns out that the slope has the prevailing effect in system performance speed. This fact will later be utilised with the aid of fuzzy logic reasoning to improve the ANN response [§6.6].

- ***ANN topology, number of the hidden neurons***

The number of hidden neurons in an ANN is one of the main characteristics of the system. The number of neurons in an ANN determines the total number of unknowns in the network. The larger the number of neurons, the more time consuming and lengthy is the learning process. Common experiments from the ANN [25] shows the optimal per-

[1] training cycle

formance of the ANN is achieved within a range of hidden unit numbers, and for the low order ANN of this study this number need not be more than two or three. To investigate the effect of number of hidden neurons on the ANN performance, the ANN with both two and three hidden neurons were simulated, and the results are shown in the figure 3-2-5.

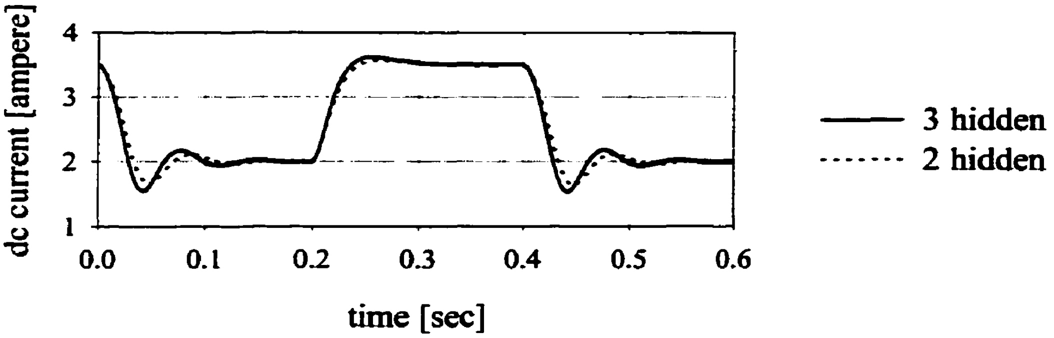

Figure 3-2-5 : Response of ANN with 2 and 3 neurons

Figure 3-2-5 shows that the ANN performance does not improve considerably by employing more hidden neurons.

- ***ANN topology, the effect of bias***

So far it is assumed that all the neurons in the ANN block, were connected through adjustable weights to a constant quantity called bias. As a further study the effect of the bias on the overall performance is investigated.

The following test as shown in figure 3-2-6 reports the response of the ANN controller with and without the bias (figure 3-2-7).

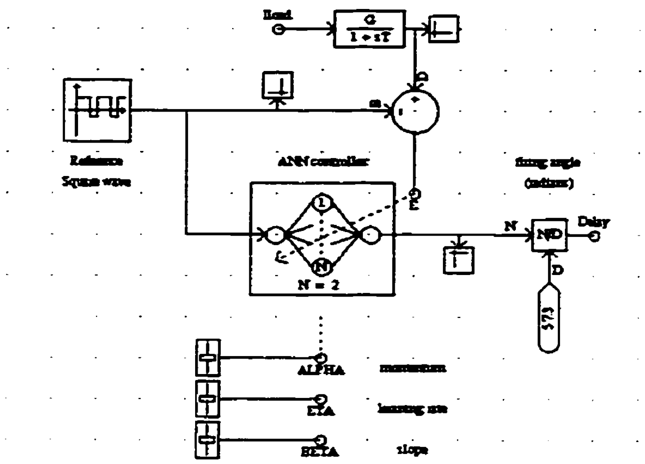

Figure 3-2-6 : ANN with and without bias

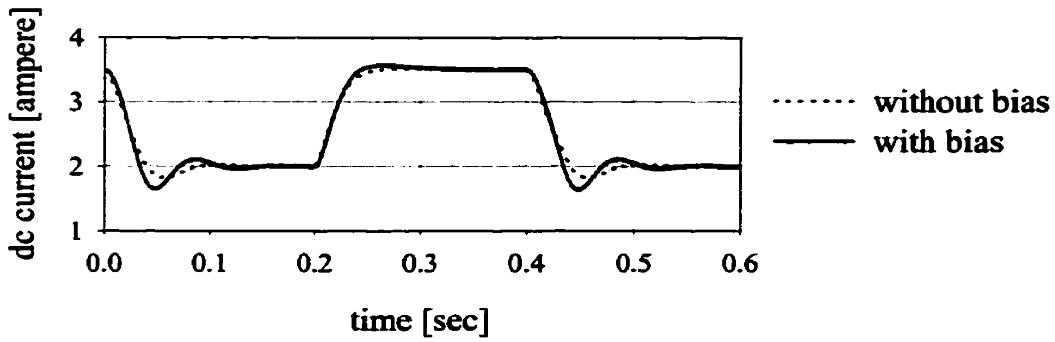

Figure 3-2-7 : Response of ANN with and without bias

The hidden units as well as the bias determine the number of unknowns associated with the ANN. Both of these tests suggest that increasing the number of unknowns for this simple ANN (one-input, one-output) does not contribute to system speed and even makes the system more oscillatory. The ANN with bias has three weights (two to hidden, one to output) more than the ANN without bias. Similarly the ANN with three hidden neurons has three (one from input, one to output, one from bias) weights more than the ANN with two hidden neurons.

Increasing the number of ANN weights does not contribute to system performance and makes the response even more oscillatory.

- ***ANN topology, input form***

As already was shown in figure 3-1-5, the input to the ANN is the reference signal, and the error signal is used for weights adjustments. Therefore any reference changes will also be sensed through the error signal. This tacitly implies the fact that the input change is also sensed by the ANN through the sudden jump of error, and the input need not necessarily be the reference value, and other signals can be taken as the ANN input. Three different inputs are investigated as the ANN input signal forms. These three different ANN topologies are schematically shown in figure 3-2-8.

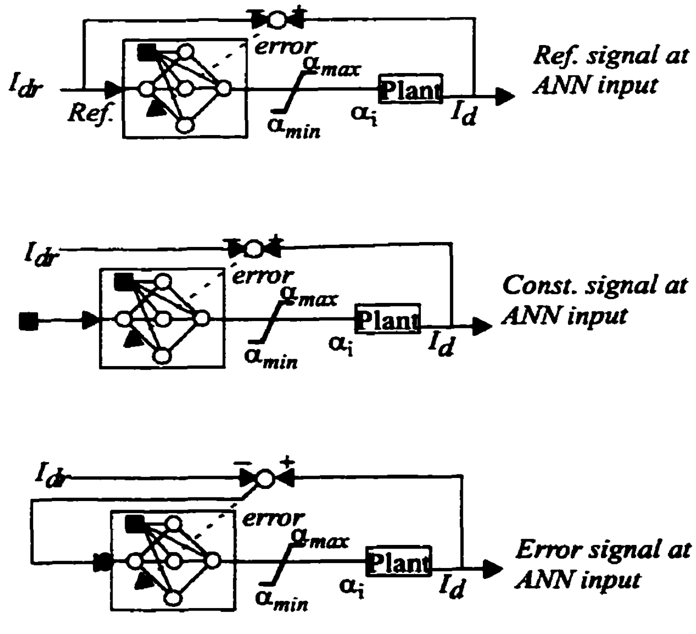

Figure 3-2-8 : ANN topologies

The result of the simulation with these three different input signals are reported in the following figure 3-2-9.

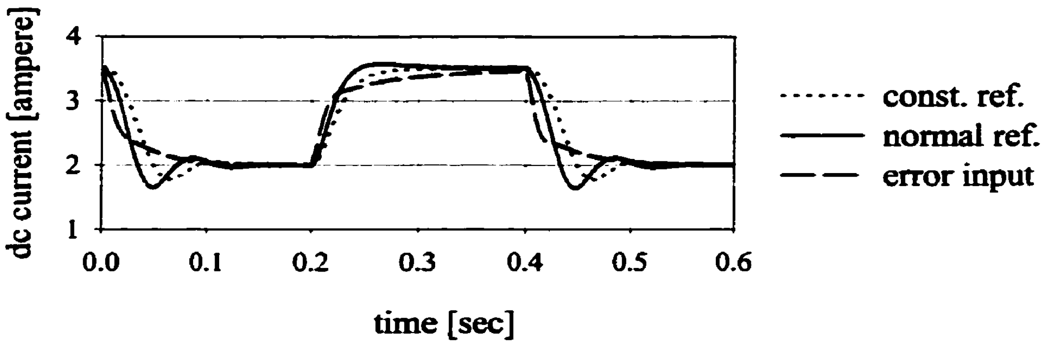

Figure 3-2-9 : Response of ANN with different reference inputs

In the second form (constant input), the ANN input can be regarded as a bias, which contributes to the output through its connection. While the third form (error input) has an input which is zero whenever the error signal is zero.

It is interesting to point out the following subtle point. Methods I and II mostly provide a large positive or negative bias on the neuron's input which drives the neuron closer to the nonlinear region of its activation function where the change of gain is not so pronounced. Conversely, the use of error as the input (method III) forces the operating point to the centre of the linear region of the sigmoid function, where the neuron activation function is linear and input change contributes to the output.

Although the third method (error input) shows slower overall response, note that this method initially responds faster than other two. Thus using the error signal as the input and increasing the speed by using steeper activation functions, lends itself to improved performance (see ANN response shown dotted in figure 6-6-6).

- ***Simulation time step***

All the studies discussed in this dissertation are based on using an electromagnetic transient program [14] type software. In this type of the study the equations for the system are solved once every time step and similarly the ANN weights are adjusted the same way. Since the back propagation is carried on in each time step, the frequency that the weights are updated is directly related to the simulation time step. Obviously the smaller time step implies more frequent weight adjustment in a run, or faster and more oscillatory response as shown in the following figure 3-2-10.

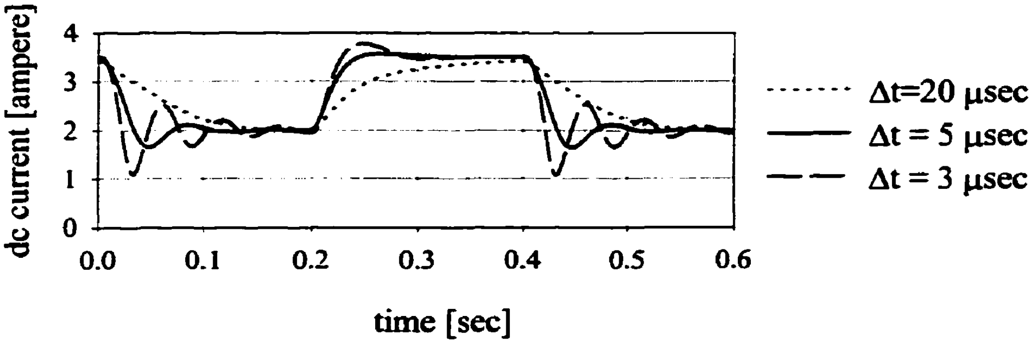

Figure 3-2-10 : Effect of simulation time step

The results of various studies on the ANN behaviour, suggest new possibilities in the ANN implementation. For example it is possible to use an ANN with low training frequency, and compensate for the reduced response speed by using neurons with steeper slopes (higher β).

3.3 Synchronized Learning

Firing angle to a converter is the only signal that controls the converter and its performance, and all the control goals are achieved via this signal. The very nature of the converter is such that the firing angle can only affect the converter performance six times during the fundamental period (for a six pulse converter). Once a firing is issued and one valve starts conducting, any subsequent changes within the $f/6$ sec. to the firing angle will not affect the converter.

Thus if the learning is carried out once in each time step, then most of the times the ANN output (firing angle) does not bring about any changes to the converter performance. For example for a simulation time step of Δt=50ms and the fundamental frequency of 60Hz, using the on-line training, the ANN is trained 400 times in each cycle, while only six of these trainings are really altering the performance and the error, while the rest 394 trainings do not affect the converter operation. Therefore for the most of the time, the learning procedure does not get any relevant information regarding its performance achievement.

In order to solve this short coming of the on-line ANN learning, the learning is carried out six times in each cycle (of fundamental frequency). The training instants are determined from a synthesized train of pulses assembled from the converter firing control circuitry. This signal is composed of unit impulses at the instants that each valve commences to conduct, or at the end of commutation period (in other words, a periodical signal consisted of six equidistant impulses within the fundamental period). Therefore this synthesized signal reproduces the instants that a change in the firing angle makes a change in converter performance. Thus the learning carried out at these instants are bound to train the ANN parameters. This synthesized signal can then be connected to the ANN enable input, or more simply multiplied by the training error. The method is named as *synchro-*

nous training. The figure 3-3-1 shows the results of comparison between normal on-line training as explained previously in this chapter with synchronized training. The results show that the speed and the accuracy of the synchronized method is considerably better than the on-line method.

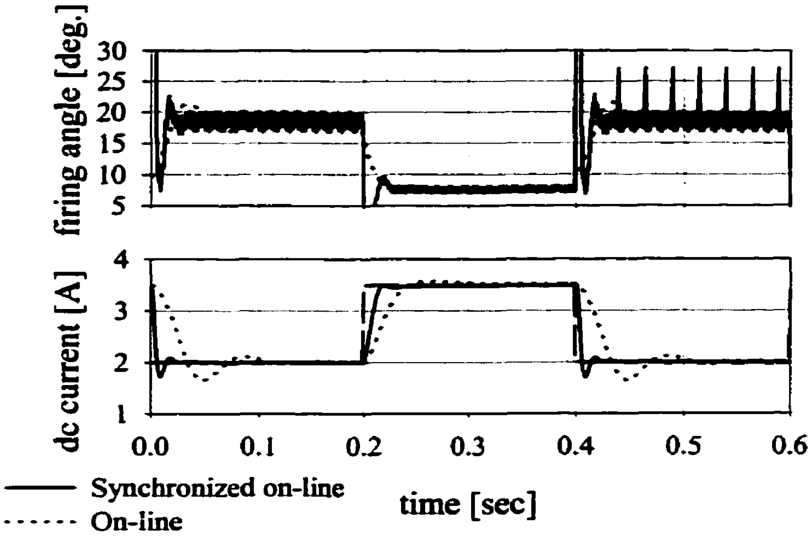

Figure 3-3-1 : Synchronized on-line training

The learning and its effect on the performance are more prominent in the synchronized learning than normal on-line learning. For example the results of the operating point change as shown in figure 3-2-1, do not show any performance improvements as the learning continues after the sudden change in the series dc source. While conducting the same test shows gradual performance improvement even for a larger change (E_{dc} = *100*).

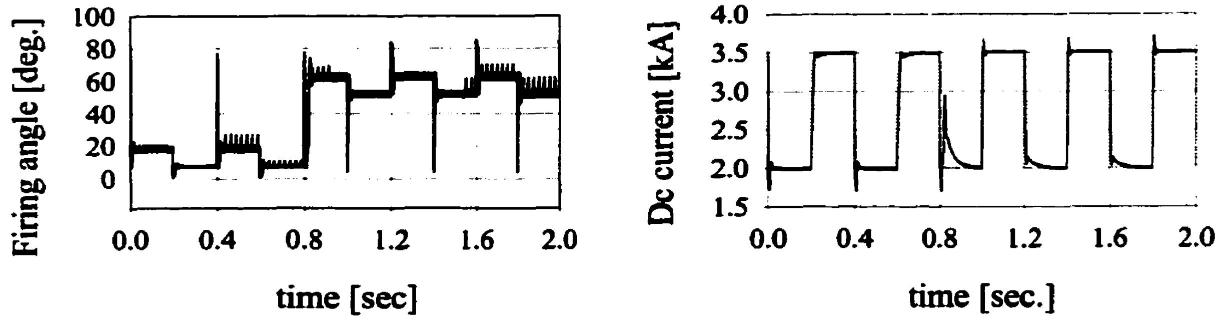

Figure 3-3-2 : Synchronized operating point change

3.4 ANN and P-I Controllers Performance Comparison

The ANN controller as discussed earlier is equipped with an adaptive procedure which guarantees that the ANN evolves with the system changes. While the P-I controller is not adaptive. The results of the two controllers on the system behaviour are shown in the figure 3-4-1.

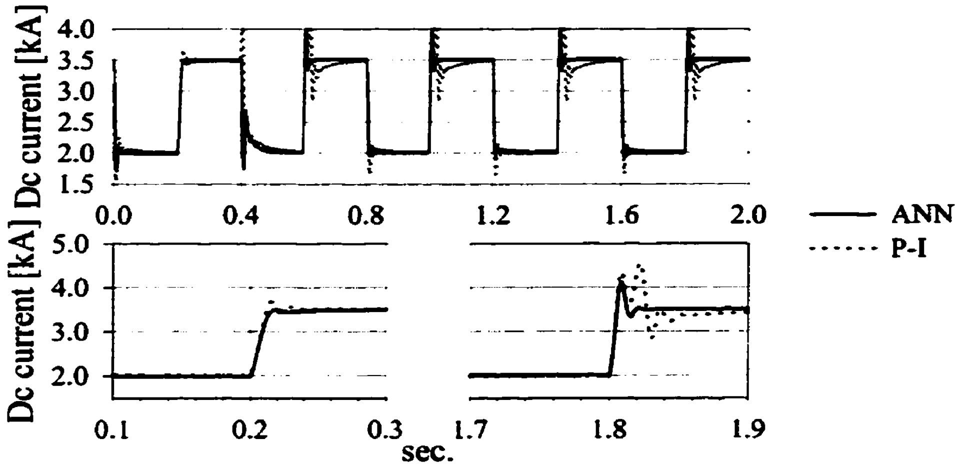

Figure 3-4-1 : P-I and ANN comparison

Both P-I and ANN as depicted in figure 3-4-1 show initially the same response speed, while the P-I has more overshoot and the change in the operating point results in substantial P-I response degradation, while the ANN controller can adaptively adjust the controller performance and behaviour due to any system changes.

In order to make the P-I response more robust, a compromise gain is usually selected in typical control systems. This gain setting gives acceptable response at each operating point, but is not the best possible response at any operating points.

3.5 Conclusion

The ANN is applied to the control of a simple rectifier connected to an active load. Preliminary studies show that the ANN provides superior performance under different system conditions. Further, the effect of the ANN parameters are investigated. It turns out that the response speed increases with activation function slope change. This idea will be followed later in §6.6. The effect of different inputs to the ANN was investigated. It is found that the error can also be used as the ANN single input. In effect throughout §4, the error is used as the single input of the ANN along with increased slope (β) for the activation function. The result of performing the on-line training procedure, six times in each cycle has shown significant improvement. This method, referred to as synchronized learning, is independent of the simulation time step.

4. The CIGRE HVDC Benchmark Model

In order to investigate the performance of ANN controllers on an HVdc system, *the first CIGRE HVdc benchmark model* is chosen [59] as the HVdc system under study. This benchmark was designed by CIGRE study group 14.02 with parameters that present a high degree of difficulty for the control studies.

Since the advent of HVdc transmission systems, their controls have been studied in great detail [20,37], and many proprietary methods [3] have been developed. These control schemes are quite complicated and includes many protective measures. They also have been utilized for many years and with ongoing modifications, are now considerably optimized.

Using a practical and complete control system for the studies conducted in this thesis is firstly very cumbersome and secondly distracts one from the primary objectives of the study. Also, many of these control systems are of proprietary nature and have not been published. Here the aim is to investigate the feasibility of applying new techniques to the HVdc control schemes. Therefore only the main modes of the HVdc control are implemented, without adding the auxiliary modifications and improvements. The main parts of the HVdc control are well explained and elaborated [59].

The FGH report [67] which describes a proposed control method for the CIGRE benchmark, is used here as the basis of the control scheme. This control scheme is referred to as the *conventional control scheme*, when being compared to the methods proposed in this dissertation.

It should be reiterated that the conventional method used in this dissertation is not the complete actual control method used in a real HVdc system. However the *conventional method* comprises the main modes common to all control schemes.

This chapter describes the CIGRE HVdc model and control, and also identifies the control parameters to be replaced with the ANN or fuzzy controllers later in this dissertation.

4.1 CIGRE Benchmark

The CIGRE benchmark model is used as a test system. The CIGRE benchmark model has been designed for conducting comparisons of performance of different dc control equipment and control strategies. The configuration is a two-terminal dc scheme, depicted as in figure 4-1-1.

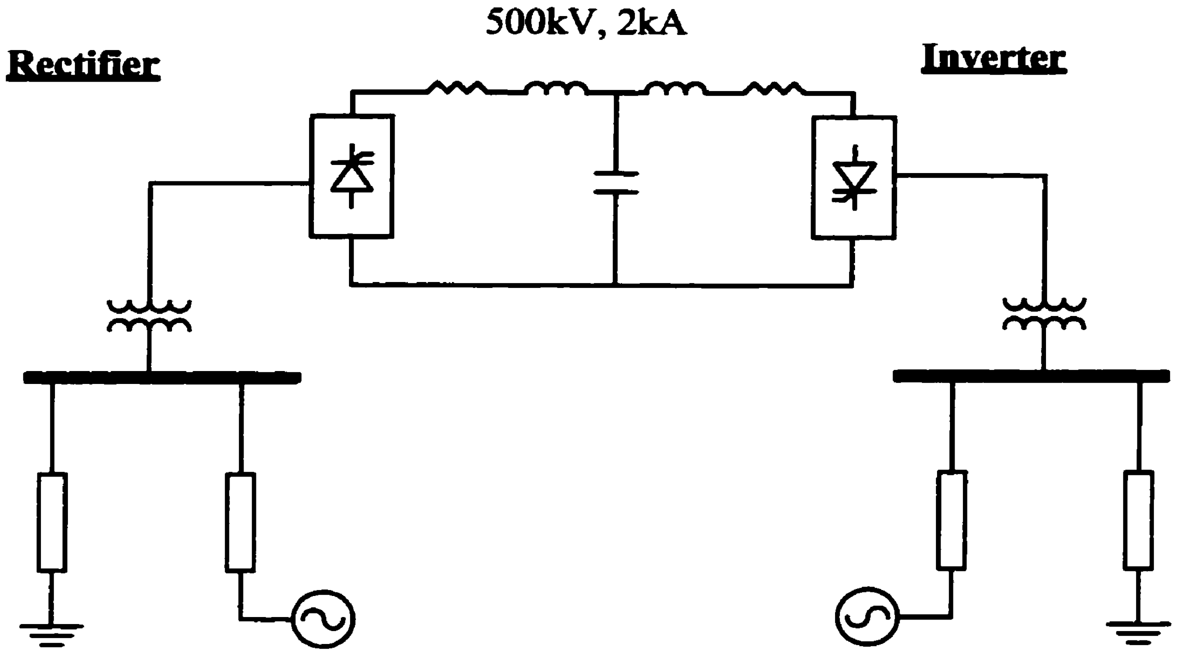

Figure 4-1-1 : CIGRE benchmark

The short circuit ratio and the effective short circuit ratio (SCR and ESCR), are important indices for characterizing the degree of expected operational problems in a dc transmission scheme. The SCR is defined as the ratio between the ac system short circuit MVA and the dc power. If the filter MVArs' are subtracted from the ac system MVA in the above calculation, the resultant quantity is the ESCR. The circuit under study [67] has the following rectifier and inverter ac system characteristics:

Rectifier SCR = $2.5\angle{-85^o}$; ESCR = $1.9\angle{-82^o}$

Inverter SCR = $2.5\angle{-75^o}$; ESCR = $1.9\angle{-70^o}$

These short circuit ratios characterize weak systems. The combination of the weak inverter system, the dc side resonance (large admittance) near fundamental, and the ac side resonance (large impedance) near the second harmonic makes the benchmark system particularly onerous for dc control operation.

4.2 HVDC Control Strategy

Both converter substations (rectifier and inverter) are provided with a current control loop including a current measuring device, a current controller and firing control equipment. Usually, one of the converters is current controlled, and the other operates in constant extinction angle as described below.

The control system for the benchmark model has two main parts.

- Rectifier constant current (CC)
- Inverter constant current (CC) or inverter constant extinction angle (CEA)

Normally the operating point is the intersection of the rectifier CC and inverter CEA (point *A* figure 4-2-1), which results in the minimum reactive power demand [5], without an excessive risk of commutation failure. With the rectifier in the CC control mode and the inverter in the CEA mode, the terminal dc voltage is the intersection of the two characteristics as shown by point A (figure 4-2-1). At this operating point the firing angle to the rectifier is above that of the limiting value α_{min} (the minimum rectifier firing angle).

There, the rectifier current controller adjusts the voltage to keep the current constant at some point on the vertical line. During transients, e.g. line faults, there are excursions of voltage. During these transients the current is temporarily different from the set value. Note that the characteristic shown in figure 4-2-1 is the locus of the operating points during the steady state operation of the HVdc system, and does show any transient operating point.

There are four reasons for keeping the power factor high; two concerning the converter itself and the other two concerning the ac system to which it is connected. The first reason is to keep the rated power of the converters as high as possible for the given current and voltage ratings of valves and transformers. The second reason is to reduce the stresses on the valves and damping circuits. The third reason is to minimize the required current rating and the copper losses in the ac iines to the converter. The fourth reason is to minimize voltage drops at the ac terminals of the converter as the loading increases. The last two reasons apply to any large ac loads.

The power factor can be raised by adding shunt capacitors, and if this is done the disadvantages become the cost of the capacitors and switching them as the load on the converter varies.

The reactive power demand of the converters is a function of firing angle. The reactive power demand of the rectifier:

$$\cos\phi = \frac{1}{2}[\cos\alpha + \cos(\alpha + u)] \qquad \textit{(eq. 4-2-1)}$$

increases with converter firing angle (α) and similarly the reactive power demand of the inverter:

$$\cos\phi = \frac{1}{2}[\cos\gamma + \cos(\gamma + u)] \qquad \textit{(eq. 4-2-2)}$$

increases with converter extinction angle (γ). In order to get a reasonably high power factor, it is preferred to operate the inverter with minimum extinction angle (γ) and the rectifier with minimum firing angle (α).

In a rectifier, it is easy: we can make $\alpha=0°$, for which $\cos\alpha = 1$. (For practical reasons, α should be about 5°). In an inverter it is more difficult, and γ must be greater than zero by some margin. The extinction angle (γ) should not breach this limit for the reason that follows.

The reason lies in the fact that, after a valve (thyristor) turns off it should regain its blocking capability, prior to re-application of the forward voltage. We can not control γ directly but instead must control the ignition advance angle $\beta = \gamma + u$ in accordance with the value of overlap angle u.

A common malfunction of an inverter is a failure of commutation. *Commutation failure* is the phenomenon in which an off-going valve (thyristor) either does not completely extinguish, or re-ignites immediately on forward voltage. Commutation failure occurs when conditions in the ac or dc circuits outside of the bridge results in inadequate line voltage which is necessary for valve turn-off.

In order to ensure successful commutation during steady state operation, the ongoing valve should be fired when there is sufficient line voltage to successfully transfer current from one valve to another. This can be achieved by maintaining a minimum commutation margin, i.e. making sure that after a valve turns off, it does not see forward voltage until the end of the margin period. This period, expressed as an electrical angle, is called the extinction angle (γ) of the valve, and the above strategy ensures that its value be kept at a constant γ_{min} (typically 15°-18°). The controller that achieves this goal is called the constant extinction angle (CEA) controller.

Under rated conditions the rectifier is in CC and inverter is in CEA control mode. System changes such as ac side voltage reduction at the rectifier end pushes the CC controller to hit the minimum firing angle limit on the rectifier side ($\alpha = \alpha_{min}$), and the controller acts as the constant firing angle.

Simultaneously the inverter controller should switch from CEA to CC. In other words the current control function is taken over at the inverter end, with the rectifier operating on its uncontrolled characteristic at the minimum firing angle. The inverter is provided with a current controller, but for this station the current reference is reduced by the amount ΔI_d, the so called *current margin.*

In the effort to further improve the control system response some other details are also incorporated into the HVdc control scheme. Some of these modifications are of general nature and common among all the control schemes, and are summarized.

In order to prevent sudden changes in the operating point during system transients (as mentioned above), the crossover sharp knee (as shown dashed-dotted figure 4-2-1) is broken with a positive resistance slope from the γ_{min} characteristic to current control characteristic of the inverter (AB instead of AB^1B figure 4-2-1).

This droop characteristic is usually called *current error control* (CEC) as shown in figure 4-3-1. In fact as long as the CEC block is active and the operating point lies on the droop line AB, the inverter is under the CEA control mode with adjusted value for the reference γ.

At point A the γ reference is γ_{min}. As the point moves along line AB a linear offset is added to γ_{min} which is equal to $\Delta\gamma$ at point B. The actual mode cross over from CEA to CC and vice versa occurs at point B. This fact will further be used in §6.

A *voltage dependent current limit* (VDCL) is usually introduced in order to reduce the current order to approximately 0.33 p.u. at low dc voltages. This ensures that if the low voltage is caused by an inverter side commutation failure, the inverter valve that has failed to turn off does not continue to carry full load dc current and hence be subjected to thermal overload. The VDCL also has the additional bonus benefit of providing improved start-up and fault recovery characteristics.

The aforementioned operation modes, lend the following characteristic.

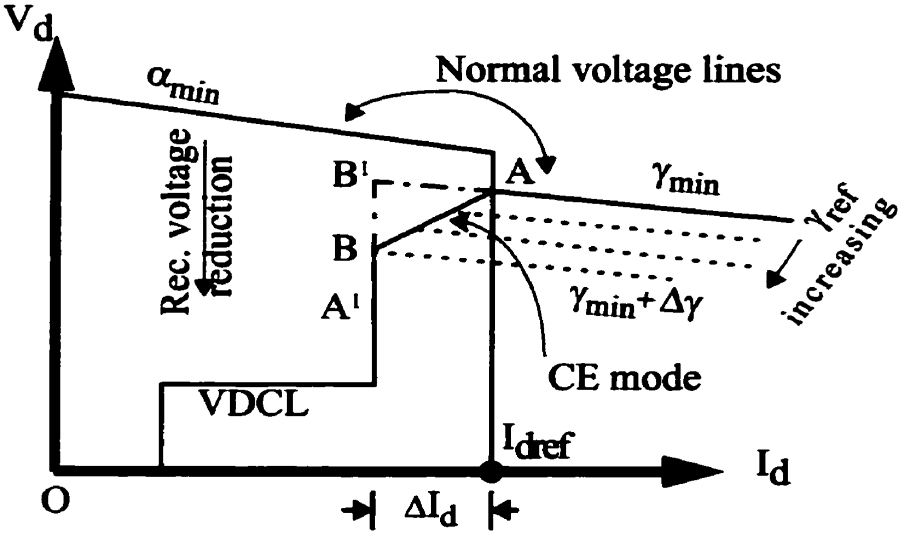

Figure 4-2-1 : HVDC Control Characteristic

4.3 HVDC Control Diagram

The basics of the HVdc control are briefly discussed in §4.2. In order to implement these basics to the CIGRE benchmark, the control diagram shown in figure 4-3-2 is used.

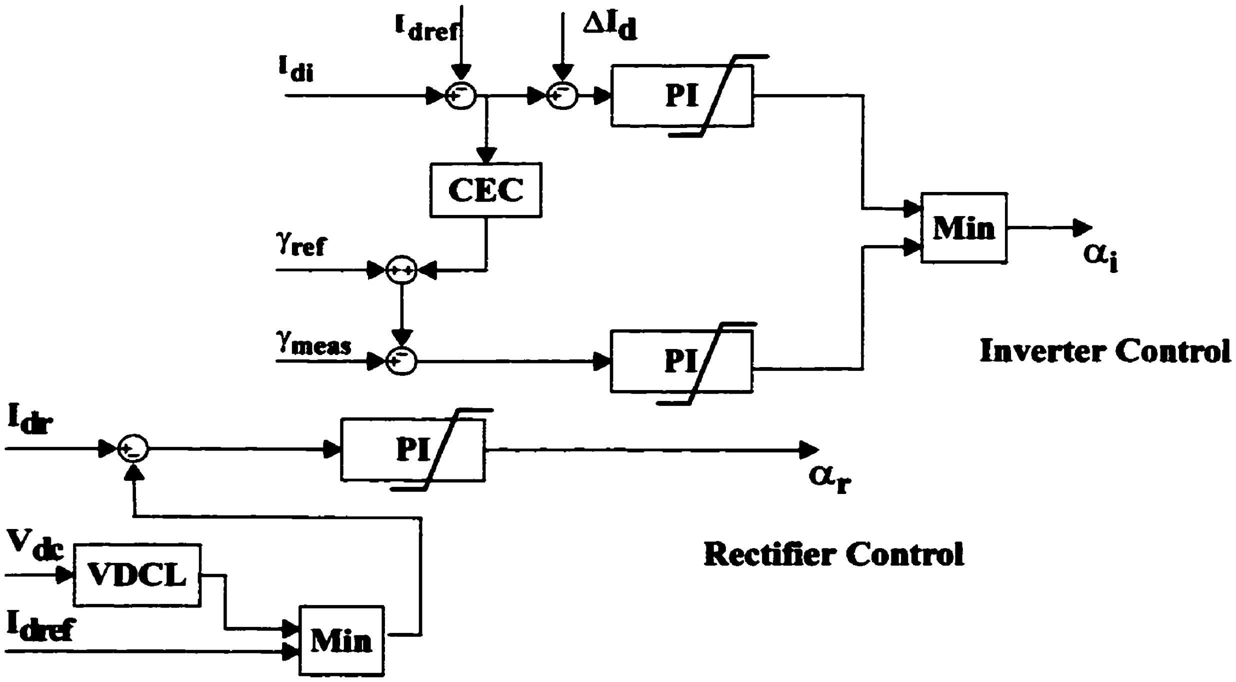

Figure 4-3-1 : Conventional Control Scheme

- Note: The limits of the P-I controllers as shown in figure 4-3-1, are shown in the P-I blocks only for the emphasis. However these limits are treated within the P-I algorithm used for simulation studies, and the P-I controllers used are non-wind-up.

Most the of parameters and terminology used in this diagram are discussed in §4.2. The inverter control circuit as shown in figure 4-3-2 is composed of two separate feedback loops. The top one is the current controller and the bottom one is the constant angle controller. The outputs of these two is fed into a minimum selector. The smallest of the two firing angles generated, is then selected as the inverter firing angle. Thus the minimum selector ensures that only CC or CEA is active. This minimum selector does the controller switch over from CEA to CC and vice verse. Besides when one of the controllers is selected, the other becomes saturated at its limit. This introduces unwanted delay or dead band when the control mode on the inverter side should be switched. In order to improve the inverter controller performance and speed up the mode switching this minimum selector provides also an auxiliary signal. This signal disables the controller which is not selected, thus prevents it from going into saturation and thus reducing the switch over dead band. This *select* signal is set to one whenever the CEA mode is chosen and zero when the inverter is in CC control mode, thus shows the inverter mode of control.

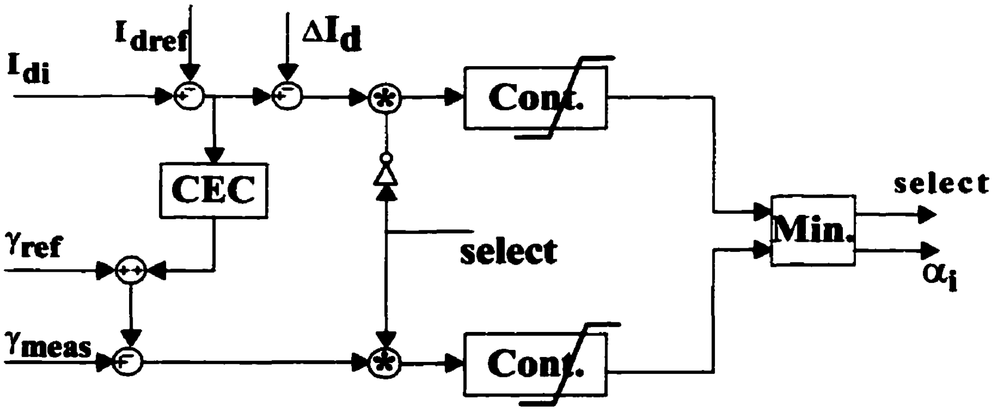

Figure 4-3-2 : De-selection method

Making the output of the de-selected controller follow the output of the selected one, a technique common to analog controllers (usually known as *follow-up*), can not be used here.

In the nominal condition, the lower path (CEA) is active thereby ensuring constancy of extinction angle at its nominal value of 15°. However, for a drop in the rectifier ac voltage, the CC path would become active. The current error (CE) mode of operation described earlier in §4.2 is implemented by modifying the extinction angle reference value with an offset which is proportional to the dc current. This block is shown as CEC in figure 4-3-2.

The rectifier control scheme is composed of a current control and a voltage dependent current limit (VDCL) block. VDCL produces a current order (say 1.5 p.u.), which under the normal operating dc (V_{dc}) voltage is more than the rated dc reference current (1 p.u.), thus the minimum operator in the rectifier control scheme chooses the actual dc current reference. However during low dc voltage this block issues a reduced current order (0.33 p.u.), and thus the reduced current order is fed to the controller. Later as the dc voltage builds up, the reduced current order is ramped up and finally the actual current reference is fed to the rectifier current controller.

The dc current reference (I_{dref}) is normally derived through a power control loop as is discussed in §4.4.

4.4 Power Flow Control

For controlling the dc power, the current reference in the current controller is derived from the ratio of the power order and the inverter side dc voltage, as shown in figure 4-4-1. The inverter side dc voltage can be estimated from the rectifier side voltage by subtracting the dc line voltage drop.

The rectifier substation as shown in figure 4-4-1, is provided with a power controller. The current reference is calculated by dividing measured dc power by measured dc voltage. The upper limit of the dc reference current is further adjusted by the measured dc voltage [30].

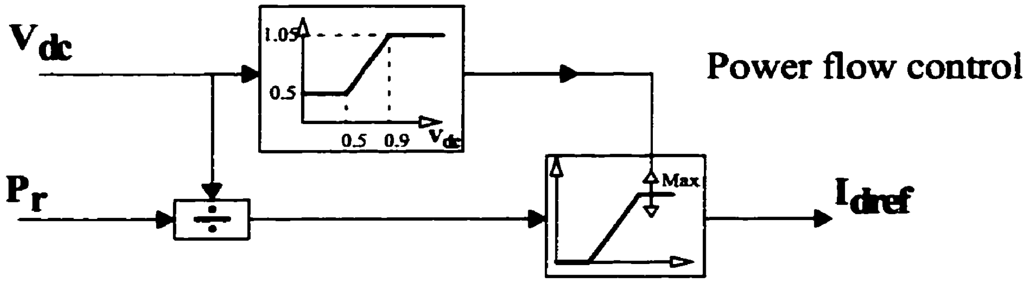

Figure 4-4-1 : Power flow control loop

The control system at the rectifier is similar, except that the dc current margin is not subtracted from the current reference (this ensures that the rectifier and inverter will not simultaneously attempt to control current).

Conventionally these controllers are P-I controllers with gains and limits set for optimal performance [67]. This control scheme is referred to as *the conventional method* all through this dissertation. Henceforth, the application of new modes and techniques to these control principles are investigated or evaluated.

5. ANN Control Studies

In this chapter the performance of the HVdc system using ANN controllers is investigated. The control diagram shown and described in §4.3, is used for the HVdc system under study. This control scheme is referred to as *conventional scheme* throughout this dissertation. In the conventional scheme the three controller blocks used as shown in figure 4-3-1, are proportional integral (P-I) type blocks. It has been verified by the studies and analyses conducted in §3, that an ANN based controller can be substituted and used instead of a P-I controller in control systems.

Using the same control basics as shown in §4, the three controllers shown in §4-3-1 are substituted with three ANN based on-line controllers.

It was shown in §3 that there are three important parameters associated with each ANN. The simulation results have shown that the best performance using ANN controllers is achieved by adjusting these parameters, discussed earlier in §2.3, as follows:

- $\alpha = 0.1$, learning momentum
- $\beta = 0.1$, activation function slope
- $\eta = 0.6$, learning rate

In order to fully evaluate the performance of the system, the following tests were conducted on the system to verify the controller behaviour.

- Current order reduction and restoration (20%)
- Rectifier ac side voltage reduction and restoration (20%)
- Rectifier ac side 3-phase fault and recovery
- Inverter ac side 3-phase fault and recovery
- Dc line fault and recovery

The objective of conducting the above tests is to investigate the behaviour of the ANN based controller in HVdc control scheme. It turns out that the ANN is not a suitable control scheme for multi-mode HVdc operation. The work presented in this chapter describes why this is so.

5.1 The Current Order Change

Normally in an HVdc system the inverter operates under the CEA mode. A current order change does not initiate any crossover from CEA to CC on the inverter side. Figure 5-1-1 shows the result for a 20% current order change on the CIGRE benchmark. The ANN controllers both on the rectifier and the inverter side perform properly, however they are slower in contrast with P-I based controllers.

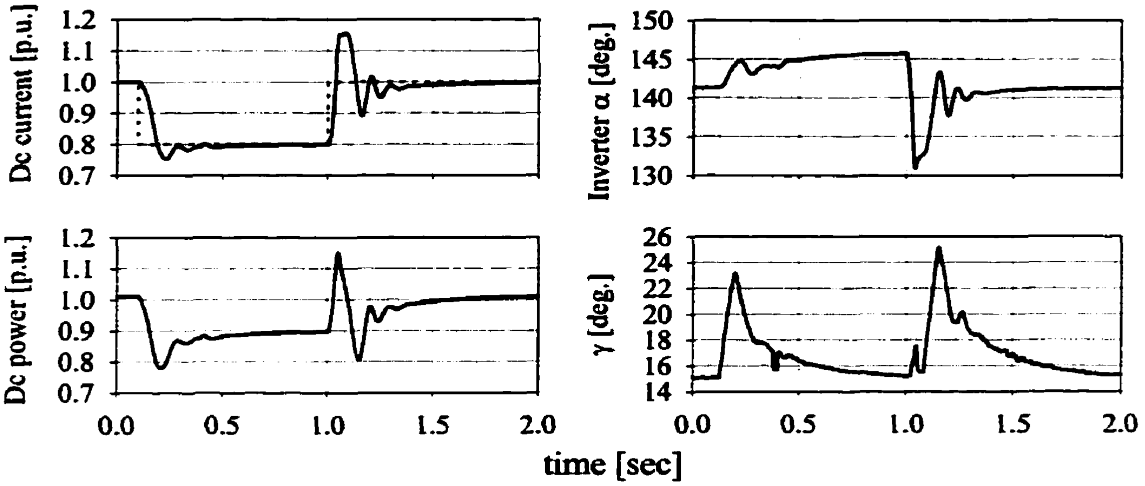

Figure 5-1-1 : Dc current change

The current order change as already mentioned above, does not initiate any control crossover on the inverter side. Thus, only the (CEA) controller is active on the inverter side during the transient while the other controller (CC) is fully de-selected. The response speed can further be improved by further adjustment to ANN activation functions' slope. However it turns out that, this can deteriorate the system responses as shown in the later tests.

5.2 The AC Voltage Reduction Test

Although an HVdc system normally works with CEA mode on the inverter side and CC on the rectifier side, the inverter sometimes assumes control of current with low rectifier voltage. The change of the operating mode is often referred to as control mode crossover. Thus any proposed control scheme such as an ANN scheme, should be tested for such a mode crossover. The example discussed earlier in §5.1 did not present a control mode crossover. Presented below is a case of rectifier side ac voltage reduction in which the lower ac voltage forces a control crossover from CEA to CC on the inverter side.

The voltage is initially reduced by 20% (figure 5-2-1) on all three phases. Following the voltage reduction, the rectifier firing angle hits the controller's lower limit and the inverter current controller, after some delay, switches to current control which adjusts the dc current to the reduced current reference ($I_{ref.}$-ΔI_d) equal to 0.9 p.u. It was observed, upon the ac voltage restoration the HVdc system undergoes a commutation failure.

As soon as the de-selected ANN controller, becomes selected again, it shows a very sluggish response. The controller behaves as if it starts to train for the first time, and the previous trainings are all forgotten. The ANN used to work fine prior to de-selection, but when it is re-selected, the ANN controller with the old parameters (weights of the ANN) does not generate a suitable output, and new training should be started, which needs more time. The ANN finally succeeds to restore the control and recover the system power to 1 p.u. dc current, which means the new training converges.

In addition, further tests and experiments which initiate control crossover on the inverter side, all ended up in the same system performance. It was concluded that control crossover on the inverter side deteriorates the system performance and results in a commutation failure. However following this commutation failure the ANN controller always succeeds to control the plant.

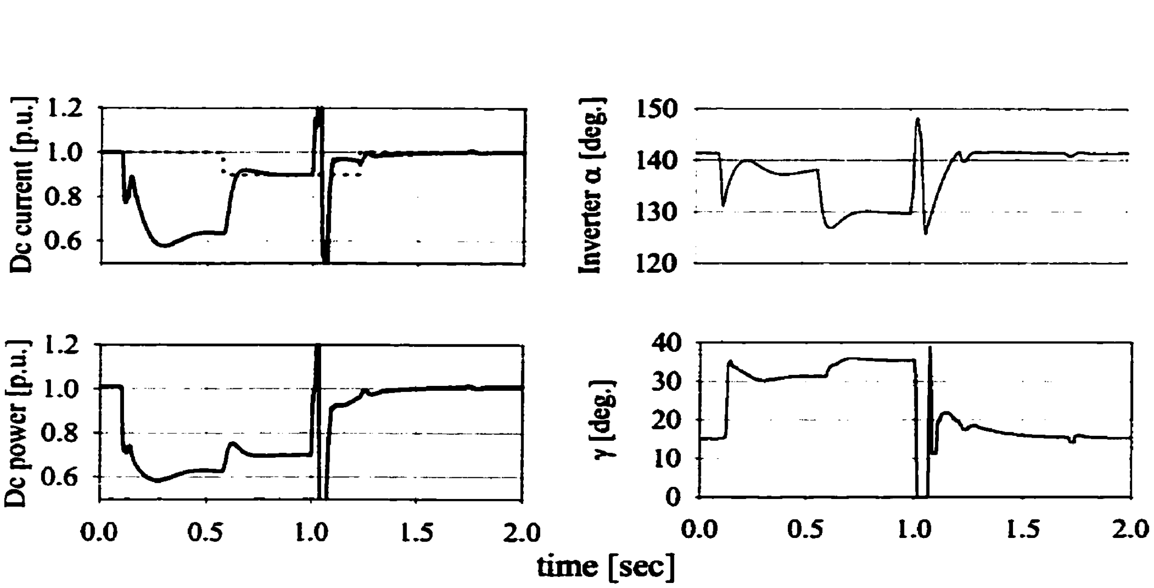

Figure 5-2-1 : Ac voltage change

Compared to the ANN, the conventional method using P-I controllers with gains and parameters given in [67], performs quite well subjected to all different tests without any commutation failure and restores the transmitted power very smoothly to one p.u.

5.3 Commentary on the Unsuitability of ANN Following Mode Crossover

The mentioned drawback of the ANN based control lies in the basic principle of the on-line training mechanism. As has already been explained, in this type of learning procedure, the ANN parameters (weights) are adjusted once every time step. Thus when the system experiences a transient, the weights of the ANN change in a direction to improve the ANN performance under this transient. When this transient finally dies out and the system reaches a new steady state operating point, the ANN parameters have been varied so many times, they hardly include any adjustments made at the instant the transient began. In other words the ANN forgets what it has learned, due to the abundant flow of information.

The P-I controller response to error change is predictable, and as long as its output lies between the output limits, one always expects to see the output changes in proportion to input changes. For the ANN controller the situation is not so straightforward. The behaviour of the ANN following the crossover is quite unexpected. Figure 5-2-1 shows that the CC controller on the inverter side does not seem to be fast enough following the voltage drop and restoration, while it shows reasonable speed elsewhere. With on-line learning, the ANN controller has to be re-trained for any new operating condition. As this takes time, the response immediately following the crossover is very poor, as the network has been trained for the pre-crossover mode.

It should be stated that we have not used any derivative information in the control algorithm. This is because an input-output rate of change for a converter is not continuous. For example, consider a simple 6-pulse rectifier as shown in figure 3-1-1, where the firing angle α is the sole input to the rectifier. Now if α is changed by an infinitesimal value equal to $\Delta\alpha$, the change in firing angle will not affect the rectifier prior to the next firing instant. This fact may also be formulated as an uncertain delay from *0* to $1/(6f)$ sec., where *f* is the ac voltage frequency (fundamental). There is no way to give a precise amount for this value, unless the instant of firing angle and firing angle change ($\Delta\alpha$) with respect to the ac voltage is known in advance. Henceforth, for a specific $\Delta\alpha$, the associated dc current change, ΔI_d, is zero from the moment that the α changes till the next the firing instant. Therefore the quantity $dI_d/d\alpha$, where I_d is the dc current, assumes zero value and then changes to some non-zero quantity, which is correlated to α changes made by the controller between firing instants. Thus, it is impossible to define a unique invertible mapping between α and the system response, as demanded by the back propagation algorithm.

Another aspect that makes the use of derivative information (Jacobian) in the control scheme difficult is that the equations which describe a converter are based on constant dc current. It should pointed that the fundamental HVdc equations shown in eq. 5-3-1 [62] only involves average and rms quantities, although invertible, is of no interest to us for defining a Jacobian.

$$V_d = 1.35 \cdot V_{do} \cdot \cos\alpha + \frac{3}{\pi} \cdot X_c \cdot I_d \qquad \text{(eq. 5-3-1)}$$

5.4 Composite Error Control

Another possible control method was proposed during the course of this thesis. This was to use *composite error*. The idea is to perform the minimum selection at the level of the control errors (γ and I_d errors) instead of doing the selection at the output of the two controllers (CEA and CC figure 4-3-2). Using this method, only one controller will be used on the inverter side and this removes the de-selection problem mentioned earlier. The method is briefly outlined in the following figure.

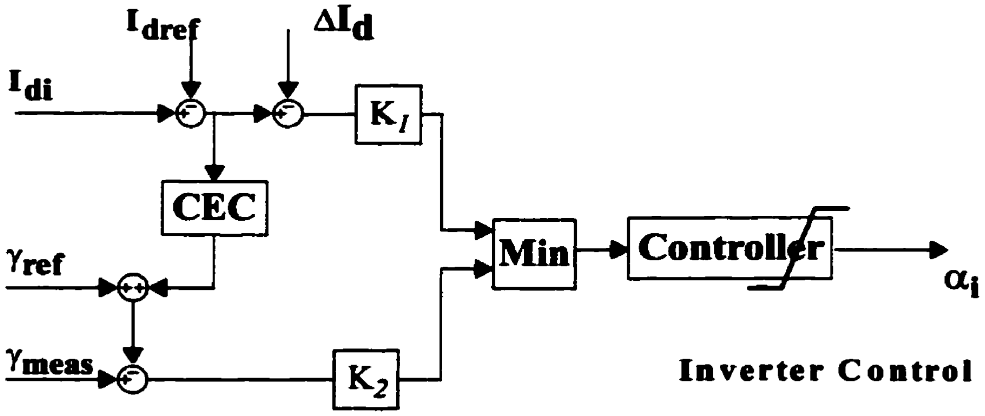

Figure 5-4-1 : Composite error control scheme

The composite error control scheme as shown in figure 5-4-1, includes only one controller instead of two, which can be either P-I for conventional method or ANN for this study.

Since only one controller is used, the two errors must be scaled with K_1 and K_2 as shown in figure 5-4-1 to make the controller parameters suitable for both options. For the purpose of argument, assume only a single gain K_C for the single controller. Let K_I and K_γ be the desired gains for the current and γ path respectively (these values could be obtained from simulation or other studies). In order for scaling to work, we must have $K_C*K_1=K_I$ and $K_C*K_2=K_\gamma$, from which the gains K_1 and K_2 can be calculated.

Using an ANN in the error composite scheme, the ac voltage test is carried out. The results do not show any improvement. Conducting the ac voltage test, following the voltage restoration the inverter experiences a commutation failure, as in the previous simulation. This further reiterates that the control mode crossover results in the ANN malfunction.

5.5 ANN Modifications

The performance of the ANN when only one controller is active at the inverter side is comparable to the P-I performance, and it is also possible to choose the ANN parameters in order to speed up the response time [57]. However the performance is quite unpredictable and sluggish when control mode crossover occurs at the inverter side.

The author tried other methods in order to improve the ANN performance. The ANN controller used so far has only one input. Therefore it may not get enough information from the system under control. A two level ANN with as many as 10 inputs, 10 hidden and one output neuron is developed using the back-propagation for the learning process. The inputs are chosen from the different system parameters and quantities both on the rectifier and inverter side.

In addition to this, the minimum selector used in figure 4-3-2 is equipped with a binary signal *(select)* in the output as shown in figure 5-5-1. This *select* signal is set to one whenever the CEA mode is chosen and zero when the inverter is in CC control mode, thus indicating the inverter mode of control. The appropriate form of this signal (*select*) is multiplied by the error used for the ANN such that the weight adjustment stops in the de-selected controller. Once a mode becomes selected, the other controller becomes deactivated.

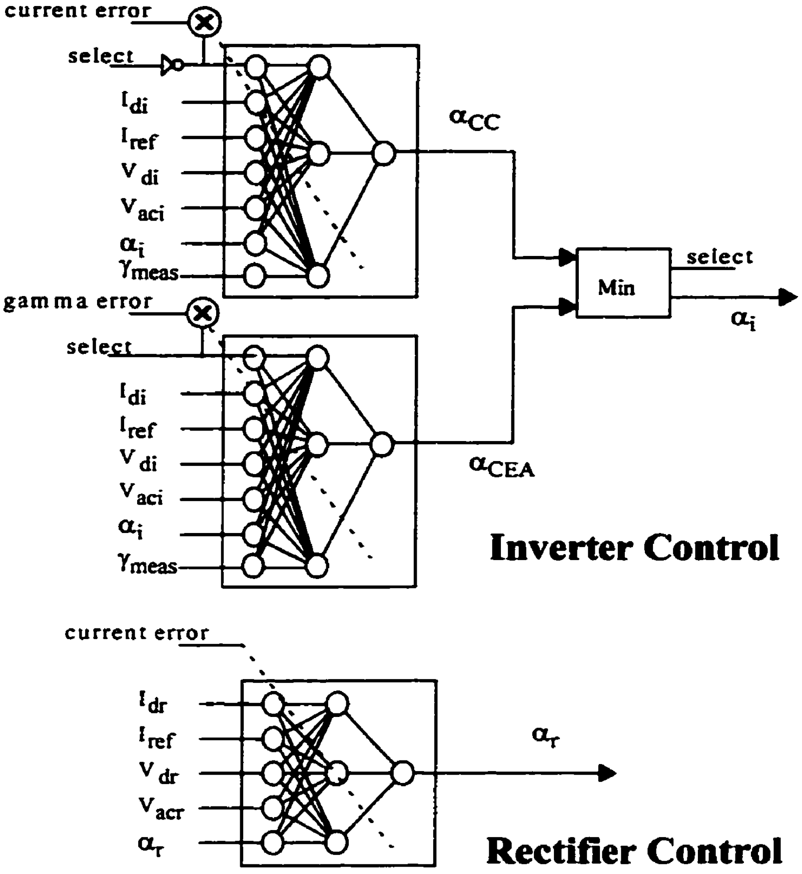

Figure 5-5-1 : Modified ANN control scheme

The rectifier current controller has five inputs which are: rectifier measured dc current (I_{dr}), dc current reference (I_{ref}), rectifier measured dc voltage (V_{dr}), rectifier measured ac bus voltage (V_{acr}) and the rectifier firing angle from (α_r) which will be the value of the firing angle from previous time step. The ANN weights for this ANN are adjusted by the current error (shown dotted). This ANN has ten hidden units.

The inverter CEA controller has seven inputs which are: *select* signal (*select*), inverter measured dc current (I_{di}), dc current reference (I_{ref}), inverter measured dc voltage

(V_{di}), inverter measured ac bus voltage (V_{aci}), inverter firing angle (α_i) and the measured extinction angle (γ_{meas}). The ANN weights for this ANN are adjusted by the gamma error (shown dotted). This ANN has ten hidden units.

On-line learning poses a special problem for the de-selected controller. If the control algorithm is allowed to keep operating, this de-selected controller moves to its extreme limit of operation. The output is thus no longer a function of its input and further training results in meaningless weights being set. Also making the output of the de-selected controller follow the output of the selected one, a technique common to analog controllers (usually known as *follow-up*), can not be used here, because if the training is allowed to continue, the de-selected controller erroneously *thinks* that its weight adjustments are actually affecting the output, thereby again resulting in incorrect training.

Freezing the weights during the de-selection mode is the only alternative, and this was used in the course of this work. This objective is carried out by the *select* signal (introduced earlier).

In order to improve this performance even further an iterative scheme was used. The on-line learning method described so far, has the shortcoming that the ANN does not learn long enough with the important patterns. Most of the time the system is under steady state condition, and therefore the patterns seen by the ANN are not a good example for training the network for transients. During the transients, such as fault recovery, the error and the system parameters contain important information about the system behaviour. But these patterns only exist during the transients, which are of short duration, and therefore the ANN may not train long enough with them and the weight adjustment may not be of satisfactory extent. Thus a simple mechanism in the learning algorithm is provided to carry out the back-propagation many times in each epoch[1], and learning iterates for a specific number of times, during each time step, instead of default only once (note: in on-line learning the weight adjustment is carried out only once in each time step). In each iteration, the weights are repeatedly adjusted using the same error and the same inputs from the system.

The modified ANN with *30* learning back-propagation iterations in each time step is modelled and used for simulation studies. The results for a 20% current reference change is shown as in the figure 5-5-2. This method shows faster response than the original ANN method. The activation functions used in this method have flatter characteristics compared to the original method discussed in §5.1. The overall performance compared to the original ANN [figure 5-1-1] is better but still far from desirable.

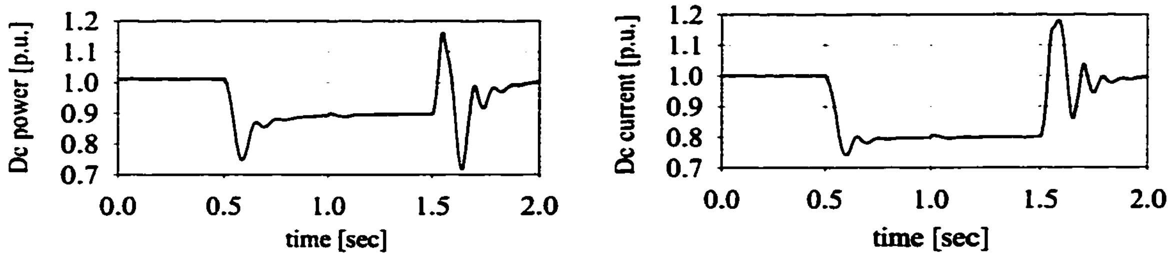

Figure 5-5-2 : Modified ANN current reference change

The control cross over on the inverter side still shows unacceptable results. Although the controllers do not get into saturation, the performance is still poor. As shown in figure 5-5-3, for 15% ac voltage change which initiates control mode crossover on the

[1] Training cycle

inverter side, upon the restoration of the ac voltage to one p.u., the inverter suffers from a commutation failure.

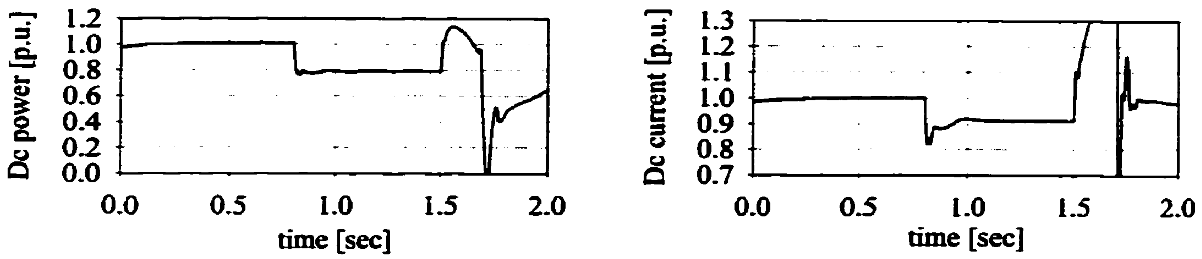

Figure 5-5-3 : Modified ANN ac voltage change

As was shown in §3.2, the ANN parameters play an important role in the speed of the ANN controller. Therefore the author tried by using a fuzzy logic based inference algorithm to vary the slope of the ANN activation function. The method will be described in the fuzzy logic section (§6.6) of the dissertation. Unfortunately, the performance of the ANN, particularly undesired delays, were not substantially improved.

The author believes that as long as the plant information is not incorporated into the learning process, the on-line training would not be a successful method. Besides by having the incessant learning process in an on-line training, the important features that ANN has learned during transients get forgotten. In addition, due to the intrinsic nature of the converter any adjustments made to the firing angle only effects the converter six times in each cycle, and any adjustments between them do not have any effect on converter performance. Thus the author believes that the provision must be made to carry out the learning six times in each cycle instead of once in each time step.

In the next section the author reports a novel fuzzy logic method for HVdc control.

6. The Fuzzy Logic Method

6.1 Basics

Fuzzy logic is a technique that allows for quantification and processing of common language rules to arrive at a decision. All the rules are considered at once or in *parallel* to arrive at a weighted decision [34,49]. In this chapter the basics of applying the fuzzy logic method to HVdc control [9] are discussed. Later the fuzzy logic modified ANN controllers are presented.

We demonstrate the application of fuzzy logic by demonstrating the conversion of the HVdc control system shown in figure 6-1-1, to the fuzzy control system shown in figure 6-1-2.

The plant in figure 6-1-1 consists of the inverter and the remaining ac/dc network. As the variables on which the control system acts are the dc current and the extinction angle, the plant appears to the controller as a one-input (α_i), two-output (I_{di}, γ_{meas}) system.

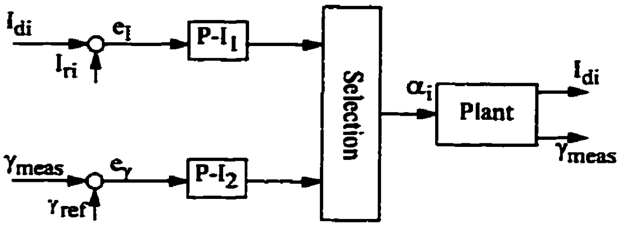

Figure 6-1-1 : General inverter control system

In the conventional method of figure 6-1-1, the plant is either under CC or CEA control mode and thus one of the two P-I controllers is selected. Note that each P-I controller has its own separate gains and error signal, and that the selection process is carried out at the *output* end of the two controllers. Thus at the transition from one control mode to another, the controlling error and the controller gains are abruptly interchanged. In the proposed fuzzy logic approach, we perform the selection procedure on the *input* side of the controllers by deriving a composite error as shown in figure 6-1-2. Two new coefficients μ_{CC} and μ_{CEA} are introduced that allow for a gradual transition in the selection process. This can be regarded as a generalization of the conventional process in figure 6-1-1, where exactly one of μ_{CC} or μ_{CEA} is one and the other zero (in CEA mode $\mu_{CC} = 0$, $\mu_{CEA} = 1$ and in CC mode $\mu_{CC} = 1$, $\mu_{CEA} = 0$). In the fuzzy logic approach these two coefficients are continuous numbers in the closed interval [0,1] and not necessarily complements. At the nominal operating point, however, the controller is in extinction angle control, with $\mu_{CC} = 0$, $\mu_{CEA} = 1$.

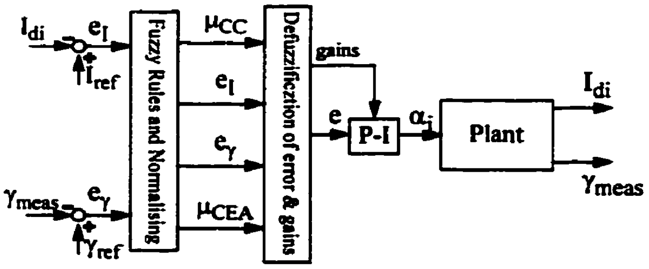

Figure 6-1-2 : Fuzzy logic control of SIMO systems

The two coefficients μ_{CEA} and μ_{CC} are derived from simple verbally stated control rules. For example whenever the measured extinction angle is smaller than its set value, the CEA mode of control should be selected in order to bring the extinction angle to its reference in order to provide sufficient commutation margin. The set of rules are explained next in §6.2. Using the fuzzy coefficients μ_{CEA} and μ_{CC}, the deriving error of the P-I controller (e in figure 6-1-2) is calculated as shown in figure 6-1-3.

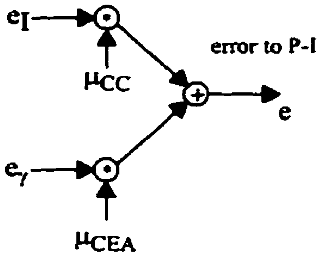

Figure 6-1-3 : Composite error derivation

In a similar fashion, the P-I controller gains and limits are also continuously adjusted through a weighting process (depending on the output errors, μ_{CEA} and μ_{CC}) and are continuously loaded into the P-I block as shown schematically in figure 6-1-2.

6.2 Fuzzy Logic Formulation

All the rules are based on two inputs, the current and the extinction angle measurements. The first step in fuzzy logic is to define the *fuzzy membership function* for the inputs. In deterministic logic, we assign a truth value of "*yes (1)*" or "*no (0)*" to the statement "*... the current is large*". In fuzzy logic, the answer can take on values between 0 and 1. At the extremities, where it is clear that the current is large (or small) we may assign a value of 1 (or 0).

Thus as in figure 6-2-1, a value of I_S=1 implies that the current is "*definitely smalI*" whereas I_S=0 means that the current is "*definitely not smalI*"; intermediate values between

0 and 1 implying something in between. Similarly I_L=1 implies that the current is "*definitely large*", and so on.

For the two inputs under consideration I_{di} and γ the following simple linear sets are used (Note: The overlap of the two sets is not necessarily 50%).

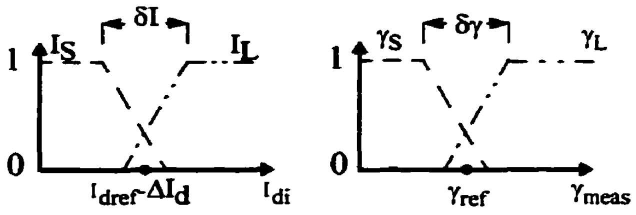

Figure 6-2-1 : Fuzzy membership functions

- Note: The definition of small or large current is defined with respect to the reference current, i.e. I_{di} is definitely small (I_S=1) if it is significantly less than the reference current. A similar argument applies for γ.

I_S and I_L are a measure of small and large dc current respectively. Using the membership values for I_{di} and γ, the following set of rules is used for control.

RULE I: IF I_S AND γ_S THEN μ_{CC}

RULE II: IF I_S AND γ_L THEN μ_{CC}

RULE III: IF I_L AND γ_S THEN μ_{CEA}

RULE IV: IF I_L AND γ_L THEN μ_{CC}

One rational behind the rule is that the extinction angle control is most important when there is a higher probability of commutation failure, i.e. at higher currents and smaller γ. If however the current is large and γ is large, then current control is still the preferred mode because the large γ indicates that commutation failure is not a problem. Similarly at the smaller current, commutation failure is not a problem and so current control is the preferred mode.

The rules are shorthand expressions for simple real-language statements which describe desired operating strategy. For example, rule IV states that *if the current is large and the extinction angle is large, current control should be used.* However, unlike deterministic logic, this rule does not assign a value of 0 or 1 to μ_{CC}, but rather just assigns a contribution. The contributions to μ_{CC} from rules I, II and IV are then used to determine its final value using some de-fuzzification method.

Shown below is the procedure for using the above rules in quantitative manner. For any typical measured I_{di} and γ_{meas}, the quantities I_L, I_S, γ_L and γ_S assume some values between 0 and 1. For example suppose that for some I_{di} and γ_{meas} we get I_S=0.3, I_L=0.6, γ_L=0.75 and γ_S=0.1. Using correlation-product inference [34] the above rules give the following:

RULE I: $\mu_{CC} = 0.3 * 0.75 = 0.225$

RULE II: $\mu_{CC} = 0.3 * 0.1 = 0.03$

RULE III: $\mu_{CEA} = 0.6 * 0.75 = 0.45$

RULE IV: $\mu_{CC} = 0.6 * 0.1 = 0.06$

The selected de-fuzzification method used to obtain a unique value for the fuzzy coefficients, is the *Maximum Membership De-fuzzification Method* [34]. In this method, we simply use the largest values generated by the rules, i.e., μ_{CEA}=0.45 and μ_{CC}=0.225.

Thus, instead of having a controlling error of e_γ or e_I as in the conventional method, we now have an error of $0.45 * e_\gamma + 0.225 * e_I$ at this operating point.

A similar approach is used to set the gains and the limits of the composite controller; with the same values of μ_{CEA} and μ_{CC} obtained above for this operating point. Thus, if the P-I controller proportional gains for the CC and CEA modes are respectively KP_{CC} and KP_{CEA}; then the value assigned to the composite gain is $KP = 0.45\ KP_{CEA} + 0.225 KP_{CC}$.

A compact form for visualizing the control rules I-IV is the *Fuzzy Associative Memory* (FAM) shown in figure 6-2-2.

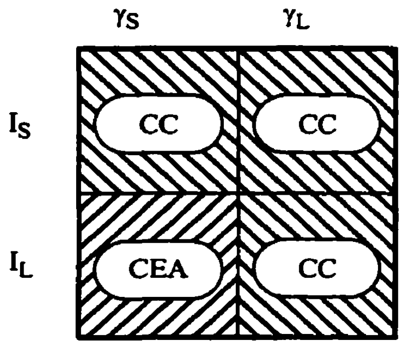

	γ_S	γ_L
I_S	CC	CC
I_L	CEA	CC

Figure 6-2-2 : FAM for the control strategy

The FAM shown above has the I_d-γ plane analogy as shown in figure 6-2-3. As shown by figure 6-2-3, in different areas of this plane, at least one specific control mode should be active. The control modes obey the same rule set explained earlier in §2.3. These rules render the two dimensional visualization as follows.

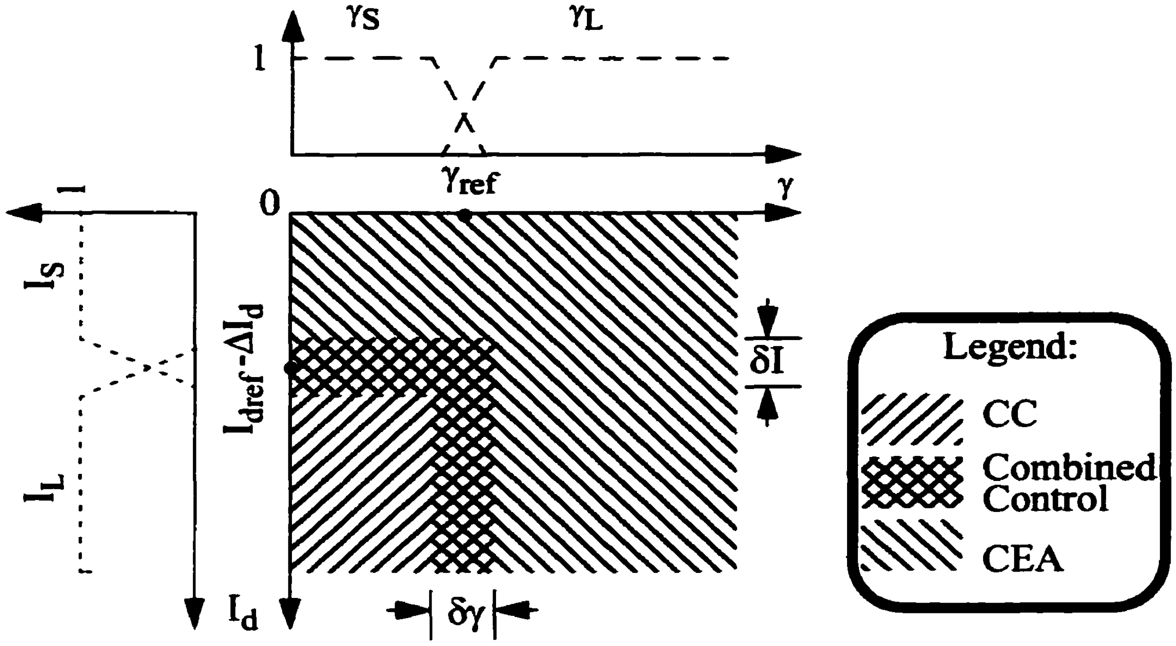

Figure 6-2-3 : Plane analogy of the FAM

On the left and the upper side of this figure the fuzzy membership functions for γ and I_d are also shown.

The μ_{CC} and μ_{CEA} participation factors are then used to evaluate the P-I gains and deriving error.

The two *participation factors* (μ_{CC} and μ_{CEA}) are calculated using the fuzzy inference method described previously. For any points on the Id-γ plane as shown in figure 6-2-3, the μ_{CC} and μ_{CEA} are driven. These factors are then used to get the P-I proportional gains. The proportional composite gain is derived as $KP = KP_{CEA}*\mu_{CEA} + KP_{CC}*\mu_{CC}$. The proportional gains for the two inverter control modes as given by [67] are: $KP_{CC}=0.62992$ and $KP_{CEA}=0.75055$, then the composite KP can be visualized as three dimensional surface as shown in the following figure.

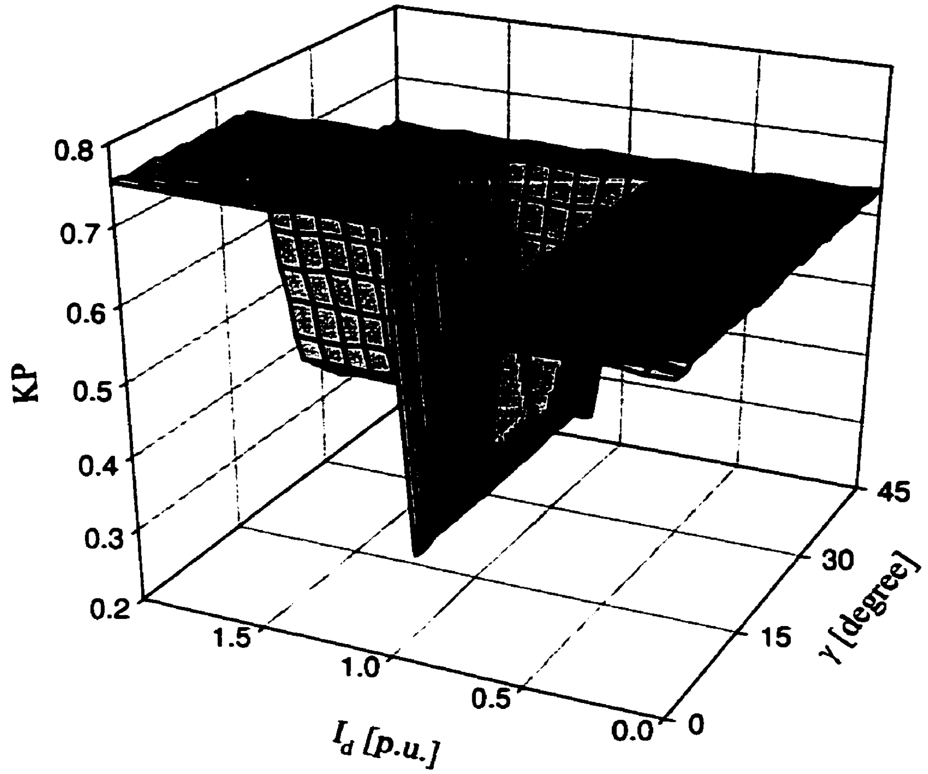

Figure 6-2-4 : Three dimensional plot of composite KP

The shape of the three dimensional plot for KP shows two plateaus which correspond to the CC and CEA modes respectively. In the transition, there appears to be a valley. However the shape of the function is strictly dependent on the selected overlap among the membership functions. The graph in figure 6-2-4 is for a 25% overlap. No such valley is seen for a 50% overlap; in which case the transition between the two plateaus is smooth. This figure depicts how the proportional gain *KP*, changes for different extinction angle and dc current quantities. The proportional gain as well as the other parameters are set according to the four simple control rules expressed earlier.

It is interesting to point that it is also possible to use even simpler set of rules for the same objective. For example, as the figure 6-2-3 justifies, the following three rules set express the same objectives as the initial four rules set. But with these three rules, instead of defining the universe of discourse as four quadrant using four rules, the three proposed rules defines the same universe of discourse by two strips and one quadrants. These rules are simpler than the initial rule set and the implementation would be more straightforward, although they both convey absolutely the same purpose.

RULE I: IF I_S THEN μ_{CC}

RULE II: IF γ_L THEN μ_{CC}

RULE III: IF I_L AND γ_S THEN μ_{CEA}

The simple four-rule FAM or the three-rule set, was used to describe and simulate the proposed fuzzy logic method. As will be shown in the §6.4, even a larger number of rules can also be used to further adjust and improve the HVDC control system.

6.3 Tests With Initial Rule-Set

Both the fuzzy logic and the conventional methods are simulated and the results are compared. The parameters and settings for the conventional controllers are taken from [67]. The thyristors' turn off time t_f is taken equal to 200 μs (4.3° at 60 Hz) and the thyristor model is forced to re-ignite if the extinction time is less than this value. The current characteristic (line AB in figure 4-2-1) is generated by adding an additional reference $\Delta\gamma$ to that of the CEA controller which is 16° at the point B in figure 4-2-1, where dc current is I_{dref}-ΔI_d.

The fuzzy parameters for membership functions (see figure 6-2-1) are selected as: $\delta I=0.1$, $\delta\gamma=10°$ and the overlap between the fuzzy sets is 25%.

During the preliminary studies it turned out that the system performance is quite satisfactory and the control system response is also comparable to the conventional scheme. Thus the two responses for the same test are reported for the sake of comparison.

The following tests were conducted for evaluating the new control method:

Fault tests:

- rectifier side ac faults
- inverter side ac faults
- dc line faults

Set-point changes:

- step changes to current order

Operating condition changes:

- rectifier ac voltage change

The performance of the fuzzy logic scheme is compared with the conventional method, and the results for different tests are reported. In all the following figures the solid line and the dotted line refer to the fuzzy logic and the conventional method respectively, unless otherwise captioned.

With the straightforward application of fuzzy control rules as shown in §6.2, the dc power recovery is not as good as the conventional method. The minimum extinction angle for the fuzzy logic scheme is larger than the conventional one, while the power recovery is poorer. Figure 6-3-1 shows the performance of the fuzzy logic method in contrast to conventional method for a rectifier ac side fault.

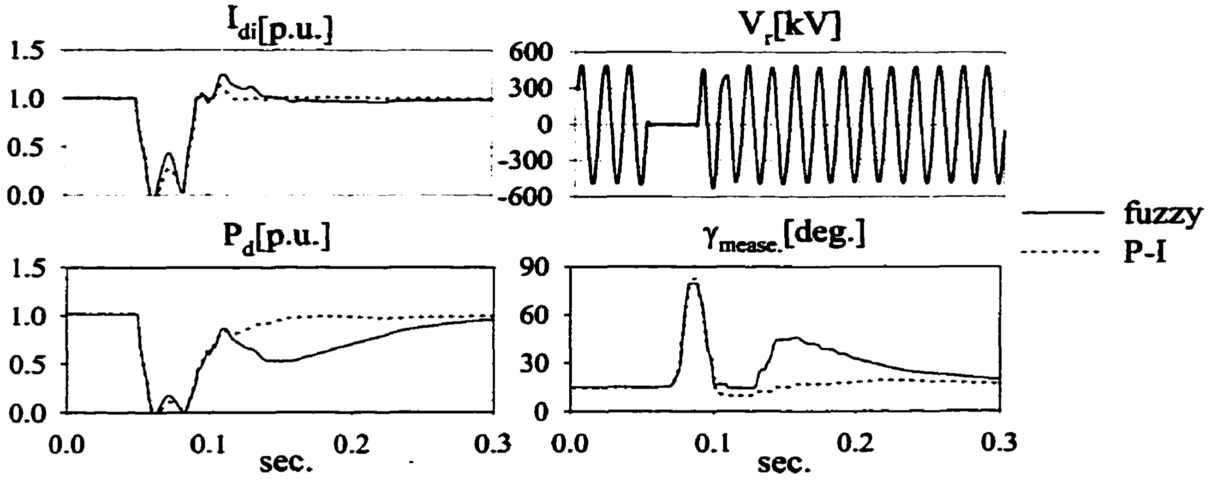

Figure 6-3-1 : Recovery from a 3-phase ac fault at rectifier

The other tests also show poor power recovery, and higher extinction angle. Since the control strategy is based on simple language rules, this drawback can be easily improved by incorporating new rules and using a more elaborate rule set. Thus additional rules are included to enhance the performance of the fuzzy logic control and improve the power recovery.

6.4 Enhanced Rule-Set

In order to speed up the dc power recovery, one additional piece of system information is included in the fuzzy reasoning. The rate of the change of the dc current ($DI = dI/dt$) is taken as this additional parameter, and the corresponding membership functions are shown in figure 6-4-1, where *SDI*, *MDI*, and *LDI* stand for small, medium and large dc current rate of change.

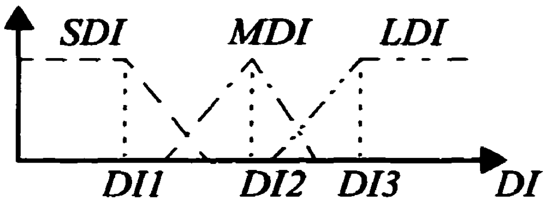

Figure 6-4-1 : Membership functions with additional parameter *DI*

From experiments, it turned out that if the rate of rise of dc current were too high then the dc power recovery would be poorer. It was observed that the rate of rise of current could be reduced by having a larger contribution towards current control from the inverter current controller. The earlier rule set, recommended current control via *Rules I, II* and *IV*. One additional rule is added in favour of the current control mode for large dI/dt values. Similarly instead of prescribing the CEA only for *Rule III* (in the previous rule set), we modify this rule, to also favour CEA for low $DI = dI/dt$.

Thus the new rule set will be as:

RULE I': IF I_S AND γ_S THEN μ_{CC}

RULE II': IF I_S AND γ_L THEN μ_{CC}

RULE III'*:** IF I_L AND γ_S ***AND SDI THEN μ_{CEA}

RULE IV': IF I_L AND γ_L THEN μ_{CC}

RULE V':IF LDI THEN μ_{CC}

The *Or* operation is carried out by a *maximum* function and the *And* is carried out by a *minimum* function. The two statements give the values for μ_{CC} and μ_{CEA} independently, based on the system information as measured dc current, rate of change of dc current and measured extinction angle.

The parameters for membership functions as shown in figure 6-4-1 are taken as, *DI1=5*, *DI2=20*, *DI3=50*, and the overlap of these sets is set to be 25%.

6.5 Simulation Results

•A Three phase rectifier fault:

As shown previously in figure 6-3-1, the power recovery from a three phase rectifier side ac fault, compared to the conventional scheme, is poorer. The results from the enhanced rule set are shown in figure 6-5-1. The power recovery is still marginally slower than with P-I option. The extinction angle γ always remains above 15° for the fuzzy approach, whereas with the P-I option, the system experiences a dangerously smaller commutation margin (7°) during the recovery. On the other hand, the smaller γ during the recovery means that the inverter side dc voltage builds up quicker which is why the recovery of the power is somewhat faster than the fuzzy option. Nevertheless the modified fuzzy rule set results in a much improved power recovery in comparison with original rule set (figure 6-3-1).

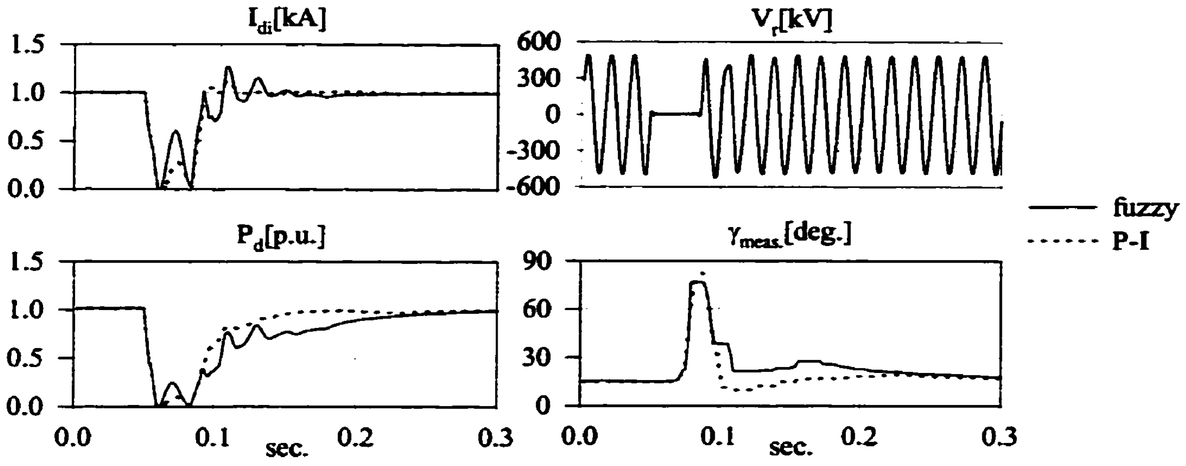

Figure 6-5-1 : Rectifier short circuit recovery

•B *Three phase inverter fault:*

Figure 6-5-2 shows the results of a two cycle ac fault on the inverter ac bus. As in the previous test the fuzzy controller results in marginally slower power recovery and a higher transient γ.

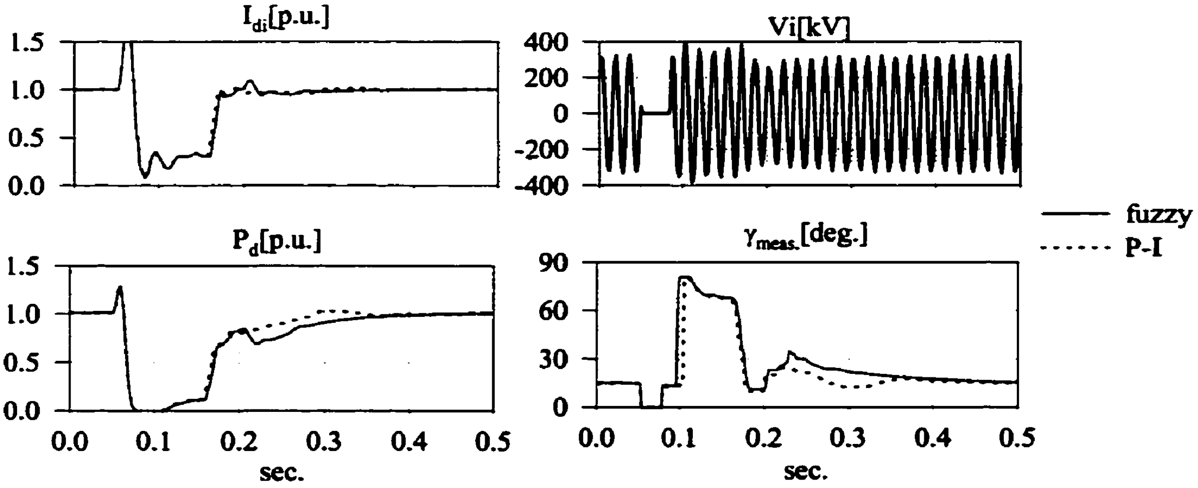

Figure 6-5-2 : Inverter short circuit recovery

•C *Dc line fault:*

A dc line fault is applied at 50 ms into the run (see figure 6-5-3). The fault is cleared by a force retard action of the rectifier in which the firing angle is increased into the inverter region (120°), kept there for 150 ms thereby de-energizing the fault, and then ramped back to the value set by the control loop. In this case, with the selected ramp rates, the conventional controller appears to suffer a commutation failure during recovery which the fuzzy controller does not.

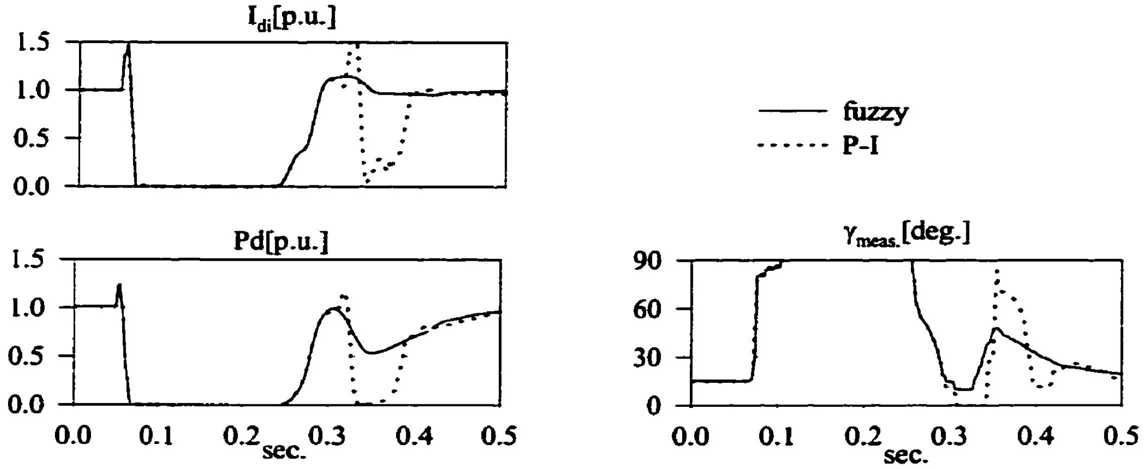

Figure 6-5-3 : DC line fault

•D *Current order change:*

The current order is changed from 1.0 p.u. to 0.8 p.u. and restored to 1.0 p.u. (20% change). During the test the rectifier side is under constant current control and the inverter side is under constant extinction angle control and no control crossover occurs. Throughout this transient the μ_{CEA} is entirely 1 except for very short instants and thus the two methods results in the approximately the same response as seen in figure 6-5-4.

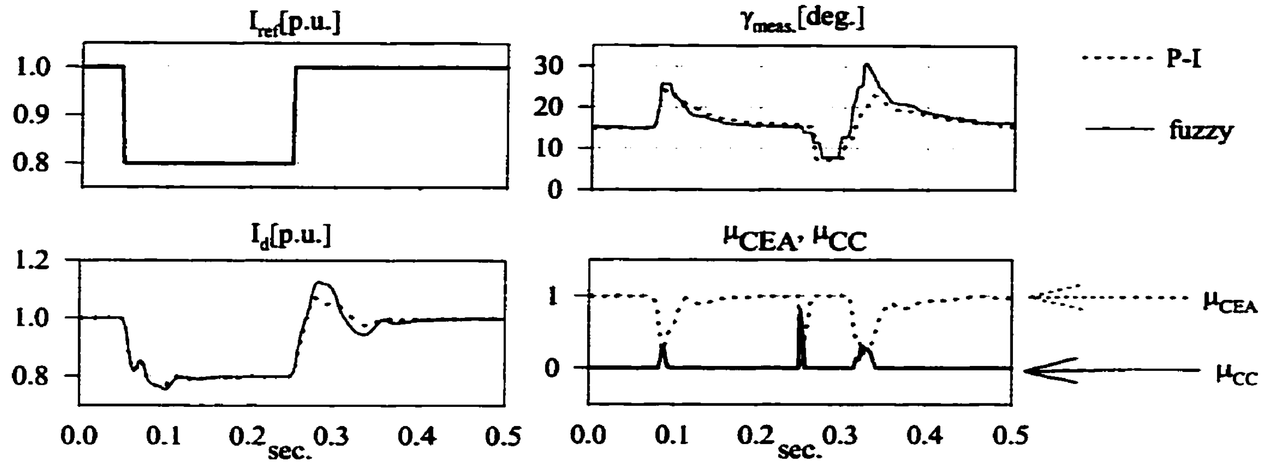

Figure 6-5-4 : Current order change

•*E* ***Rectifier AC voltage change:***

This test is carried out in order to investigate the control transition between CC and CEA. The ac voltage on the rectifier bus is reduced by 20% and then restored to its rated value. As previously pointed out, a rectifier side AC voltage reduction causes the crossover on the inverter side control from CEA to CC, and vice-versa during the voltage recovery. For 20% voltage reduction and restoration the results are shown in figure 6-5-5.

With the fuzzy option the response is better than with the P-I option, particularly on voltage restoration. During this transition, a commutation failure is experienced with the conventional approach. The fuzzy controller's tight regulation of the extinction angle γ allows for much better recovery. Also shown in figure 6-5-5 are the membership coefficients μ_{CEA} and μ_{CC} which give an idea of the participation of the CC and CEA control modes during the transient. Interestingly, during the voltage depression, the CEA controller is disabled as expected, but the CC controller is almost 65% active. This is analogous to having an adaptive gain in the CC controller which takes on smaller value during the disturbance.

Note that during the disturbance, the depressed voltage means that the inverter has to operate at a firing angle closer to 90°. Hence, the sensitivity of the dc voltage to small changes of firing angle is increased (note: $dV_d/d\alpha \approx -kV_{ac}\sin\alpha$). The reduced CC gain during this voltage depression compensates for the higher sensitivity.

The maximum voltage change limit that the conventional control scheme for the HVdc CIGRE benchmark may successfully tolerate without ending up in commutation failure is 15%, while the fuzzy logic method is able to handle 20% voltage change, where the minimum extinction angle following the ac voltage restoration is 12°. Considering the fact that the fuzzy method uses the same gains and limits as the P-I controllers in the conventional scheme, the fact that the composite fuzzy controller is adaptable becomes more pronounced. For example the fuzzy P-I controller has a proportional gain as pictured in figure 6-2-4.

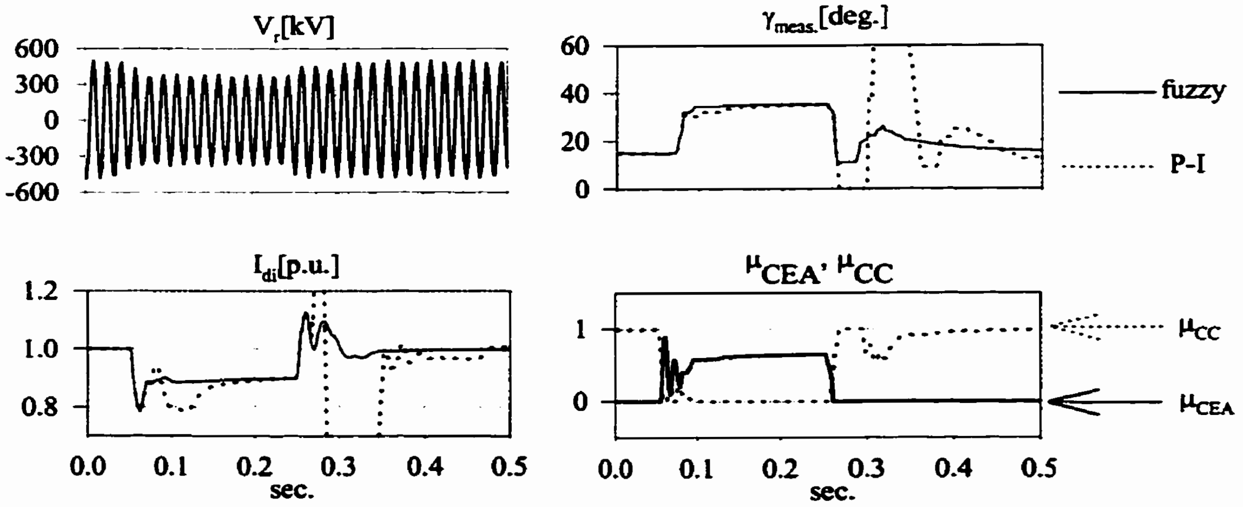

Figure 6-5-5 : 20% Voltage change

As is shown in the figure 6-5-5, the 20% voltage change results in commutation failure for the conventional method while with the fuzzy logic method the lowest γ is more than 10°.

6.6 Fuzzy Modification to the ANN Controller

The ANN based controller has been briefly discussed and analysed in §3.1, and the effect of ANN parameters such as learning rate (η), momentum (α) and activation function slope (β) are shown, and it has been shown how the controller speed varies with these parameters variation.

We expected that using the fuzzy logic control in a supervisory role [49] to change the ANN parameters (α,β,η) could improve the HVdc controller response significantly compared to the results presented in §5. However the results only showed a marginal improvement for the HVdc multi-mode control, although significant improvement was observed for single mode control. This section discusses the attempt made toward these improvements. Here a fuzzy controller is used to adjust the ANN parameters and the learning algorithm. The primary role of the fuzzy controller is to tune up the numerical algorithm by advising on the most relevant values of the learning parameters. The fuzzy controller produces a numerical factor based on the rule set inference, which will be multiplied to any of the ANN parameters. Therefore the ANN parameter(s) can be dynamically varied.

Consider the simple six-pulse rectifier as presented in §3.1. The learning parameter β directly effects the learning and simultaneously the response speed. The error (e) and the rate of change of the error ($de/dt = \dot{e}$) are taken as the fuzzy variables. In order to assign an order of granularity for e and $\dot{e}$, the discrete plot of error e versus the rate of change of the error $\dot{e}$ for some arbitrary run is plotted as follows.

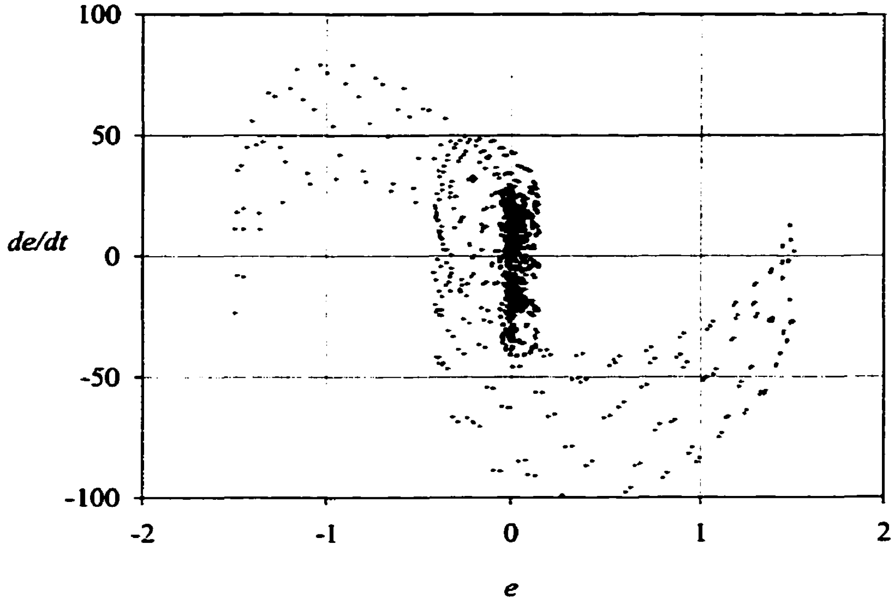

Figure 6-6-1 : Discrete plot of *e* and $\dot{e}$

The figure 6-6-1, shows the phase plane plot for the two fuzzy variables e and $\dot{e}$ (referred to in fuzzy terminology as the *universe of discourse* [49]). Considering the characteristics of the distinct points as well as the their density in different areas the following fuzzy membership functions are proposed in terms of values for e and $\dot{e}$.

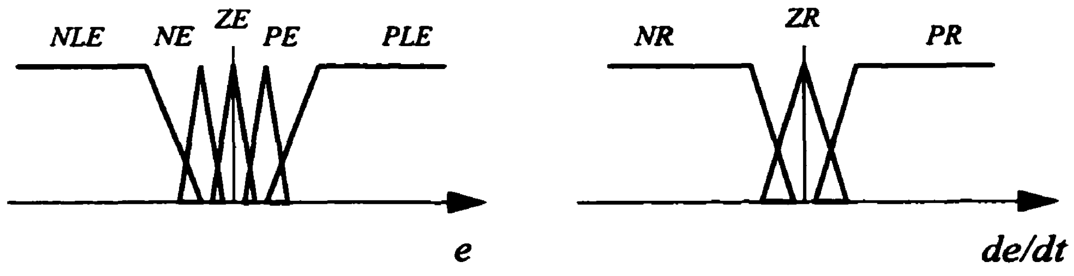

Figure 6-6-2 : Fuzzy membership functions

The fuzzy membership functions are implemented within the DRAFT module of PSCAD/EMTDC™ using the necessary developed blocks. The following figure shows the derivation of the e, $de/dt = \dot{e}$ and the corresponding fuzzy variables in the DRAFT palette.

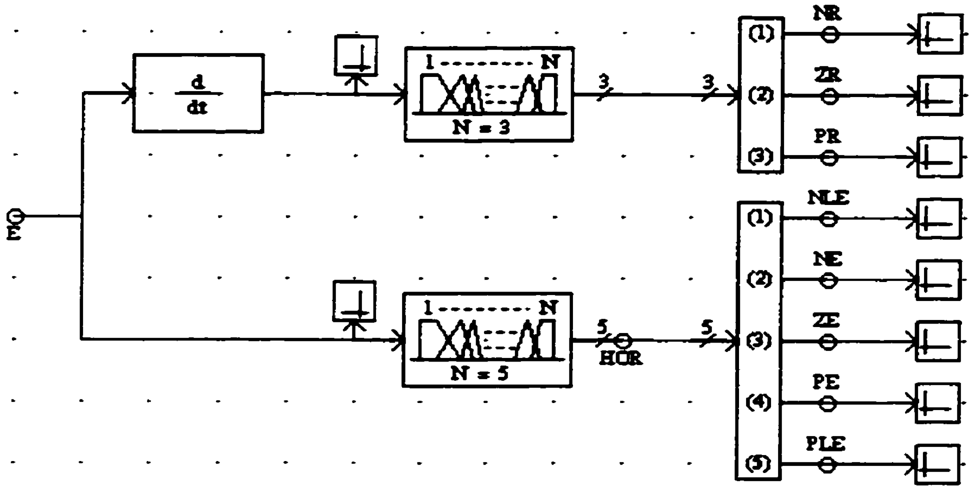

Figure 6-6-3 : Derivation of e and $\dot{e}$ in DRAFT

As previously indicated, increasing β, decreases the ANN response time and increases the control system speed, and it was shown that among all the ANN parameters the response has the highest sensitivity to β.

The error to the ANN controller, which is used to adjust the controller parameters, is also a measure of controller performance. In other words, large error means that the controller has not achieved its goal, thus faster control measures (larger β) are required. On the other hand, a small error means the controller is achieving its goal, therefore the controller may slow down in order to avoid oscillations.

The comments quoted in the above paragraph, yield themselves easily to fuzzy logic formulation. The method closely resembles the one discussed by Rueda and Pedrycz

[53]. We next move forward to specify the fuzzy rules or the bank of the *fuzzy associative memory* (FAM). The rules are based on the two quantity e and $\dot{e}$, and produce a factor that will further be utilized to tune the ANN parameters.

The following FAM is used as the fuzzy inference rule set.

		e				
		NLE	NE	ZE	PE	PLE
	NR	LA	ME	NC	NC	NC
$\frac{de}{dt}$	ZR	ME	NC	NC	NC	ME
	PR	NC	NC	NC	ME	LA

Figure 6-6-4 : FAM bank of the modified ANN

The fuzzy variables *LA*, *ME* and *NC* are respectfully stand for *Large*, *Medium* and *No-Change*. The fuzzy outputs are then a large or a medium numerical value based on the type of the ANN parameter, and is one for the no-change case. Therefore each of the 15 cells used for this analysis individually generates 15 coefficients such as:

$$IF\ e=NLE\ And\ \dot{e}=NR\ Then\ output=LA \qquad (eq.\ 6\text{-}6\text{-}1)$$

which should later be de-fuzzified and the final fuzzy inference output will be a single quantity. Multiplying this final derived quantity by the activation function slope (β) as shown in figure 6-6-5 introduces an activation function slope change in the range of 1-5 times the nominal value. This factor continuously increases the slope (β) of the ANN activation functions as the measured signal tends to deviate from the reference value, and as the measured signal approaches the reference value, continuously decreases and finally becomes one. The method is briefly shown in figure 6-6-5.

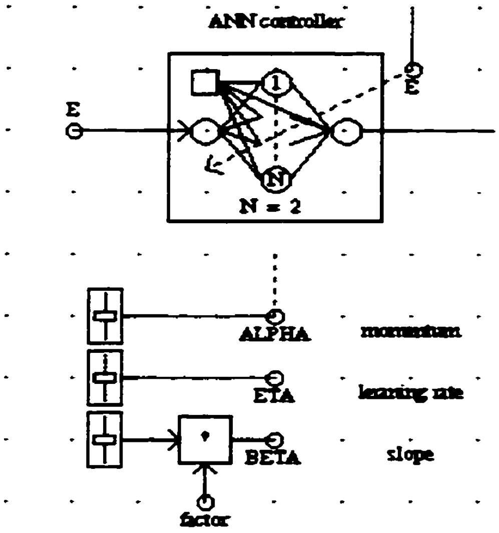

Figure 6-6-5 : Activation function slope change

The modified ANN response is faster and has smaller overshoot compared to the original ANN response (figure 3-1-6).

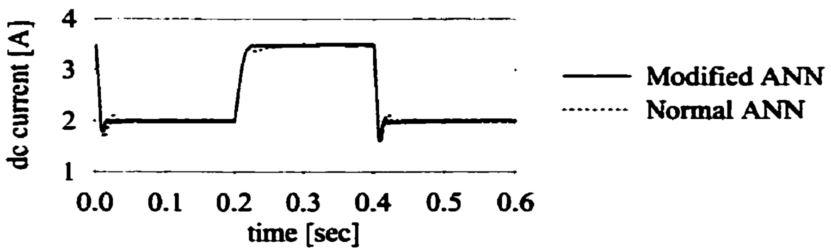

Figure 6-6-6 : Modified ANN response

The above figure shows that the modified ANN is both faster and the has lower overshoot compared to the initial ANN response. It is therefore deduced that for single mode control, say CC or CEA the modified ANN gives the necessary speed as well as the minimal response overshoot.

However in an HVdc system the control mode crossover is of particular interest and any proposed controller should be subjected to it. In order to apply this method to the HVdc ANN based control scheme three separate fuzzy inference algorithm should be implemented for the three controllers in the HVdc control scheme (§4.2).

Applying the same procedure as discussed for the simple six-pulse converter in this chapter to the three HVdc controllers, the modified control scheme is subjected to different tests and faults as cited in §6.4. The modified ANN approach still suffers from the a commutation failure following the control mode crossover on the inverter side. The result for the 20% current order change is depicted in the figure 6-6-7.

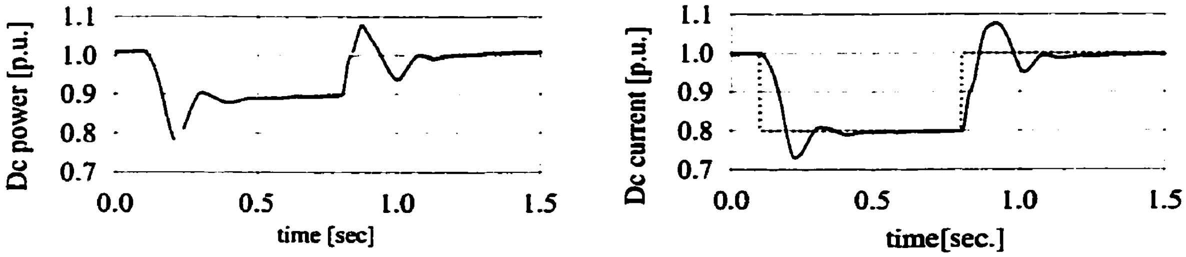

Figure 6-6-7 : 20% DC current change

The above procedure was an attempt to improve the response of the ANN controller described in §3. However, the results show that although in comparison to figure 5-5-2, the response for the restoration of dc current has improved, it is still far from desired. This shows that, for the reasons discussed in §5.3 the ANN controller still behaves poorly following mode crossover.

6.7 Conclusions and Recommendations

The fuzzy logic method allows for the incorporation of simple rules into a control system. The rules are first stated in simple language and then are quantified for inclusion into the control system by using the fuzzy reasoning approach. If the performance is does not meet some requirements, additional parameters and rules can be added.

In the fuzzy logic approach, the basic control unit is still the P-I controller, but its gain and time constant are adjusted by fuzzy reasoning. The limiting values of the gains and the time constants are the same as the conventional system, so as to ensure similar small signal behaviour when it is clear in which control mode the controller should be operating.

Converting the P-I controller based control system for an HVdc scheme to one based on fuzzy logic results in improved immunity to commutation failure during recovery from dc faults and ac voltage dips. Although initial implementation showed poor recovery of dc power following ac side fault, the inclusion of additional parameters and rules improved the power recovery remarkably.

The area of stability analysis of the fuzzy control is still under investigation. There have been some papers [49] that address this issue, but are applicable when the plant is of a small order. Also, the approach of this thesis involves fuzzy supervisory control applied to a P-I controller. The mathematics for this are yet not developed. Thus for the kind of problem being considered here, digital simulation seems to be the only viable approach. Although not reported in the text, the controllers were robust and operated well with different system configurations.

The most important merit of the fuzzy logic approach is higher extinction angle. Since the extinction angle γ for the fuzzy logic method is greater than when the conventional method is used, the ordered γ can be made smaller. This means lower reactive power consumption on the inverter side.

It is shown that more elaborated rules and information can be incorporated in decision making in order to achieve different goals. More extensive rules which incorporate some protective measures or modulation to damp out the sub-synchronous oscillations of other machines in the system can be incorporated in the formulation of the rules, and will be discussed in §7.

7. High Level Control Studies

So far, the application of new techniques were solely considered for the level HVdc control loops such as current and extinction angle control loops. The advantages and disadvantages of applying such techniques to low level control were fully described and analysed in §6. In this section fuzzy logic techniques are applied to higher level control functions.

Other authors have used such techniques for ac and dc systems such as, damping of the tie line oscillations [63], power swing damping [11], gain scheduling [12] and tuning of DC link controllers [13]. The ANN technique has also been applied to HVdc systems for fault identification and detection [36,58].

In this section the applications of the fuzzy logic method to two high level control problems are presented. This includes, damping of the two synchronous machines connected to the converter ac side, and as well as the damping of SSR (sub-synchronous resonance) oscillations.

7.1 Mechanical Damping

The CIGRE benchmark is composed of two ac sources, one at the inverter and one at the rectifier side. Each of these ac sources, is assumed to be the *Thevenin* equivalent of a real source. However in actuality a machine (generator or synchronous condenser) is a part of the ac source at a converter station. The mechanical and the electrical parts of the machine constitute a dynamical system which may develop oscillations under faults or system changes [69]. These include the so called the SSR oscillation. The CIGRE benchmark model is modified to reflect this situation by replacing the rectifier ac source with a synchronous machine driven by a multi-mass steam turbine model. The steam turbine complex is composed of one high, one intermediate and two low pressure turbines. The synchronous machine is equipped with an static exciter which varies the dc field such that the terminal ac voltage remains constant [28]. The parameters such as shaft constants, mutual damping and inertia constant for the multi mass turbine are obtained from the IEEE SSR benchmark [29] and scaled to fit the MW ratings of the dc scheme. The complete data for this study are given in the §B.1. The HVdc system with the rectifier side generator and the equivalent six mass mechanical system are shown in 7-1-1.

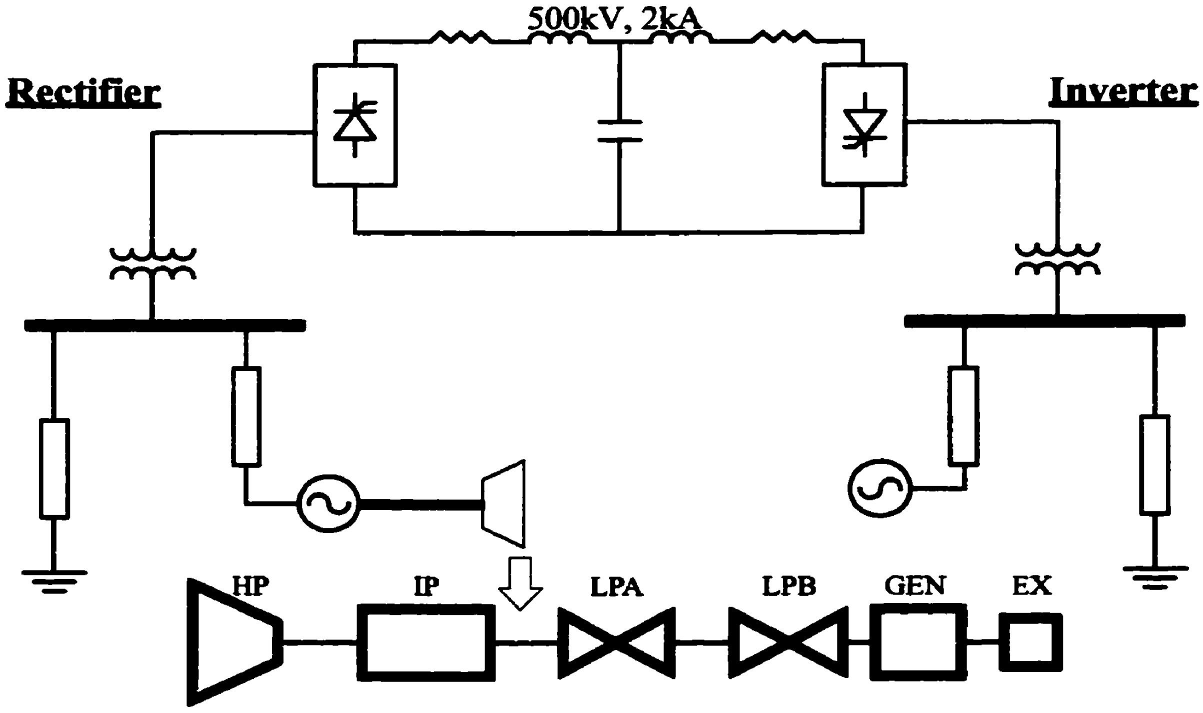

Figure 7-1-1 : HVDC system and the six-mass spring model

Starting from steady state a system perturbation initiates and builds up oscillations at SSR frequencies in the mechanical multi-mass system, in which the different turbine sections oscillate with respect to one another. These oscillations apply severe stress on the shaft between the two masses and leads to failure or loss of life expectancy.

Studies conducted using the transient program verified that a dc line fault and recovery generates a sufficient perturbation and would cause oscillations to build up in the system. Therefore a dc line fault and recovery test is conducted on the HVdc model. The results for the multi-mass system are shown in the figure 7-1-2.

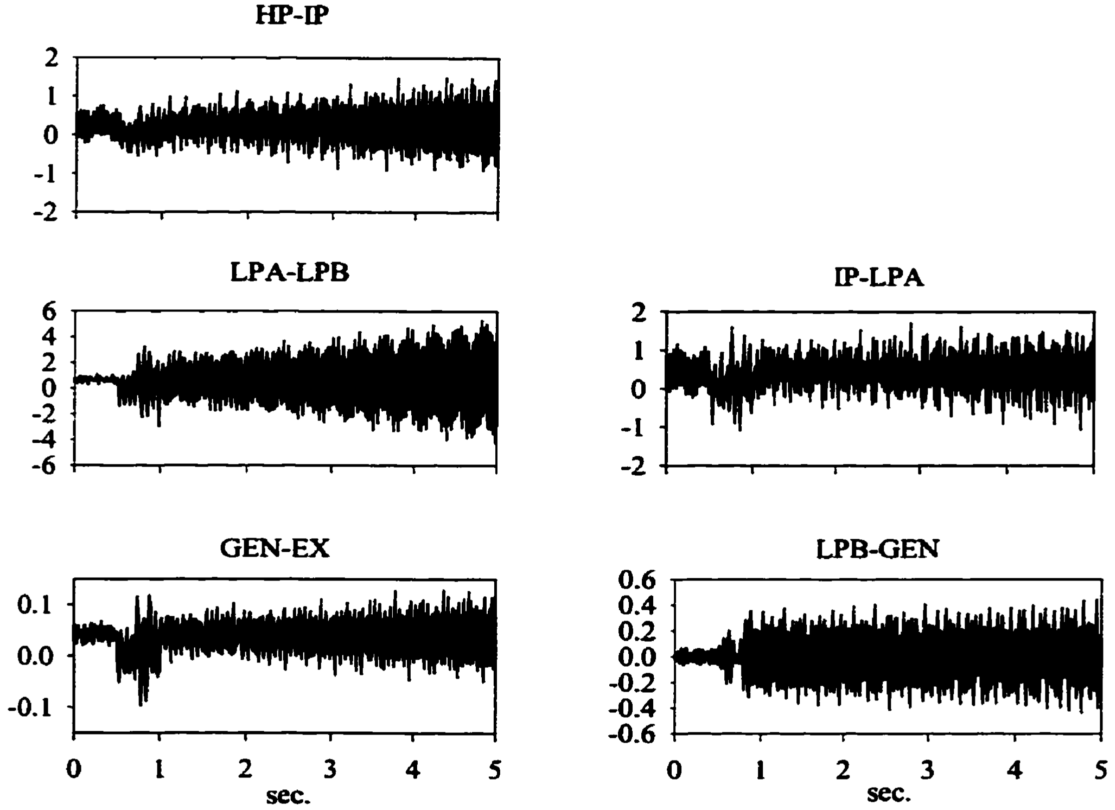

Figure 7-1-2 : Torsional oscillations

The results show that the amplitude of the oscillations tends to grow; the oscillation amplitude between LPA and LPB turbines being particularly severe. These oscillations result in the fatigue of the steel shaft and decreases the shaft life expectancy.

HVdc systems are very fast acting systems, and it is possible to control such systems six times (for six-pulse bridges) or 12 times during each period of ac waveform. Such a possibility lends itself easily to be used for system control both in low and high level modes.

A particularly serious possibility for sub-synchronous resonance arises when there is a single large synchronous generator connected in the vicinity of an HVdc rectifier station [15]. The fuzzy logic method used to damp out these oscillation is briefly outlined in figure 7-1-3. The controller input is the synchronous machine angular velocity (ω), and the output is the Δα, which is added as an auxiliary signal to the α order derived from the rectifier control scheme, as shown in figure 4-3-1.

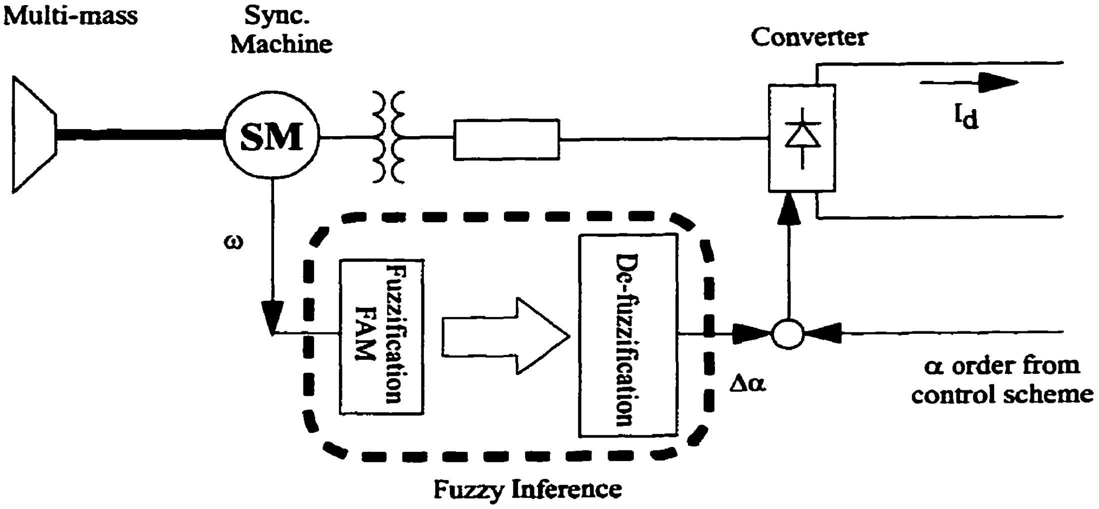

Figure 7-1-3 : Fuzzy logic oscillation damping

In order to develop a fuzzy inference scheme to mitigate the oscillation magnitude, the angular velocity of the synchronous machine (ω) is chosen as the control signal. This signal is readily measurable either on the electrical or mechanical side. The machine angular velocity ω and its rate of change *dω/dt* are the only two inputs to the fuzzy damping system. The fuzzy membership functions for the ω and the *dω/dt* are depicted in figure 7-1-4.

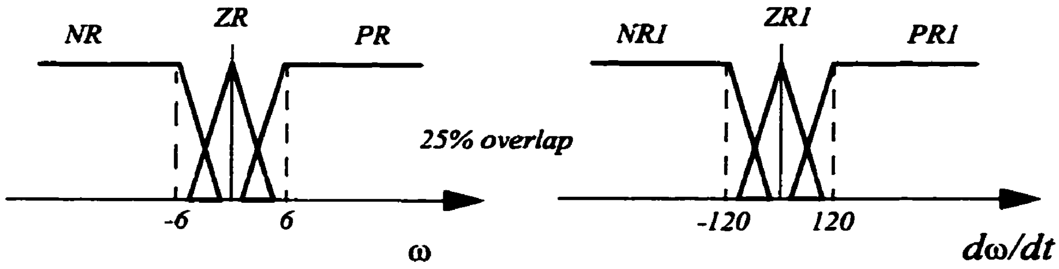

Figure 7-1-4 : Fuzzy membership functions

The fuzzy inference scheme generates an additional modulation in the firing angle via the signal Δα. The inference operation norms required in the fuzzy algorithm, such as AND and OR are chosen to be minimum and maximum respectively [49], and the fuzzy centroid de-fuzzification scheme is used. Using the correlation-product inference [34], the de-fuzzification process is significantly facilitated, and the output centroids are only used in the de-fuzzification procedure.

The fuzzy associative memory [34] (FAM) for this case, is composed of five rules and is shown in figure 7-1-5.

			ω	
		NR	ZR	PR
$\frac{d\omega}{dt}$	NR1	NL		
	ZR1	NM	ZE	PM
	PR1			PL

Figure 7-1-5 : FAM bank for oscillation damping

The parameters *NL*, *NM*, *ZE*, *PM* and *PL* used in this FAM stand for *Negative Large*, *Negative Medium*, *Zero*, *Positive Medium* and *Positive Large* respectively. Each of these fuzzy values refer to a fuzzy membership function, but as already explained previously, only their centriods participate in the de-fuzzification procedure. Thus each can be represented by numerical values of the area and the centroid of the FAM rule's consequence. The numerical values for each one is assumed to be $NL = -4$, $NM = -1$, $ZE = 0$, $PM = 1$ and $PL = 4$.

The fuzzy logic scheme output is then used to modulate the firing angle order to the rectifier converter.

The fuzzy logic inference scheme as shown in figure 7-1-3, modulates the rectifier firing angle. This control scheme results in a substantial reduction in the SSR oscillation following a dc line fault. The results of the proposed system following a dc line fault and recovery are shown in figure 7-1-6, and should be compared with the case without SSR damping (figure 7-1-2).

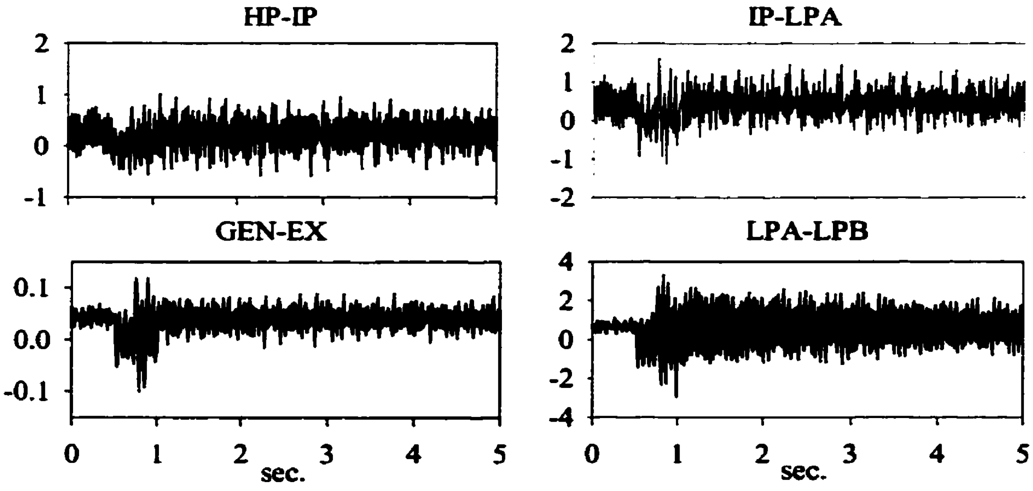

Figure 7-1-6 : Torsional oscillations damping

The following figure 7-1-7, shows the modulated firing angle as superimposed on the rectifier firing angle.

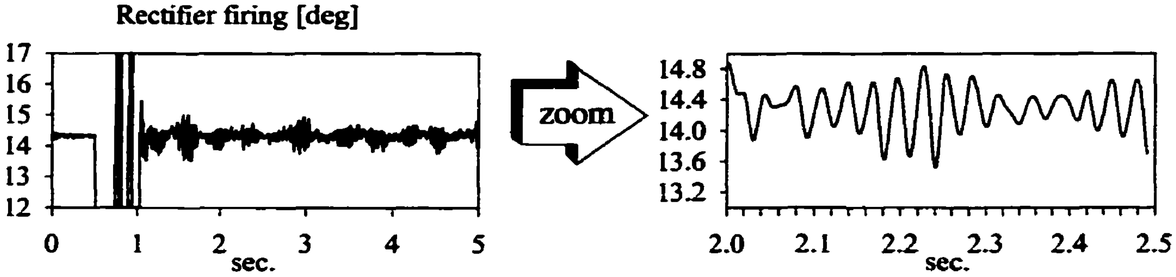

Figure 7-1-7 : Rectifier firing angle

As shown small modulation of the rectifier angle (which has an approximate magnitude of about 1° peak-peak) successfully stabilizes the oscillations, especially the LPA-LPB oscillation as is seen by comparing the figure 7-1-2 with figure 7-1-6. Since the firing angle modulation is of small magnitude, it does not contribute to non-characteristics harmonics generation.

The delivered dc power for the two cases shown is in figure 7-1-8. This figure shows that the fuzzy controller reduces the power oscillations in the dc line significantly compared to the case without the controller.

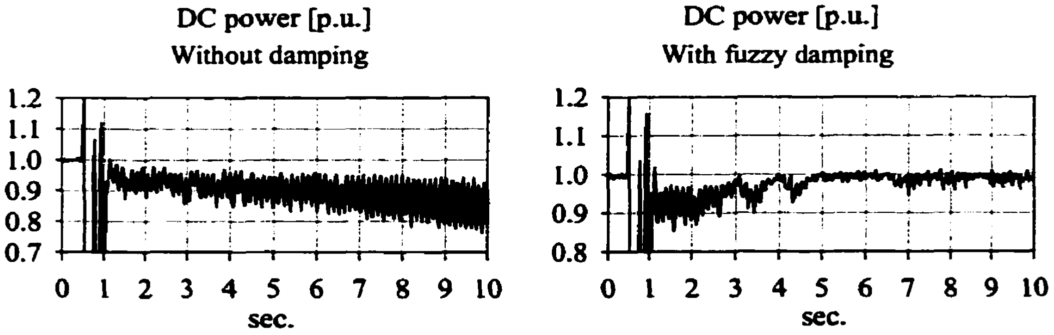

Figure 7-1-8 : Power response

Therefore the fuzzy controller can successfully reduce the oscillations in the mechanical part as well as the electrical counterpart of the system.

7.2 Power Oscillation Damping

As another example of the application of the fuzzy control to a high level control scheme, power oscillation damping is investigated. In this case the inverter side source of the CIGRE benchmark is substituted with an equivalent synchronous machine model equipped with the solid state exciter and hydro governor. The ratings of the synchronous machine, exciter and hydro governor are given in §B.2. In addition a synchronous condenser is also connected to the inverter side ac bus, which supplies about 30% of the inverter bridge reactive power under the rated steady state codition.The ratings of this synchronous condenser as well as the corresponding exciter are given in the §B.2.

The combined system on the inverter side which is now composed of two synchronous machines, shows new dynamical performance. The two machine are now able to oscillate either with respect to a fixed rotating frame or relative to each other. The former will be detected through external system performance while the latter would be left undetected. The circuit is shown in the figure 7-2-1.

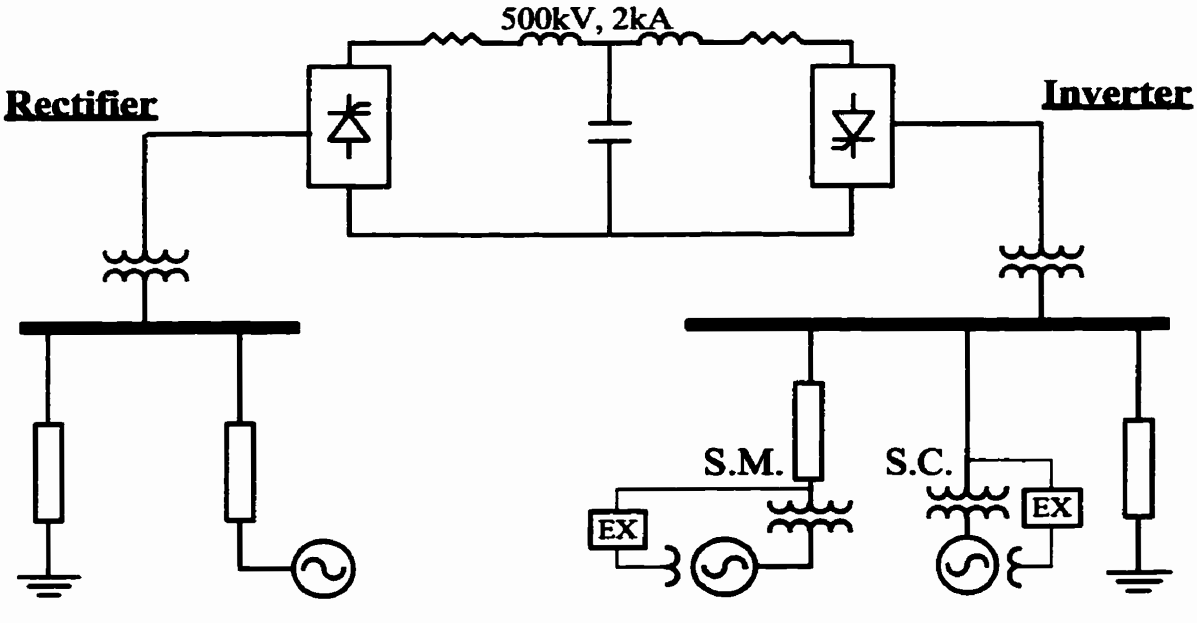

Figure 7-2-1 : CIGRE benchmark with modified inverter

The results of the simulation show that even the start-up process is very oscillatory which damps out very slowly (roughly 10 sec.).

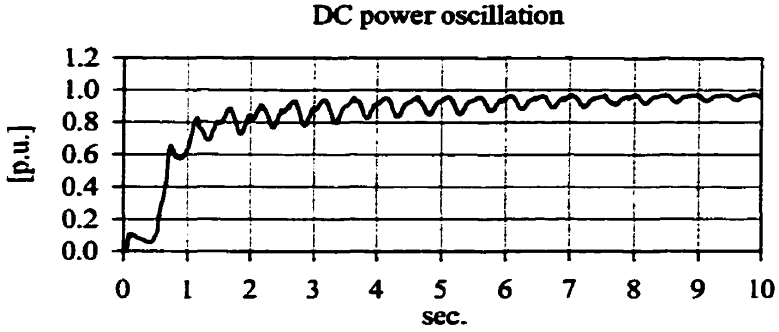

Figure 7-2-2 : Dc power oscillations during the start-up

In order to be able to damp out the oscillations, one should be able to measure the frequency and the deviation of the line voltage. The main obstacle in these kind of problems is that, there is no reference frame for comparison. In order to elaborate more on this subtle point, consider that the ac voltage phasor on the inverter bus is aligned with an arbitrary but synchronized phasor under the steady sate condition. It is obvious that under a new steady state condition long after any changes on the inverter side the voltage phasor does not remain aligned with the arbitrary phasor. Figure 7-2-3 shows this fact. The voltage phasor (solid vector) which is initially aligned with the arbitrary reference phasor (dotted vector), will not remain aligned with the reference phasor following a system change.

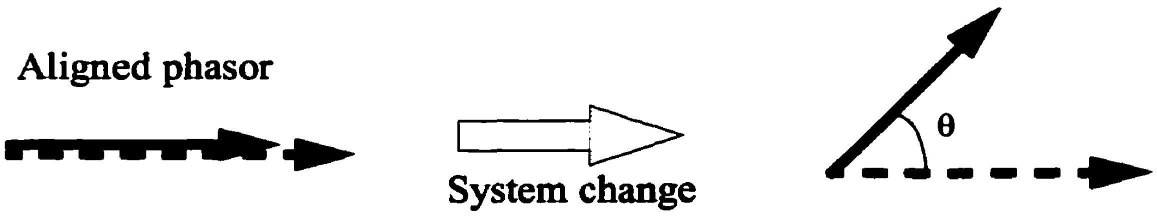

Figure 7-2-3 : Reference phasor

This reference phasor is only required to be at synchronous speed. Obviously the static deviation of the two phasors, does not contribute to any system oscillations, while the dynamic deviations such as oscillation of the voltage phasor about the arbitrary phasor directly related to system oscillations. The high frequency deviations of the voltage are not important either, because of the existing harmonics in the system. In order to differentiate between these three distinct cases the following filtering scheme is utilised.

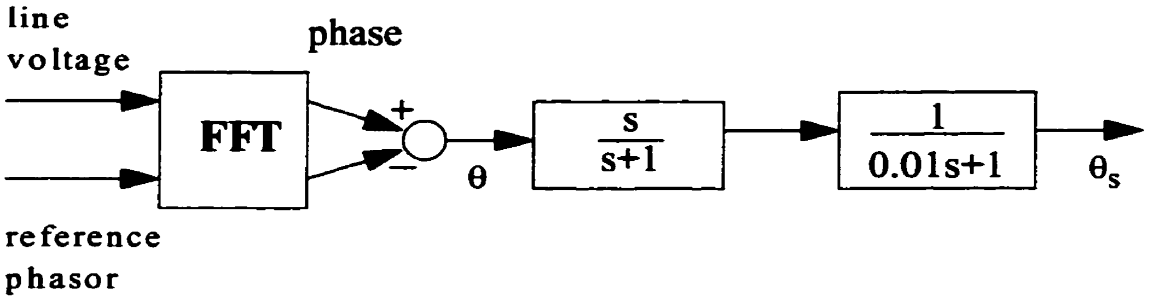

Figure 7-2-4 : Load angle measurement scheme

The FFT block calculates the fundamental phase angles associated with each vector. Then the difference between the two phases (θ) is fed into two cascaded filters. The first filter allows the output to follow the sudden changes of the input but washes out the slow changes in the input from appearing in the output. The second filter is used to filter low frequencies from the signal. Thus the overall filtering is like a medium pass filter and therefore the output as named in figure 7-2-4 by θ_S, is a close measure of the voltage angle deviation from the reference phasor within the proper frequency band.

The Bode plot (phase and magnitude) for the series connection of the washout and the real pole filters in figure 7-2-4 is shown in figure 7-2-5.

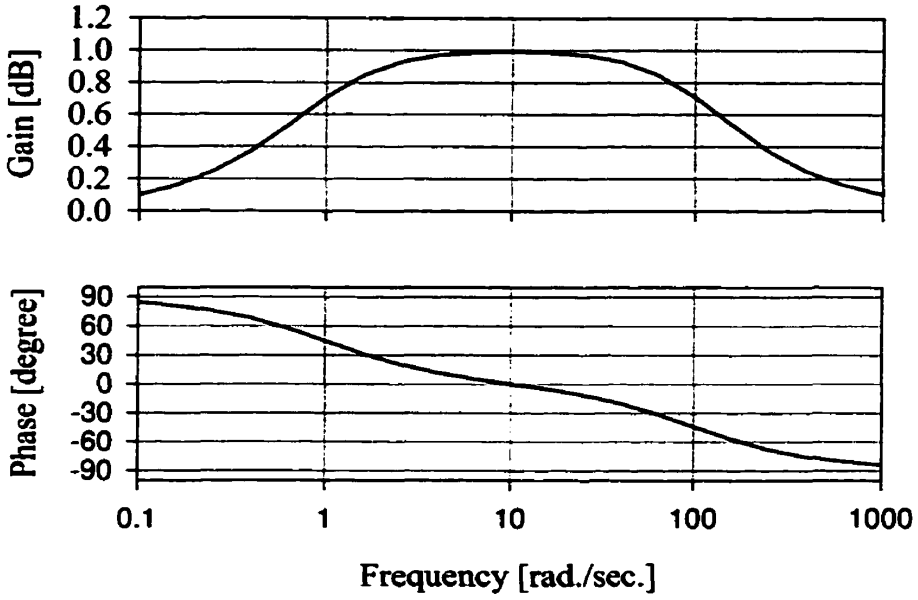

Figure 7-2-5 : Bode plots of the filter

Using such a measuring scheme applied to the line voltage of the ac bus, the θ_S plot versus time during the start up process is measured and shown in the figure 7-2-6. A close look at this figure shows that the line voltage oscillates with a frequency of about 2 Hz, at synchronous speed.

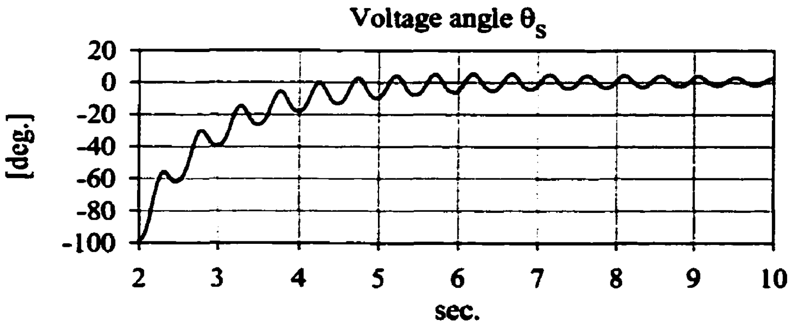

Figure 7-2-6 : θ_S angle oscillation

In order to damp the generated oscillations, a fuzzy inference algorithm is developed using the θ_S angle as the input.

The figure 7-2-7, shows the overall fuzzy control scheme used here. The line voltage is measured at the converter bus, and the synchronous machine is connected through the Thevenin equivalent impedance to this bus. The constant capacitor, filters and the synchronous condenser are all connected to this bus.

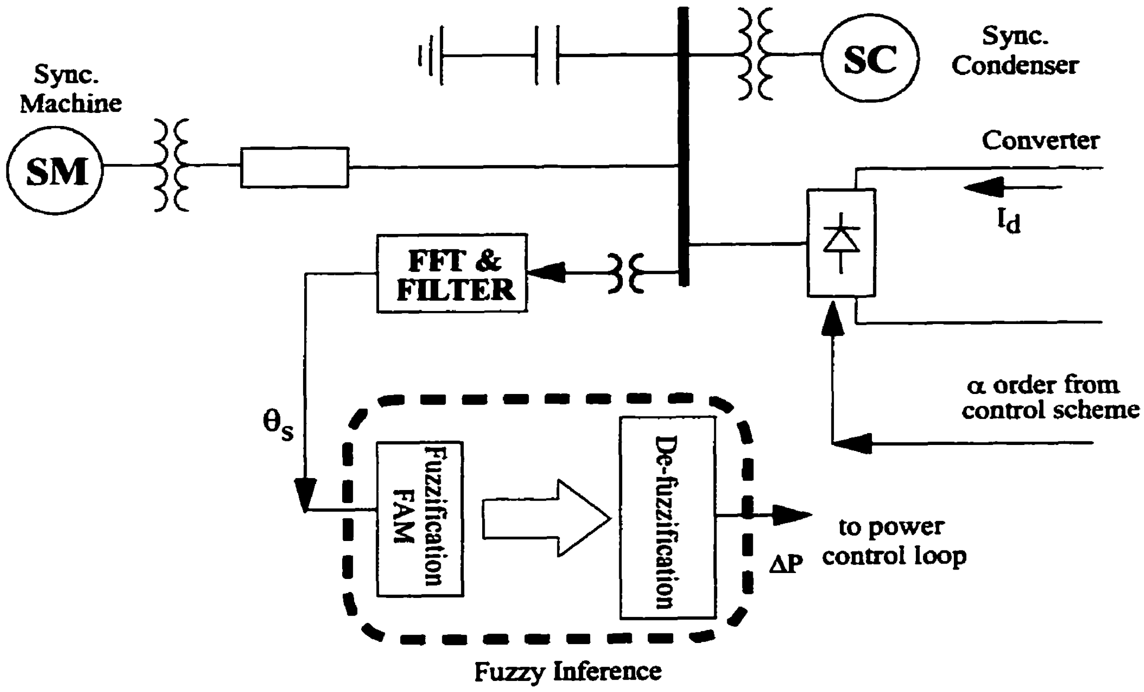

Figure 7-2-7 : Fuzzy inference diagram

The fuzzy inference controller shown in figure 7-2-7 generates a signal ΔP, which can be considered as the power order modulation. This power order modulation is used as an auxiliary input in the power control loop, shown in figure 4-4-1.

The signal ΔP derived through the fuzzy inference algorithm is added as an auxiliary input signal to the power reference signal in the power control loop.

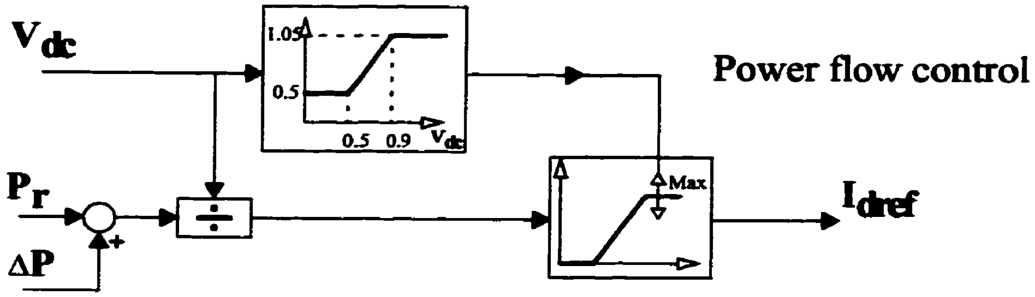

Figure 7-2-8 : Power control loop

Thus the power modulation is applied through ΔP in the power control loop, modulates the dc current reference and the converter's firing angle.

The fuzzy membership functions for the θ_s, the $d\theta_S/dt$ and the FAM consisting of the fuzzy rules are shown in figure 7-2-9.

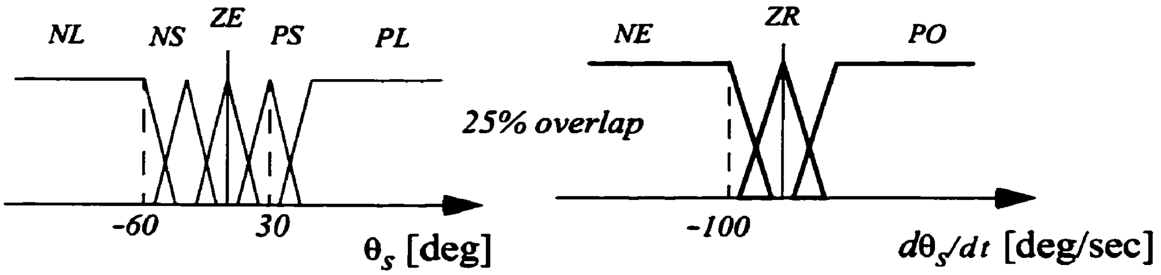

		$d\theta_S/dt$		
		NE	ZR	PO
θ_S	NL	NG	NM	PM
	NS	NM	Z	PM
	ZE	NM	Z	PM
	PS	NM	NM	PM
	PL	NG	NM	PG

Figure 7-2-9 : Fuzzy memberships and FAM

The acronyms NL, NM, Z, PM and PL stand for Negative Large, Negative Medium, Zero, Positive Medium and Positive Large.

The use of the fuzzy controller results in significant damping of the oscillations shown earlier. For example the dc transmitted power during the start up as shown earlier in figure 7-2-2, is significantly improved as is shown in figure 7-2-10.

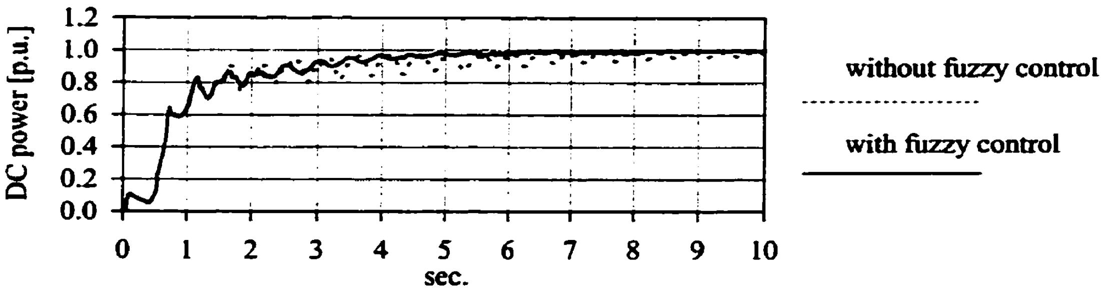

Figure 7-2-10 : Improved power recovery

The fuzzy controller also improves the line voltage oscillations. The oscillations in the voltage angle θ and the filtered phase θ_s are significantly reduced using the fuzzy controller.

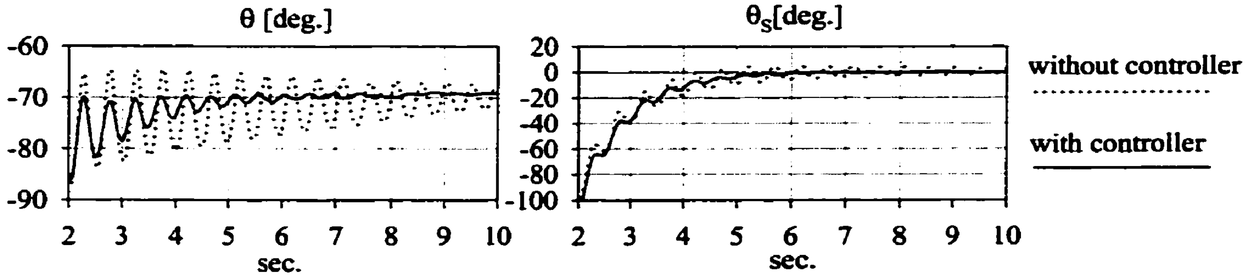

Figure 7-2-11 : θ and θ_S responses with the fuzzy controller

7.3 Conclusion

The fuzzy logic method has been successfully applied to high level HVdc control. The implementations outline the basics of the method, and the results show significant improvements in the system performance.

8. Conclusion

8.1 Contributions

In this dissertation the application of the artificial neural network and fuzzy logic control was studied and presented. Throughout this work several important contributions were made. The eminent contributions made in this dissertation can be summarized as follows:

- ANN control of HVdc systems was investigated. Various candidate networks were considered and it was concluded (with the justification in §2.4) that the off-line ANN would not show any improvement over conventional P-I controller. On the other hand, on-line ANN controllers were shown to be more applicable (§2.3).

- Using the case of a three phase rectifier connected to an R-L load, the ANN on-line based controller was shown to have very favourable response in comparison to a P-I based controller. The gain setting in a P-I controller can not be adaptively changed, thus the P-I controller can only be optimized at one operating point. Because of the learning feature of the ANN controller, it provides a favourable response over entire operating range.

- The on-line controller worked very well with the HVdc system as long as there is no control mode crossover. However, with control mode crossover, the response following the mode change was very poor. Various attempts such as freezing the weight adjustments did not improve the response to an acceptable level (§5.4 and §5.5). Finally a justification was presented for such unfavourable behaviour (§5.3).

- Fuzzy logic was also successfully implemented in the primary control loops of the HVdc systems. The general technique in order to improve and incorporate more control rules into the control scheme is also presented [§6]. The fuzzy logic method allows for the incorporation of simple rules into a control system. The rules are first stated in simple language and then are quantified for inclusion into the control system by using the fuzzy reasoning approach. If the performance is does not meet some requirements, additional parameters and rules can be added.

- The application of fuzzy logic to high level control problems of the HVdc system, resulted in improved stability of the electric system. The successful application of fuzzy logic to problems such as SSR and power swing damping are presented [§7].

- The topic of ANN controller which showed poor behaviour for mode crossover, was revisited. An attempt was made to use the fuzzy logic as a supervisory loop for the ANN on-line control blocks. Although this did result in some improvement, the overall response proved to be less than desired.

8.2 Additional Conclusion

- A MATLAB-PSCAD/EMTDC™ interface was developed. This interface allows one to integrate MATLAB's powerful computational engine into the electromagnetic transients simulation software PSCAD/EMTDC™ and allows for direct incorporation of MATLAB Toolboxes into the transient simulation.

8.3 Future Recommendations

1. The ANN studies have indicated that the on-line based ANN controller fails to achieve

a satisfactory result for the HVdc control mode crossover. The following areas for future works are recommended.

- The response speed of the ANN with synchronized learning was significantly improved with the technique presented in §3.3. One area for future study could be the inclusion of the plant Jacobian into the learning process. The derivatives can be substituted with discrete rate of change between input-output pairs. In other words, substituting $dI/d\alpha$ with $\Delta I/\Delta\alpha$ computed for each commutation interval.

- Another area for the improvement could be changing the optimization in the ANN such that it behaves as a CC or CEA controller in different operating regions, with the aid of a different cost function than the one used here.

- Other activation function such as *radial basis* function [25] should also be investigated.

- The application of ANN to high level control studies such as SSR and power swing damping may also be investigated.

2. The application of fuzzy logic to both low and high level control were studied in this thesis. The results have shown satisfactory results. Following is a list of recommendations for future works in this field.

- The inclusion of more control rules into the rule set was represented. The incorporation of protective control rules into the controlling rule set may also be studied.

- Domain knowledge such as specific characteristics of ac or dc systems can also be included as a fuzzy inference algorithm into the HVdc control scheme. This may also be considered as a potential field in this area.

Appendix A. MATLAB Aided Simulation

A.1 Introduction

Previous experiences with ANN and fuzzy logic as reported in §5 and §6 respectively, have shown that it is not straight forward to implement a new ANN or fuzzy logic algorithm into the simulation software. The simulation software PSCAD/EMTDC™ as any other electromagnetic transient simulation program is developed to study electric systems, and many common control blocks (such as P-I) are also provided in the default libraries provided by their vendors.

However when one tries to introduce new areas in conjunction with the simulation studies, one has to develop the necessary software in order to successfully implement this new technique into the study. Thus one has to initially achieve an in-depth familiarity with the new field and then spend a long time, developing and customizing the necessary programs.

MATLAB is a well known computational package with rich built-in commands and numerous Toolboxes. These Toolboxes are mainly developed and customized for technical fields such as artificial neural network and fuzzy logic.

The author believes that the possibility of synergy between MATLAB and the PSCAD/EMTDC™ facilitates the incorporation and study of new fields into the simulation studies by saving the time spend to develop new models and programs into the

PSCAD/EMTDC™. This interface would then be regarded as a great asset and useful tool in the studies.

This chapter describes the procedure and results for interfacing the computational engine of the MATLAB program with PSCAD/EMTDC™ program. The interface is developed using conversation pipes on UNIX platforms. Such pipes are used for the inter-process communication between the two separate programs.

Using this approach, it is possible to run the two programs simultaneously on separate computers even when they have different architecture. For ease of use, the interface is incorporated into the PSCAD/DRAFT. This allows the entry of MATLAB commands merely by clicking on the appropriate PSCAD/DRAFT icon. In addition to the description of the interface, a typical simulation example of an artificial neural network based controller for an ac-dc controlled rectifier (same as §3) is presented [10].

The emtp-type program PSCAD/EMTDC™ [22] has been designed to take advantage of piped communication. The popular mathematics and control systems design software package MATLAB [41] also has this capability.

The synergy of an electromagnetic transient program with MATLAB has several advantages. Although the power system network equations can be programmed into MATLAB, this requires the user to manually enter these equations. The emtp-type programs are optimized for power-network simulations and automatically generate the network equations directly from the topological description and constraints of the network. They also usually run faster than interpreted MATLAB code.

The DRAFT available with PSCAD/EMTDC™ is also customized for power-industry applications. On the other hand, MATLAB offers a large library of control functions, and through its Toolboxes, it also offers a wide range of preprogrammed algorithms.

Incorporating new techniques of control for power systems using simulation, requires that the user be quite familiar with the new control area, and write the necessary code in a programming language which is mostly FORTRAN. This requires an extensive effort especially during the preliminary studies just to investigate the feasibility of such applications. Thus during the preliminary studies, it is convenient to use MATLAB built-in function and Toolboxes.

Previous work on the subject includes writing of the emtp-type algorithm using MATLAB [40]. An approach similar to the one used here has been reported with the ATP program[31]. However in this chapter we describe an automated approach where the new component and the necessary interface files are generated automatically. The resulting component is then available in graphical form as a block in PSCAD/EMTDC™.

A.2 Structure of the Interface

The structure of the interface is as shown in figure A-2-1. PSCAD/EMTDC™ has a FORTRAN file called DSDYN through which external FORTRAN subroutines can be called. A FORTRAN subroutine is therefore developed which starts the MATLAB engine and sets up the data communication pipe between this subroutine and the MATLAB engine. Through this FORTRAN file, the M-file[1] containing the MATLAB commands is

[1] The file name extension (*.m) for a file containing MATLAB commands. The file is referred to in MATLAB terminology as m-file.

also passed to the MATLAB engine. The MATLAB part of the simulation is, of course, independently written and stored in the M-file.

It should be noted that the FORTRAN subroutine is not user-written but is automatically generated using a program specially developed for this purpose. This program generates all the necessary files for a new MATLAB block. This block is added to the DRAFT repertoire. The program and the interface have been successfully tested on Sun and DEC Alpha platforms.

Since the MATLAB computational engine is invoked using a FORTRAN subroutine and the data communication is established between PSCAD/EMTDC™ and MATLAB, it is possible in a network to run these two programs on two separate platforms; even when the two machines have different architecture. The resultant parallelism gives a speed-up in the total execution time.

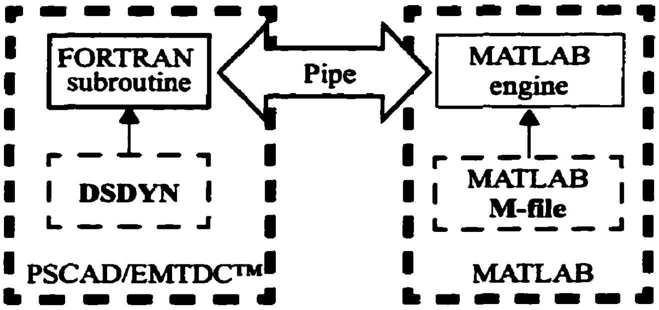

Figure A-2-1 : Structure of PSCAD/EMTDC™–MATLAB interface

A.3 Development of the MATLAB Block

The MATLAB block in PSCAD/EMTDC™ is seen as a graphical icon on the DRAFT palette. Connections to this block from other PSCAD/EMTDC™ blocks are made by dragging and dropping connecting wires. With each MATLAB block there are three associated files. The main file is the M-file which is interpreted by the MATLAB engine and includes all the commands that will be executed by MATLAB engine. The second file is the FORTRAN file. This FORTRAN file incorporates the main interface commands, such as starting the MATLAB engine and data sending and retrieving from MATLAB. The third file comprises the DRAFT description for the icon.

A new MATLAB block can be developed using a program specially developed for this purpose. This program asks for the name of the new component, the number of inputs and outputs and their names. A graphical icon of the block is then automatically generated along with an empty M-file, which is opened for user input in a text-editor shell. The user should then enter the appropriate MATLAB statements into this M-file.

It should be mentioned that the developed piece of code written in C, generates the necessary commands and calls the necessary functions to establish the data exchange between the FORTRAN subroutine and the MATLAB engine.

On one side of this data exchange, FORTRAN deals with floating point and integers values, while on the other side of the data exchange, MATLAB deals with dynamical pointers to arrays.

Therefore in order to pass data from FORTRAN to MATLAB, first a pointer must be assigned to the data and the address of the pointer should be passed to the MATLAB and conversely for passing data from MATLAB to FORTRAN. Therefore one variable has many assigned names which are all kept in a record. However the user only deals with a single name that appears both in the DRAFT graphical user interface and the MATLAB M-file.

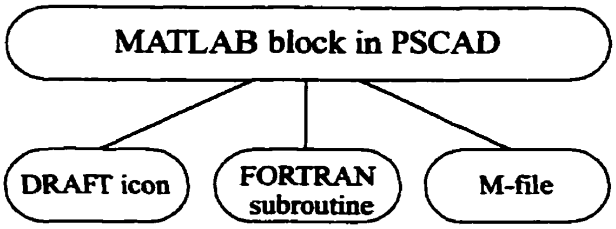

Figure A-3-1 : The PSCAD MATLAB block and its constituents

Figure A-3-2 shows a typical PSCAD/EMTDC™ case in which the MATLAB component labelled "MATLAB" is being used. Inputs or outputs can be scalars or arrays. The input in figure A-3-2 is an array of two components (Ref. and error), and the output is a scalar (α).

Once the component is developed, it may be used later merely by dragging and dropping the icon on the DRAFT palette from user library. The user can even edit the developed component's M-file directly from DRAFT via a popup menu that is selected by clicking on the component's icon.

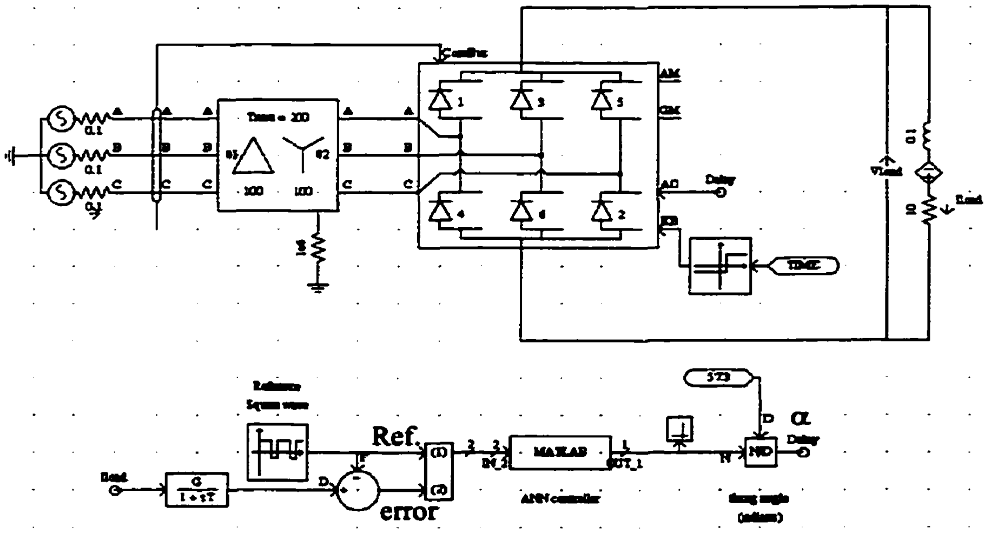

Figure A-3-2 : PSCAD/EMTDC™ palette with MATLAB block

A.4 Simulation Example

The example presented here describes the application of the PSCAD/EMTDC™ interface to the ac-dc converter being controlled by an artificial neural network (ANN) based controller. This case is identical to the example already presented in §3.2. A similar simulation is also developed using the fuzzy logic method, using the fuzzy logic Toolbox [21]. Here the ANN is trained in *incremental* or *on-line* training mode which tries to make the dc current follow the reference value and reduce the error to zero. The ANN is modelled using the MATLAB neural network Toolbox. The ANN is comprised of one input (in ANN terminology only Ref. is the input to ANN), two hidden and one output neurons. The current error is used to adjust the weights using the back-propagation as shown schematically in figure A-4-1.

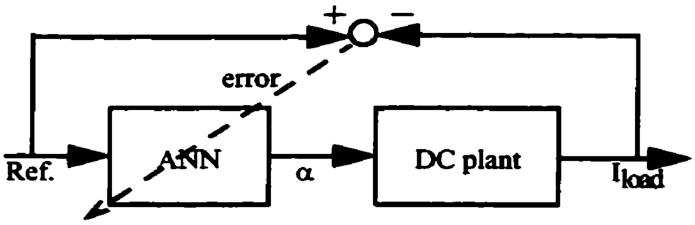

Figure A-4-1 : On-line ANN controller basics

The schematic diagram can be seen in the DRAFT palette shown in figure A-3-2, with the associated M-file shown in figure A-4-2. In the simulated case, the current reference is switched between two set-points (2.0 kA and 3.5 kA) at 200 ms intervals.

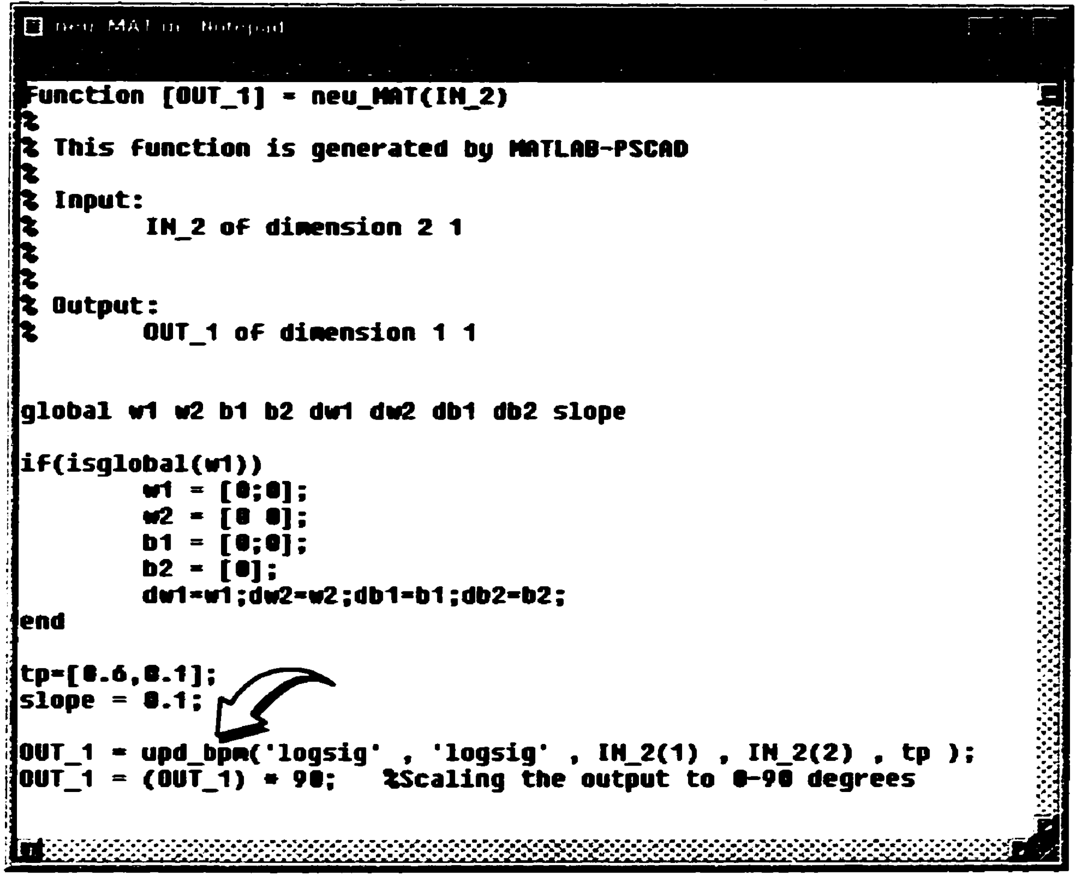

```
function [OUT_1] = neu_MAT(IN_2)
%
% This function is generated by MATLAB-PSCAD
%
% Input:
%        IN_2 of dimension 2 1
%
%
% Output:
%        OUT_1 of dimension 1 1


global w1 w2 b1 b2 dw1 dw2 db1 db2 slope

if(isglobal(w1))
        w1 = [0;0];
        w2 = [0 0];
        b1 = [0;0];
        b2 = [0];
        dw1=w1;dw2=w2;db1=b1;db2=b2;
end

tp=[0.6,0.1];
slope = 0.1;

OUT_1 = upd_bpm('logsig' , 'logsig' , IN_2(1) , IN_2(2) , tp );
OUT_1 = (OUT_1) * 90;   %Scaling the output to 0-90 degrees
```

Figure A-4-2 : M-file for PSCAD/MATLAB block "MATLAB"

This M-file shown in figure A-4-2 calls another M-file named upd_bpm.m (see arrow). This M-file (shown in figure A-4-3) executes the back-propagation algorithm using MATLAB neural network Toolbox commands. The entries in the M-file are directly entered using the popup editor window which appears when the ‘MATLAB’ component in the DRAFT palette (figure A-3-2) is clicked upon.

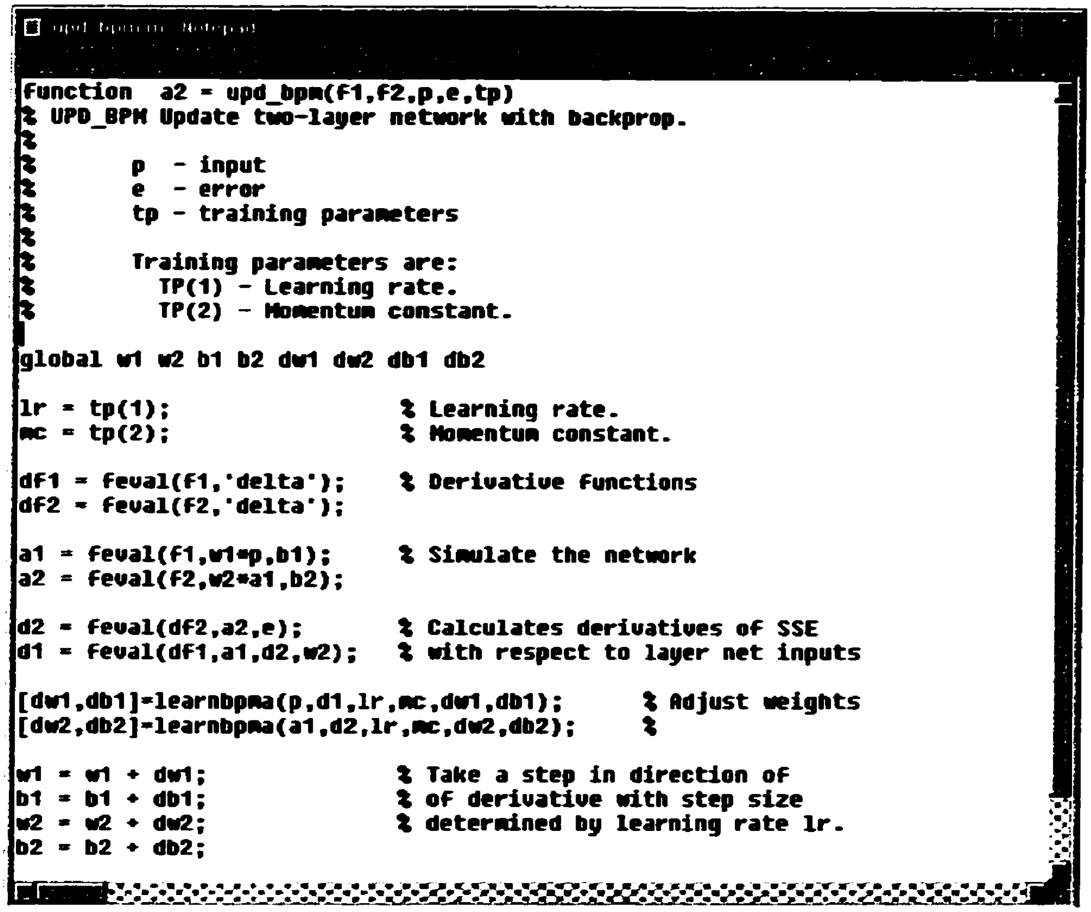

```
function  a2 = upd_bpm(f1,f2,p,e,tp)
% UPD_BPM Update two-layer network with backprop.
%
%       p  - input
%       e  - error
%       tp - training parameters
%
%       Training parameters are:
%         TP(1) - Learning rate.
%         TP(2) - Momentum constant.

global w1 w2 b1 b2 dw1 dw2 db1 db2

lr = tp(1);                  % Learning rate.
mc = tp(2);                  % Momentum constant.

df1 = feval(f1,'delta');     % Derivative functions
df2 = feval(f2,'delta');

a1 = feval(f1,w1*p,b1);      % Simulate the network
a2 = feval(f2,w2*a1,b2);

d2 = feval(df2,a2,e);        % Calculates derivatives of SSE
d1 = feval(df1,a1,d2,w2);    % with respect to layer net inputs

[dw1,db1]=learnbpma(p,d1,lr,mc,dw1,db1);      % Adjust weights
[dw2,db2]=learnbpma(a1,d2,lr,mc,dw2,db2);     %

w1 = w1 + dw1;               % Take a step in direction of
b1 = b1 + db1;               % of derivative with step size
w2 = w2 + dw2;               % determined by learning rate lr.
b2 = b2 + db2;
```

Figure A-4-3 : The on-line back-propagation algorithm

The results from the simulation are seen in figure A-4-4. The first plot shows the dc load current and the reference current order, and the second one shows the associated firing angle that is generated at the output of the ANN controller.

Although the overall simulation time required for the example is larger than that if the ANN component were directly programmed in FORTRAN as a standard PSCAD/ EMTDC™ block, the interface allows one to investigate a large number of control strategies using the preprogrammed libraries of the MATLAB Toolboxes, thereby saving much effort in developing and utilizing the new models. However, once the control strategy is finalized, it may be worthwhile to reprogram the algorithm into a standard PSCAD/EMTDC™ block written in FORTRAN. This also allows for the block to be compiled and made into a library within PSCAD/EMTDC™ and thus speeds up the simulation process.

In a similar manner any other function available in the basic MATLAB program or its Toolboxes can be included into PSCAD/EMTDC™. One additional advantage of this approach is to that of animated output rendering. For example, during the program's execution, the path of the flux-current point on a saturation curve of a typical transformer can be traced via MATLAB commands or the locus of a relay trajectory can be seen superposed on the relay characteristic. Similarly three dimensional plotting commands in MATLAB can reveal interesting features of the simulation during execution time.

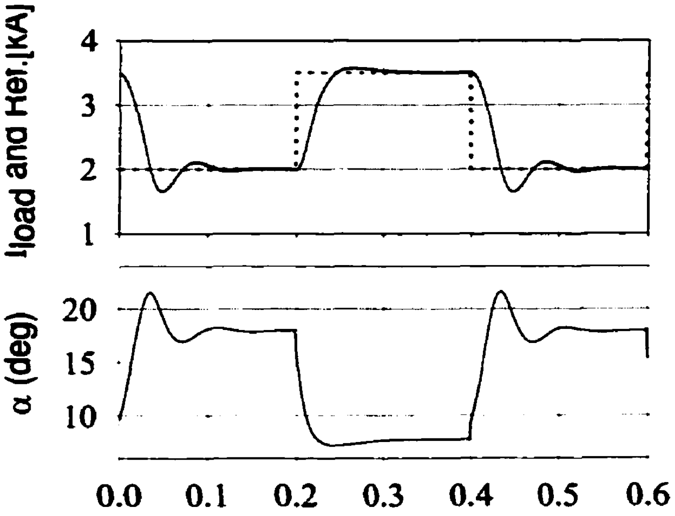

Figure A-4-4 : Simulation results

A.5 Conclusions

The powerful control system modelling capabilities in MATLAB were accessed through the PSCAD/EMTDC™ simulation program. The FORTRAN Interface available in PSCAD/EMTDC™ coupled with the data exchange over inter-process communication pipes on the UNIX platform allows for such an interface to be easily constructed.

A special program that performs the automatic generation of the component icon and associates the corresponding files with the icon, was found to greatly simplify the process of new component design. The newly developed component is then accessible through the graphical user interface of PSCAD/EMTDC™ just like any other component in its repertoire.

The technique allows for immediate access to a whole range of pre-developed MATLAB control libraries as shown by the example of the ANN based controller for an ac-dc converter. It also offers the possibility of using advanced MATLAB graphics commands for animated on-line displays.

The CPU time required for the combined PSCAD/EMTDC™-MATLAB simulation is more than if the MATLAB component were modelled directly in PSCAD/EMTDC™. Thus the above simulation approach is recommended during the evaluation stage in which several different control algorithms are being investigated. For the fastest possible runs, the component should be compiled and used in PSCAD/EMTDC™.

Although this powerful technique could have been used extensively during the progress of this thesis, it was only completed toward the end of the research. By that time the author already gained sufficient experience with the artificial neural networks and fuzzy logic, and directly developed the components in PSCAD/EMTDC™.

Appendix B. Data for §7

B.1 Data for §7.1

EXCITER PARAMETERS:

T1	“Rectifier Smoothing Time Constant”	“0.02 sec”
Ta	“Controller Lead Time Constant”	“1.43 sec”
Tb	“Controller Lag Time Constant”	“7.04 sec”
Te	“Exciter Time Constant”	“0.032 sec”
K	“Exciter Gain”	“500 p.u.”
Emax	“Maximum Field Voltage”	“5 p.u.”
Emin	“Minimum Field Voltage”	“-5 p.u.”
Vbase	“L-G Voltage Base”	“199.18584 kV, rms”
Ibase	“Line Current Base”	“2 kA, rms”
Rrev	“Reverse Resistance”	“14285 Ohms”

“Exciter Voltage Supply Bus Fed”

MULTI-MASS PARAMETERS:

N	“Number of Turbines (1 to 5)”	“4”
MVA	“Machine 3 phase MVA”	“1200 MVA”
F	“Electrical base frequency”	“60.0 Hz”
RPM	“Machine rated speed”	“3600.0 rpm”

“INERTIA CONSTANTS”

H1	“Turbine #1 Inertia Constant”	“0.0929”
H2	“Turbine #2 Inertia Constant”	“0.1556”
H3	“Turbine #3 Inertia Constant”	“0.8587”
H4	“Turbine #4 Inertia Constant”	“0.8842”

Data for §7

HG	“Generator Inertia Constant”	“0.8685”
HE	“Exciter Inertia Constant”	“0.0342”

“MUTUAL DAMPING”

“ALL SET TO ZERO”

“SHAFT SPRING CONSTANT”

K12	“Spring Constant From Turbine #1 to #2”	“7277”
K23	“Spring Constant From Turbine #2 to #3”	“13168”
K34	“Spring Constant From Turbine #3 to #4”	“19618”
KLG	“Spring Const. From Last Turb. to Gen.”	“26713”
KGE	“Spring Const. From Generator to Exciter”	“1064”

“TURBINE TORQUE SHARE”

TF1	“Torque Share for Turbine #1”	“0.30 p.u.”
TF2	“Torque Share for Turbine #2”	“0.26p.u.”
TF3	“Torque Share for Turbine #3”	“0.22 p.u.”
TF4	“Torque Share for Turbine #4”	“0.22 p.u.”

SYNCHRONOUS MACHINE PARAMETERS:

H	“Inertia Constant”	“2.89 MWs/MVA”
OMO	“Base Angular Frequency”	“376.992 rad/s”
Vbase	“Rated RMS Phase Voltage”	“15.011 kV”
Ibase	“Rated RMS Phase Current”	“26.5477 kA”

“GENERATOR FORMAT”

Xp	“Potier Reactance”	“0.130 p.u.”
Xd	“Direct-Axis Reactance”	“1.79 p.u.”
Xd’	“Direct-Axis Transient Reactance”	“0.1690 p.u.”
Xd”	“Direct-Axis Sub-Transient Reactance”	“0.135 p.u.”
Xq	“Quad-Axis Reactance”	“1.71 p.u.”
Xq”	“Quad-Axis Sub-Transient Reactance”	“0.2 p.u.”
Ra	“Armature Resistance”	“0.02 p.u.”

Tdo’	“Direct-Axis Transient Time Constant”	“4.3 sec”
Tdo”	“Direct-Axis Sub-Transient Time Constant”	“0.032 sec”
Tqo”	“Quad-Axis Sub-Transient Time Constant”	“0.05 sec”

B.2 Data for §7.2

SOURCE PARAMETERS

“GOVERNER PARAMETERS”

f	“Base Frequency”	“60.0 Hz”
T1	“Controller Real Pole Gain”	“0.88 “
T2	“Controller Proportional Gain”	“3.7 “
T3	“Controller Integral Gain”	“0.44 “
T4	“Controller Real Pole Time Const”	“0.02 sec”
T5	“Turbine Lead Time Constant”	“0.8 sec”
T6	“Turbine Lag Time Constant”	“0.4 sec”
TS	“Governor Time Constant”	“0.05 sec”
C1	“Inverse Gate Velocity Limit”	“4.8 sec/p.u.”
C2	“Gate Velocity Time Constant”	“0.1 sec”
C3	“Permanent Droop Gain”	“0.04”
C4	“Gate Position Control Rate Limit”	“0.22 pu./sec”
C5	“Temporary Droop Gain”	“0.0”
C6	“Temporary Droop Time Constant”	“1.0 sec”
Tmax	“Conversion Constant”	“0.957”
Tm0s	“Time Constant for Smoothing Tm0”	“0.02 sec”

EXCITER PARAMETERS:

T1	“Rectifier Smoothing Time Constant”	“0.02 sec”
Ta	“Controller Lead Time Constant”	“1.5 sec”
Tb	“Controller Lag Time Constant”	“1.0 sec”

Data for §7

Te	“Exciter Time Constant”	“0.02 sec”
K	“Exciter Gain”	“100 p.u.”
Emax	“Maximum Field Voltage”	“5 p.u.”
Emin	“Minimum Field Voltage”	“-5 p.u.”
Vbase	“L-G Voltage Base”	“132.79 kV, rms”
Ibase	“Line Current Base”	“3.7653 kA, rms”
Rrev	“Reverse Resistance”	“15000 Ohms”

“Exciter Voltage Supply Bus Fed”

SYNCHRONOUS MACHINE PARAMETERS:

H	“Inertia Constant”	“5 sec”
OMO	“Base Angular Frequency”	“376.992 rad/s”
Vbase	“Rated RMS Phase-to-Ground Voltage”	“10.392 kV”
Ibase	“RMS Phase Current (MVA/ [3*Vbase])”	“48.1125 kA”
VT	“Terminal Voltage Magnitude at t=0”	“0.94839130 p.u.”
Pheta	“Terminal Voltage Phase at t=0”	“-0.429351 rad”
P0	“Real Power at t=0 (+=Out)”	“-25.0 MW”
Q0	“Reactive Power at t=0 (+=Out)”	“-270.0 MVAr”

“EQUIV. CIRCUIT FORMAT”

XS1	“Stator Leakage Reactance”	“0.14 p.u.”
XMDO	“Unsaturated Magnetizing Reactance”	“1.445 p.u.”
X3D	“Damper Leakage Reactance”	“0.0437 p.u.”
X2D	“Field Leakage Reactance”	“0.2004 p.u.”
XMQ	“Quad-Axis Magnetizing Reactance”	“0.91 p.u.”
X2Q	“Quad-Axis Damper Leakage”	“0.106 p.u.”
Rs1	“Stator Resistance”	“0.0025 p.u.”
R2D	“Field Resistance”	“0.00043 p.u.”
R3D	“Direct-Axis Damper Resistance”	“0.0051 p.u.”
R2Q	“Quad-Axis Damper Resistance”	“0.00842 p.u.”

Data for §7

SYNCHRONOUS CONDENSER PARAMTERES

EXCITER PARAMETERS:

T1	“Rectifier Smoothing Time Constant”	“0.02 sec”
Ta	“Controller Lead Time Constant”	“1.5 sec”
Tb	“Controller Lag Time Constant”	“1.0 sec”
Te	“Exciter Time Constant”	“0.02 sec”
K	“Exciter Gain”	“100 p.u.”
Emax	“Maximum Field Voltage”	“5 p.u.”
Emin	“Minimum Field Voltage”	“-5 p.u.”
Vbase	“L-G Voltage Base”	“132.7906 kV, rms”
Ibase	“Line Current Base”	“0.6276 kA, rms”
“Exciter Voltage Supply Bus Fed”		

SYNCHRONOUS MACHINE PARAMETERS:

H	“Inertia Constant”	“1.7 sec”
OMO	“Base Angular Frequency”	“376.992 rad/s”
Vbase	“Rated RMS Phase-to-Ground Voltage”	“10.392 kV”
Ibase	“RMS Phase Current (MVA/ [3*Vbase])”	“35.283 kA”

“GENERATOR TYPE FORMAT”

Xp	“Potier Reactance”	“0.2 p.u.”
Xd	“Direct-Axis Reactance”	“1.56 p.u.”
Xd’	“Direct-Axis Transient Reactance”	“0.300 p.u.”
Xd”	“Direct-Axis Sub-Transient Reactance”	“0.280 p.u.”
Xkf	“Damper-Field Mutual Reactance”	“0.0 p.u.”
Xq	“Quad-Axis Reactance”	“1.560 p.u.”
Xq”	“Quad-Axis Sub-Transient Reactance”	“0.230 p.u.”
Ta	“Armature Time Constant”	“0.332 sec”
Tdo’	“Direct-Axis Transient Time Constant”	“1.1 sec”
Tqo”	“Quad-Axis Sub-Transient Time Constant”	“0.05 sec”

9. References

[1] - Aggoune M., El-Sharkawi M. A., Park D.C., Damborg M.J. and Marks II R.J., "Preliminary Results of Neural Networks for Security Assessment." IEEE PAS 6 (1991): 890-896.

[2] - Aggoune M. E., Atlas L. E., Cohn D. A., El-Sharkawi M. A. and Marks R. J., "Artificial Neural Networks for Power System Static Security Assessment." IEEE International Symposium on Circuits and Systems, Portland, Oregon, May 9 - 11, 1989, 490-494.

[3] - Ainsworht, J.D., "The Phase-Locked Oscilator—A new Control System for Controlled Static Converters." IEEE PAS 87 (1965): 859-865.

[4] - Alves, J.E.R.; Pilotto, L.A.S.; Watanabe, E.H, "Adaptive digital controller applied to HVDC transmission." IEEE Transactions on Power Delivery 8 (1993): 1851-1859.

[5] - Arrillaga, J. High Voltage Direct Current transmission. London: Peter Pereginus 1983.

[6] - Beaufays, F., et al.,:"Application of Neural Networks to Load-Frequency Control in Power Systems." Neural Networks, 7.1 (1994): 183-194.

[7] - Chen, Fu-Chuang, "Back-Propagation Neural Networks for Nonlinear Self-Tuning Adaptive Control." IEEE Control Systems Magazine, (1990): 44-48.

[8] - Daneshpooy, A., Gole, A.M. (1994):"HVDC Control with On-line Learning Based Neural Network" Proceedings of the International Confefernce on Power System Technology, ICPST'94, Oct. 18-21, Beijing, China, 479-483.

[9] - Daneshpooy, A., Gole, A.M., Chapman,D.G., Davies,J.B., "Fuzzy Logic Control for HVDC Transmission", IEEE Winter Meeting, New York, 1997.

[10] - Daneshpooy, A., Gole, A.M. "Linking Computational Engine to Electromagnetic Transients Program" Proceedings of the Second International Conferernce on Digital Power Systems Simulators, ICDS 97, Montréal, Québec May 28-30, 1997 143-147.

[11] - Dash, P.K., et. al. , "High performance controllers for HVdc transmission links.", IEE Proc. Gener. Trans. Dist. 5 (1994): 422-428.

[12] - Dash, P.K.; Routray, Aurobinda; Panda, S.K.,"Gain scheduling adaptive control strategies for HVDC systems using fuzzy logic", Proceedings of the IEEE International Conference on Power Electronics, Drives & Energy Systems for Industrial Growth, PEDES v 1 1996. IEEE, Piscataway, NJ, USA. 134-139.

[13] - Dash, P.K.; Panda, S.K.; Liew, A.C. "Fuzzy tuning of DC link controllers.", Proceedings of the International Conference on Energy Management and Power Delivery, EMPD v 1 1995. IEEE, Piscataway, NJ, USA,95TH8130. 370-375

[14] - Dommel, W. H., "Digital Computer Solution of Electromagnetic Transients in Single and Multiphase Networks" IEEE PAS 88 (1969): 388-398.

[15] - Electric Power Research Institute (EPRI), "HVDC System Control for Damping of Subsynchronous Oscillations", EPRI EL-2708, Project 1425-1, Final Report, October 1982.

[16] - El-Sharkawi M. A., Marks R.J., Oh S., Huang S.J., Kerszenbaum I. and Rodriguez A., "Localization of Winding Shorts Using Fuzzified Neural Networks." IEEE Transaction on Energy Conversion 10 (1995): 140-146.

[17] - El-Sharkawi M. A., Marks R. J., Aggoune M. E., Park D. C., Damborg M. J. and Atlas L. E., "Dynamic Security Assessment of Power System Using Back Error Propagation Artificial Neural Networks" Second Symposium on Expert Systems Application to Power Systems, Seattle, Washington, July 17 - 20, 1989, 366-370.

[18] - El-Sharkawi M. A., Marks R. J., Damborg M. J., Atlas L. E., Cohn D. A. and Aggoune M., "Artificial Neural Networks as Operator Aid for On-Line Static Security Assessment of Power Systems" Power Systems Computation Conference, Graz, Austria, August 19-24, 1990, 895 - 901.

[19] - El-Sharkawi M. A., Oh S., Marks R. J., Damborg M. J. and Brace C. M., “Short Term Electric Load Forecasting Using an Adaptively Trained Layered Perceptrone” First International Forum on Applications of Neural Networks to Power Systems, Seattle, July 23 - 26, 1991, 3-6.

[20] - Engström, P.G., “Operation and Control of H.V.D.C. Transmission.”, IEEE PAS 83 (1964): 71-77.

[21] - Gole, A.M., Daneshpooy, A., “A PSCAD/EMTDC™ to MATLAB Interface”, IPST 97, 22-26 June, Seattle, USA

[22] - Gole A.M., Nayak O.B., Sidhu T.S. , Sachdev M.S. , "A Graphical Electromagnetic Simulation Laboratory for Power Systems Engineering Programs”, IEEE PES Summer Meeting, Portland, OR, July 1995.

[23] - Hecht-Nielsen, R. Neurocomputing. NewYork:Addison-Wesley Publishing co., 1990.

[24] - Hect-Nielsen, R. ”Theory of the Backpropagation Neural Network.”, Proceedings of the International Joint Conference on Neural Network June 1989. , New York: IEEE Press, vol. I, .593-611.

[25] - Hertz, J., et al. Introduction to the Theory of Neural Computation. Lecture notes I, Santa Fe Institute in Sciences of Complexity, New York: Addison-Wesley Publishing co. 1991.

[26] - Huang T., Weerasooriya S. and El-Sharkawi M. A., "Novel Approaches to Drives Control: Neural Networks and Fuzzy Control" The Third International Conference on Advances in Communications and Control Systems, Victoria, B.C., October 16-18, 1991.

[27] - Hayashi, Yoichi; Czogala, Ernest; Buckley, James J.,"Fuzzy neural controller" IEEE Int Conf Fuzzy Syst FUZZ-IEEE. Publ by IEEE, IEEE Service Center, Piscataway, NJ, USA (IEEE cat n 92CH3073-4) 197-202

[28] - IEEE Committee, "Computer representation of excitation systems.", IEEE PAS 100 (1981): 494-509.

[29] - IEEE Committee, "First Benchmark Model for Computer simulation of Subsynchronous Resonance.", IEEE PAS 96 (1977): 1565-1572.

[30] - Jotten,R., Bowles,J.P., Liss,G., Martin,C.J.B., Rumpf,E., "Control in HVdc systems, the state of art, Part I: Two Terminal Systems", CIGRE 14-10, 1978.

[31] - Kezunovic, M., Chen, Q.," A Novel Approach for Interactive Protection System Simulation", IEEE T&D Conference, Los Angeles, September 1996.

[32] - Kimbark,E.W. Direct Current Transmission. New York: Wiley-Interscience 1971."

[33] - Kong, S. G., Kosko, B., "Adaptive Fuzzy Systems for Backing up a Truck and Trailer.", IEEE Trans. on Neural Networks, 3 (1992): 211-223

[34] - Kosko, B. Neural Networks and Fuzzy Systems. Toronto: Prentice Hall, 1992.

[35] - Kirkpatrik, S. C. D., et al., (1983):"Optimization by Simulated Annealing.", Science 220 (1983): 671-680

[36] - Lai L.L., Ndeh-Che F., Chari Tejedo, "Fault identification in HVDC systems with neural networks", Proceedings of the 5th European Conference on Power Electronics and Applications, IEE Conference Publication v 1 n 388 1994. Publ by IEE, Michael Faraday House, Stevenage, Engl. 231-236.

[37] - Lamm, U., "Control System", Direct Current, 4 (1959): 162-163.

[38] - Madan, S.; Bollinger, K.E.; Banerjee, S.K., "Microprocessor based HVDC converter protection", Canadian Conference on Electrical and Computer Engineering v2, 1996. IEEE, Piscataway, NJ, USA, 96TH8157. 750-753.

[39] - Maharsi, Y.; Do, V.Q.; Sood, V.K.; Casoria, S.; Belanger, J.,"HVDC control system based on parallel digital signal processors", IEEE PAS 10 (1995): 995-1002.

[40] - Mahseredjian, J. and Alvarado, F.; "The Design of Time Domain Simulation Tools: the Computational Engine Approach" Proceedings of the International Conference on Power System Transients, Lisbon, Portugal, Sept. 3-7, 1995, 493-498.

[41] - The Mathworks Inc. MATLAB Reference Guide. 1992.

[42] - Narendra,K.G., Khorasani,K., Sood,V.K., Patel,R.V., "Intelligent Current Controller for an HVDC Transmission link", Proceedings of the 20th International Conference on Power Industry Computer Applications, May 11-16, 1997, columbus, Ohio, 67-74.

[43] - Narendra,K.G., Sood,V.K., Khorasani,K., Patel,R.V., "Investigation into an Artificial Neural Network based On-Line Current Controller for an HVDC Transmission link", IEEE Power Engineering Society Winter meeting 97, N.Y., 1997.

[44] - Narendra, K.G.; Sood, V.K.; Patel, R.; Khorasani, K.,"Neuro-fuzzy VDCL unit to enhance the performance of an HVDC system", Canadian Conference on Electrical and Computer Engineering v 1 1995. IEEE, Piscataway, NJ, USA,95TH8103. 441-446.

[45] - Nguyen,H.D., Widrow, B.:"Neural Networks for Self-Learning Control Systems.", IEEE Control System Magazine 8 (1990) 18-23.

[46] - Nguyen,H.D., Widrow, B.:"The Truck Backer-Upper: An Example of Self-Learning in Neural Networks", Int. Joint Conf. on Neural Networks, June 1989,v II, 357-363.

[47] - Park D. C., El-Sharkawi M. A., Marks R. J., Atlas L. E. and Damborg M. J., "Electric Load Forecasting Using An Artificial Neural Network." IEEE Transactions on Power Systems. 6 (1991) 442-449.

[48] - Park D.C., Mohammed O., El-Sharkawi M. A. and Marks R. J., "Adaptively Trained Neural Networks and Their Application to Electric Load Forecasting" IEEE International Symposium on Circuits and Systems, Singapore, June 11 - 14, 1991, 1125-1128.

[49] - Pedrycz, W. Fuzzy Control and Fuzzy Systems. Somerset: Research Studies Press Ltd., 1993.

[50] - Psaltis, D., et al."A Multilayer Neural Network Controller.", IEEE Control System Magazine 8 (1988): 17-21.

[51] - Reeve, John; Sultan, Mansour, "Gain scheduling adaptive control strategies for HVDC systems to accommodate large disturbances.", IEEE Transactions on Power Systems 9 (1994) 366-372.

[52] - Reeve, John; Sultan, Mansour, "Robust Adaptive Control of HVDC Systems.", IEEE Transactions on Power Systems 9 (1994) 1487-1493.

[53] - Rueda, A.; Pedrycz, W., "Design method for a class of fuzzy hierarchical controllers", IEEE International Conference on Fuzzy Systems Second IEEE Int Conf Fuzzy Syst 1993, Publ by IEEE, IEEE Service Center, Piscataway, NJ, USA,Manit, 196-199.

[54] - Sanpei, Masatoshi; Kakehi, Atsuyuki; Takeda, Hideo, "Application of multi-variable control for automatic frequency controller of HVDC transmission system.", IEEE Transactions on Power Delivery 9 (1994): 1063-1068.

[55] - Schiffmann, W.H., Geffers, H.W. "Adaptive Control of Dynamic Systems by Back Propagation Networks.", Neural Network 6 (1993): 517-524.

[56] - Sood, V. K., et al.,(1991):"Neural Network Based Current Controller for HVDC Transmission Systems", Second IEE Int. Conf. on Neural Networks, Bournelmouth, U.K., 18-20 Nov.1991, 373-378.

[57] - Sood, V. K., et al., (1992):"Comparative Evaluation of Neural Network Based and PI Current Controllers for HVDC Transmission.", IEEE Trans. Power Electronics, 9 (1994): 288-296.

[58] - Swarup, K.S.; Chandrasekharaiah, H.S.,"Fault detection and diagnosis of power converters using artificial neural networks", Proceedings of the IEEE International Conference on Power Electronics, Drives & Energy Systems for Industrial Growth, PEDES v 2 1996, IEEE, Piscataway, NJ, USA. 1054-1058.

[59] - Szechtman. M, et al.,(1991):"First Benchmark Model for HVDC Control Studies.", Electra 135 (1991): 54-73.

[60] - To, K.W.V.; David, A.K., "Multi-variable adaptive control of AC-DC systems.", IEE Proceedings Generation, Transmission and Distribution 141 (1994): 658-664.

[61] - Venugopal, K. P., Pandaya, A. S., Sudhakar, R., "A Recurrent Neural Network Controller and Leraning Algorithm for the On-Line Learning Control of Autonomous Underwater Vehicles.", Neural Networks, 7.5 (1994): 833-846.

[62] - Uhlmann, E. Power Transmission by Direct Current. Berlin: Springer-Verlag., 1975

[63] - Uhlmann, E. "Stabilisation of an AC link by a parallel DC link.", Direct Curret, August 1964, 89-94.

[64] - Weerasooriya S., El-Sharkawi M. A., Damborg M. and Marks R., "Towards Static Security Assessment of a Large Scale Power System Using Neural Networks" IEE Proceedings-C, 139(1992): 64-70.

[65] - Weerasooriya S. and El-Sharkawi M. A., "Laboratory Implementation of Neural Network Trajectory Controllerfor a dc Motor" IEEE Transaction on Energy Conversion, 8 (1993): 107-113.

[66] - Werbos, Paul J.,"An overview of neural networks for control", IEEE Control Systems Magazine 11-1 (1991): 40-41.

[67] - Wess, T., Ring, W. "FGH controls for the HVDC benchmark model study", FGH report presented to CIGRE WG 14.02, Oct. 1988.

[68] - Wood, A.R., Arrillaga, J. "Frequency dependent impedance of an HVdc converter", IEEE Transactions on Power Delivery 10 (1995): 1635-1641.

[69] - Yu, Yao-Nan. Electric Power System Dynamics. Newe York: Academic Press, 1983.